

POLITECNICO DI TORINO

SCUOLA INTERPOLITECNICA DI
DOTTORATO

Doctoral Program in Biomedical Engineering – XXVIII cycle

Final Dissertation

**A versatile platform for three-dimensional
dynamic suspension culture applications**



Giuseppe Isu

Tutor

prof. Umberto Morbiducci
Dr. Diana Massai

Co-ordinator of the Research
Doctorate Course

prof. Cristina Bignardi

April 4th, 2016

Abstract

In the last decades, the rapid upgrading in cell biological knowledge has bumped the interest in using cell-based therapeutic approaches as well as cell-based model systems for the treatment of diseases. Given the rapid translation towards cell-based clinical treatments and the consequent increasing demand of cell sources, three-dimensional (3D) suspension cultures have demonstrated to be an advantageous alternative to monolayer techniques for large scale expansion of cells and for the generation of three-dimensional model systems in a scale-up perspective.

In this scenario, a versatile bioreactor platform suitable for 3D dynamic suspension cell culture under tuneable shear stress conditions is developed and preliminarily tested culturing cancer cell spheroids. By adopting simple technological solutions and avoiding rotating components, the bioreactor exploits a laminar hydrodynamics, enabling dynamic cell suspension in an environment favourable to mass transport. Technically, the bioreactor is conceived to produce dynamic suspension cell culture under tuneable shear stress conditions without the use of moving components (from ultralow to

moderate shear stress). A multiphysics computational modelling strategy is applied for the development and optimization of the suspension bioreactor platform. The in silico modelling is used to support the design and optimization phase of the bioreactor platform, providing a comprehensive analysis of its operating principles, also supporting the development/optimization of culture protocols directly in silico, and thus minimizing preliminary laboratory tests. After the technical assessment of the functionality of the device and a massive number of in silico simulations for its characterization, the bioreactor platform has been employed for two preliminary experimental applications, in order to determine the suitability of the device for culturing human cells under dynamic suspension. In detail, the bioreactor platform has been used to culture lung cancer cells for spheroid formation (Calu-3 cell line) under ultralow shear stress conditions, and for human induced pluripotent stem cell (hiPSC) dynamic suspension culture.

The use of the bioreactor platform for the formation of cancer cell spheroids under low shear stress conditions confirms the suitability of the device for its use as dynamic suspension bioreactor. In fact, compared to static cell suspension, after 5 days of dynamic suspension culture the bioreactor platform preserves morphological features, promotes intercellular connection, increases the number of cycling cells, and reduces double strand DNA damage. Calu-3 cells form functional 3D spheroids characterized by more functional adherence junctions between cells. Moreover, the computational model has been used as a tool for assisting the setup of the experimental framework with the extraction of the fluid dynamic features establishing inside the bioreactor culture chamber.

As second proof of concept application, the bioreactor platform has been tested for the dynamic suspension of hiPSCs. Starting from the ‘a priori’ knowledge gained by the development of the in silico culture protocol, the agglomeration of human induced pluripotent stem cells has been modulated by means of the combination of moderate intermittent shear stress and free-fall transport within the bioreactor culture chamber. The inoculation of single cells suspensions inside the bioreactor chamber promotes cell-cell interaction and consequently the formation of human induced pluripotent stem cell aggregates.

In conclusion, the impeller-free functioning principle characterizing the proposed bioreactor platform demonstrates to be promising for human cell dynamic suspension culture. In the future, this bioreactor platform will be further optimized for the realization of impeller-free dynamic suspension bioreactors dedicated and optimized to specific applications in stem cell and cancer cell culture.

Contents

Contents	2
1 Three-Dimensional Dynamic Suspension Cell Culture	8
1.1 Motivations.....	8
1.2 Stem cells for Regenerative Medicine and Tissue Engineering.....	11
1.3 3D Dynamic Suspension Culture: Bioreactors for Regenerative Medicine, Tissue Engineering and Cancer Biology	14
1.4 Computational Multiphysics Modelling in Tissue Engineering	17
1.4.1 Multiphysics Modelling as Bioreactor Design Tool.....	18
1.4.2 Multiphysics Modelling for Process Design	19
1.5 Research Objectives.....	20
1.6 Thesis Outline	22
References.....	25
2 Versatile Bioreactor for Reproducible and Scalable Dynamic Suspension	36
2.1 Introduction.....	36
2.2 Bioreactor Platform Description	38
2.2.1 Design Requirements	38
2.2.2 Bioreactor Platform Functioning Principle	39
2.2.3 Original Architectural Design and Constitutive Elements....	39
Culture Chamber	40
Check Valve (original configuration)	41
Filter System	42
Closed loop Recirculation Circuit.....	43

2.3 In Silico Multiphysics Model-Based Design Optimization.....	46
2.3.1 Multiphysics Modelling for Fluid Dynamics Characterization	47
Methods	47
Results and Discussion	52
2.3.2 Multiphysics Modelling for in silico Protocol Development ..	58
Methods	59
Results and Discussion	63
2.3.3 In silico Supported Check Valve Optimization	70
Revised Check Valve System: Concept	70
Methods	72
Results	74
2.4 Bioreactor Platform Optimization	76
2.4.1 Continuous Perfusion Feeding Circuit	76
2.4.2 .Control and Monitoring System	79
Sensing Flow Chamber	82
References.....	88
Appendix I.....	91
Sizing of the Closed-loop Recirculation Circuit	91
Oxygen Transport Computational Model.....	101
References.....	104
Appendix II.....	105
Sensors and Conditioning Circuit for Monitoring System	105
pH Sensor.....	105

Dissolved Oxygen (DO) Sensor	108
Amplification and Current/Voltage circuit.....	110
Monitoring System Characterization	112
pH sensor Characterization	113
DO sensor Characterization	115
Monitoring and Control System: Control Unit.....	116
References.....	119
3 Application to the Culture of Cancer Cell Spheroids.....	124
3.1 Introduction.....	124
3.2 Materials and Methods.....	127
3.2.1 Dynamic Suspension Bioreactor	127
3.2.2 Computational model	129
3.2.3 <i>In vitro</i> cell culture	131
3.2.4 Assessment of <i>In vitro</i> cell culture	132
3.3 Results	133
3.3.1 Flow dynamics within the bioreactor culture chamber	133
3.3.2 <i>In vitro</i> culture outcome	138
3.4 Discussion and Conclusion	141
References.....	146
4 Application with human induced Pluripotent Stem Cells: Preliminary Study.....	152
4.1 Introduction.....	152
4.1. Materials and Methods	155
4.1.1. Bioreactor Platform	155

4.1.2.	Qualitative Suspension Analysis	156
4.1.3.	Monolayer Culture Passaging of hiPSCs	157
4.1.4.	Orbital-Shaker Spheroid Aggregate Formation of hiPSCs 158	
4.1.5.	hiPSCs Dynamic Suspension Culture with the Bioreactor Platform	158
4.1.6.	Flow Cytometry	160
4.2.	Results.....	161
4.2.1.	Qualitative Suspension Analysis	161
4.2.2.	hiPSCs Dynamic Suspension Culture within the Bioreactor Platform	162
4.3.	Discussion and Conclusion.....	171
	References.....	174
	5 Discussion and Conclusion	178
	References.....	185
	Industrial Bioengineering Group Activity	190
	Abstract: Comparison of Symmetrical Haemodialysis Catheters using Computational Fluid Dynamics	190
	Introduction.....	192
	Materials and Methods.....	193
	Results	196
	Discussion	200
	References.....	206
	Figures.....	210

Chapter 1

Three-Dimensional Dynamic Suspension Cell Culture

1.1 Motivations

In the last decades, the rapid improvement in cell biological knowledge have bumped the interest in using cell-based approaches for the treatment of diseases. Regenerative medicine approaches have grown up as a good deal of prior clinical activities, such as surgery, surgical implants, and clinical procedures including bone marrow and organ transplants [1]. Human somatic, adult, embryo-derived or induced ‘pluripotent’ stem cells and their possible use for clinical treatments are the main focus for the researchers in this field [2,3].

As a result, regenerative medicine deals with the *restoration* of physiological structure and function of the organ or tissue, in contrast with organ or tissue repair, which entails the adaptation of the organ or tissue to non-physiological damage (e.g. scar tissues) [4]. This aspect widens the scope of interest of regenerative medicine not only on regeneration of injured tissues,

but also on congenital pathological abnormalities, where normal function has never been present (e.g. thalassemia, absence of corneas, etc.). This field is extremely interdisciplinary, involving at the same time tissue, genetic and molecular engineering. Greenwood et al. [5] considers regenerative medicine as *'an emerging interdisciplinary field of research and clinical applications focused on the repair, replacement or regeneration of cells, tissues or organs to restore impaired function resulting from any cause, including congenital defects, disease, trauma and aging. It uses a combination of several technological approaches that moves it beyond traditional transplantation and replacement therapies. These approaches may include [...] stem cell transplantation, tissue engineering and the reprogramming of cell and tissue types.'*

However, there is still a philosophical difference in the way to apply advances in cell-biology to translational regenerative medicine. Biomaterials scientists indicate the future medicine strictly connected with nanotechnology improvements, conceiving the use of nanodevices for 'futuristic' clinical treatments [6]. By contrast, there is a part of the scientific community which is interested in emulating natural renewal capabilities employing the minimal artificial materials [1]. In this perspective, living cells are a key raw material for therapeutic applications, often required in trillions of quantities to reach the required curative potential [7].

Stem cells are the ideal cellular source for cell-based therapies. There are, though, controversial observation from animal models which make numerous investigators sceptical of their direct use for clinical treatments [8,9]. This contrast concerns, firstly, the choice of the most suitable cell type to be used for organ regeneration. Secondly, there is still the underlying question of

whether regenerate a pathological organ by means of delivering primitive undifferentiated stem/progenitor cells (which differentiation will be guided by in vivo signals), or transplanting mature, in vitro engineered tissues [7]. Indeed, tissue engineered constructs are now considered the modern healthcare revolution for their increasing potential to regenerate tissues or organs from non-physiological conditions [10].

Besides the possible clinical applications, the necessity to better understand disease development, as well as the comprehension of the mechanisms which regulate stem cell self-renewal potential and cancer development are the principal purposes of cell research [11]. Cancers are complex and heterogeneous pathological ‘organs’, which have a dynamic interaction with their host. Thus, cancer research is oriented to the constitution of validated in vitro preclinical models capable of incorporating the main features of pathological cancer tissues, in order to limit the preclinical failure of innovative therapeutic molecules and drugs [12]. Since solid tumours grow three-dimensionally, two-dimensional cancer models are not completely capable of capturing the complexity of the in vivo cancer pathology. This requisite brings to the necessity to recreate a functional microenvironment resembling constitutive and morphological features of solid tumours [12].

These aspects imply the massive use of human cells in different fields of biology, biotechnology, and medicine: for drug discovery [13], toxicology studies [14], in vitro personalized disease modelling and cancer cell biology. Due to this fact, it is necessary to reach high standard of safety and efficacy in living cell biomanufacture. Biomanufactured cells or constructs must be produced consistently through economically viable processes while adhering to

good manufacturing and good tissue practise (GMP/GTP) standards. The innovative technologies needed for the scale up in the production of living cells are the crucial factor for obtaining successful applications of in vitro tissue models, disease modelling, and regenerative medicine [10].

1.2 Stem cells for Regenerative Medicine and Tissue Engineering

Stem cells are largely considered the preferred cell source for cell and scaffold based regenerative medicine and tissue engineering therapies. Stem cells have the potential to develop into many different cell types inside a living organism from early life stage, during growth, and while adult life time. Typically they are unspecialized cells capable of renewing themselves through cell division, sometimes after long periods of senescence [15]. Under specific physicochemical stimuli they are able to become differentiated cells with specialised functions. Inside an adult subject, it is possible to find adult stem cells which regularly divide and contribute to repair and regenerate damaged organ regions (e.g. in the gut and bone marrow), as well as stem cells which stay in specific cell niches and divide only under specific conditions (e.g. within heart and pancreas) [15].

Compared to muscle, neuronal, or blood cells, which usually do not replicate themselves, stem cells have shown their capability of long-term self-renewal. Indeed, starting from a stem cell population in laboratory, it is possible to maintain the population in a proliferative state preserving their unspecialized characteristics [16]. Moreover, single stem cells are able to generate a line of genetically identical cells from their division process, allowing to enhance their self-renewal and differentiation potential (i.e. clonogenic cells) [7].

The enormous interest in stem cells is related to their possible employment for therapeutic applications. In this case, the use of stem cells is a promising source of human cell types which are not otherwise available in vitro [7].

Stem cells extracted from many organs and tissues in adults (adult stem cells, ASCs) can typically differentiate to one or limited cell lines (multipotent stem cells) [15,16]. Adult stem cells are thought to reside in a specific area of each tissue (called 'stem cell niche'). Another source of stem cells is the embryo. When stem cells are derived from blastocyst stage embryos (embryonic stem cells, ESCs), their specialization potential can give origin to almost every cell line in the body (pluripotent stem cells) [17]. The necessity to destroy the early human embryo in order to obtain ESCs to be cultured in vitro has led to different limitations and regulations for every different country, in the name of distinct moral and ethical positions [18,19]. As a consequence, the most of the research in translational medicine has focused on ASCs which can be isolated from patient own tissue and subsequently transplanted (i.e. autologous cell transplant). Indeed, autologous approaches avoid donor cell rejection and the risk of teratoma formation (benign tumours containing various differentiated cells, possibly imposed by ESCs) [7]. However, the heterogeneity of stem cell types and the difficulties to isolate specific stem cell-types with supposed therapeutic potential limit the use of well-defined 'autologous cell-based cocktails', causing uncertainty in the expected clinical outcomes [8,7,20]. Furthermore, the isolation of adult stem cells with sufficient degree of purity and sufficient cell number is still problematic, also due to the lack in the definitive identification of type markers for cell-type selection amongst an isolated population [21].

In 2006, researchers demonstrated that mouse somatic cells (any body cell other than gametes) might be genetically reprogrammed to an embryonic stem cell-like state. These reprogrammed cells have been called “induced pluripotent stem cells” (iPSCs) [22]. Subsequently, in 2007, direct reprogramming was achieved in human cells. Human iPSCs are ideally equivalent to human ESCs in terms of both self-renewal and differentiation capacity, contemporarily overcoming obstacles related to immunological rejection after transplantation and ethical concerns. As a matter of fact, human iPSCs could solve the current lack of primary somatic cells in biomedicine. In fact, human iPSCs are normally derived from dermal fibroblasts because of their accessibility and relatively high reprogramming efficiency [23]. Blood cells are considered another valid source because easily accessible and does not present the risk of chromosomal aberration caused by ultraviolet light-exposure [24]. For this reason, this cell type is currently largely employed for the development of their mass production, in order to reach standardized and reproducible protocols for cell expansion with therapeutic purposes [25,26,27].

Many problems remain before iPSC medical and pharmaceutical applications can be fully realized. After the initial excitement, several reports revealed serious concerns about genomic integrity of the cells: epigenetic remodeling, aberrant expression of reprogramming factors, clonal selection, and prolonged in vitro culture are potential pathways of genomic alterations [28].

Nevertheless, besides the current limitations in the use of human stem cells for therapeutic purposes, there is still enormous attraction in stem cell culture as a source for basic stem cell research [29], drug screening and dis-

covery [30], in vitro personalized disease modelling [31], and cell-based personalized regenerative therapies [32]. In this context, beyond the main clinical purpose, there is a crescent interest in stem cells for the development of novel, scalable screening in vitro platforms for essays, compound discovery, drug toxicity testing [33], study of differentiation/development processes, study of malignancy and genetic disorders [7].

1.3 3D Dynamic Suspension Culture: Bioreactors for Regenerative Medicine, Tissue Engineering and Cancer Biology

In order to accelerate the translation from regenerative medicine/tissue engineering to clinical practice, large scale production is a mandatory step: scalability and standardization in cellular manufacturing processes are now the major challenge especially for applications which require large numbers of cells (10^{10} - 10^{12}). In a scaling-up perspective and inspired by the manufacturing processes of therapeutics in biopharmaceutical industry [34,35], three-dimensional (3D) suspension culture has demonstrated to be an advantageous alternative to monolayer techniques for large-scale expansion of cells [7,36,10]. Suspension culture techniques, with or without cell micro-carriers, have demonstrated their potential for low cost scalable cell expansion and long-term cell viability maintenance [37,25,38,27]. They have been largely employed for multicellular aggregate formation [39,40,41], to guide differentiation of stem cells [42], to prevent the dedifferentiation process that occurs under traditional two-dimensional (2D) cell culture conditions [43], for the production of native-like three dimensional (3D) engineered tissues [44], and

for the generation of 3D cancer models reproducing the solid tumour micro-environment [45,46]. The provision of a 3D environment, with suspension mimicking the microenvironment of the cellular niche, has proven to be beneficial, promoting cell proliferation and retaining cell properties in vitro [7,47,48].

Typically, suspension culture is obtained by means of bioreactors. A bioreactor can be defined as a system capable to simulate physiological environments in order to facilitate physical conditioning of cells, (engineered) tissues and organs in vitro. These devices allow to study the effects of biophysical factors under closely monitored and controlled culture conditions and to generate tissues in vitro, assuring greater reproducibility, traceability, scalability, and almost operator-independence [49,50]. In general, bioreactors provide the possibility to develop platforms for automated, repeatable, and scalable: (1) cell expansion, (2) cell seeding in scaffolds, (3) cellular differentiation and tissue maturation, (4) drug screening, and (5) in vitro disease model investigation [51].

In the specific field of suspension culture, the use of bioreactors is favourable for all biotechnological or clinical applications in which large quantities of cells ($\geq 10^7$) are demanded [52]. When suspension is obtained by means of dynamic mixing of the culture medium, the formation of pH, dissolved oxygen, and nutrient gradients is prevented, mass transport is increased and sedimentation is avoided, overcoming the intrinsic limitations of static culture systems [7,49,34].

The most commonly-used suspension bioreactors for scalable production and differentiation of cells are the stirred flask and rotating wall bioreactors [53].

Stirred flask (also known as spinner flask) bioreactors are typically small vessels (in laboratory scale around 120 mL in volume) in which culture medium is agitated by the magnetic stirring of an impeller. The interaction between the impeller and the culture medium produces a complex flow field inside the vessel volume, resulting in eddies and turbulent instabilities. Transitional flow and turbulence are conceived to enhance fluid transport through the suspended particles and constructs (isotropic turbulence may be considered) [54], even if agitation rates for stem cell culture are mild compared to original biotechnological applications. Indeed, typical agitation rates for laboratory scale bioreactors are between 30 to 80 rpm [25,27,55]. Such devices, designed to provide a 3D homogeneous culture environment, have been demonstrated to lead to more reproducible, robust and cost effective processes for stem cell proliferation and differentiation [27,25,26,10]. As a matter of fact, these devices are usually equipped with a control and monitor system for the most significant culture parameters such as pH, dissolved oxygen, and biomass detection [7,25]. Nevertheless, due to the local turbulence and the high shear rate generated between the impeller and the vessel walls, stirred bioreactors are characterized by non-physiological shear stress and consequent unfavourable conditions, affecting cell growth rate and metabolism, interfering with stem cell pluripotency, and limiting efficiency and reproducibility of the culture process [7,56,57].

Rotating wall vessels (RWV) were designed to minimize shear stress and turbulence in suspension culture devices [43,58]. These bioreactors exist in two different configurations: high aspect ratio vessel (HARV) and slow turning lateral vessel (STLV), but they are both characterized by the same operating principle [36]. The cylindrical culture vessel is continuously rotated, about its horizontal axis. The permanent rotation produces specimen suspension, resulting in circular free-fall paths developing as a function of rotational velocity. This circular paths ensure suspended particles to move sufficiently inside the culture medium in order to guarantee homogeneous nutrient, oxygen and waste distribution and favouring aggregate formation by cell-to-cell contact [59]. This operating basis encourages a uniform growth of the constructs, avoiding the possible mechanical damage to suspended cells and tissues caused by mechanical stress, both including shear stress and detrimental cell-wall or cell-impeller collisions [50]. RWVs has been successfully employed for osteogenic [60,61,62] and cardiomyogenic differentiation [63,64]. Nevertheless, the complexity of the technological solutions adopted for rotation makes these devices not easily scalable and unsuitable for continuous medium replacement and real-time monitoring [36,43].

1.4 Computational Multiphysics Modelling in Tissue Engineering

One of the most striking issues in regenerative medicine and tissue engineering is the lack of quantitative measures and procedures to increase the reproducibility of the generated products [65,66]. In general, protocols and procedures followed inside the most of the laboratories are still commonly established by trial and error approaches. In a perspective of the scaling up

of the technologies to an industrial manufacturing level, the lack of intelligent process design makes difficult the realization of products that may meet the quality standards imposed by the international regulatory bodies (e.g. EMA or FDA) [67]. As a consequence, in the last years, it was proposed to include commonly used engineering techniques into tissue engineering in order to orient the research towards robust, observable, and controllable procedures. Typically, the first step of the design phase in industrial manufacturing, from chemical to automotive engineering, is to devise *in silico* models with the aim to increase the process quality and optimization. This approach gives the possibility to extrapolate the key process-parameter and to predict with a certain degree of accuracy the final product behaviour [67].

1.4.1 Multiphysics Modelling as Bioreactor Design Tool

As mentioned in the previous paragraphs, bioreactors are characterized by a dynamic culture environment capable of increasing transport phenomena inside the culture vessel as well as guaranteeing optimal conditions for cultured cells. Besides the two commercial bioreactor designs highlighted in paragraph 1.3 (stirred and rotating wall bioreactors), single research groups in tissue engineering and regenerative medicine have designed, developed, and studied other novel bioreactor architectures. Different bioreactor configurations may result in different fluid dynamics inside the extracellular environment which may affect cellular activities [57]. As a matter of fact, fluid dynamics inside bioreactors must be optimized in order to determine the optimal environment conditions to cells in terms of mass transport and flow-induced mechanical stimulation. Multiphysics modelling of different culture platforms is usually carried out by means of computational fluid dynamics

(CFD). The high efficiency achieved in the last years in computational performance enables to generate relevant information on the flow field and transport efficiency of soluble factors or nutrients to cells, even in complex designs and multiphysics problems. CFD simulations serve as a tool to accelerate the transition from the conception of a new idea to the realization of the prototype, giving the possibility to identify the most important parameters to be taken into account during the design of a cell culture platform. Moreover CFD allows to improve with quantitative measures the bioreactor performance obtaining a comprehensive description of its functioning [68,69].

1.4.2 Multiphysics Modelling for Process Design

Multiphysics models are largely employed to extract knowledge on the process in progress inside the bioreactor platform [70]. Starting from the on-line monitoring of culture parameters (e.g. pH, dissolved oxygen, metabolite concentrations, etc.) it is possible to develop control approaches such as model-based predictive controllers. The set-up of a model, that is complex enough to capture the process dynamics of interest inside the bioreactor platform, is useful to establish a fully-defined culture method allowing to predict with a good degree of accuracy the outcome of the experiment [71]. The importance of adopting multiphysics modelling in tissue engineering/regenerative medicine processes is self-evident when, for the proficient setup of the experiment, it is necessary to integrate knowledge about biomass distribution, culture medium flow, mass transport, together in the same device [72]. Several examples of multiphysics models in process development have been proposed: optimization of the generation of engineered vascular grafts [73], opti-

mization of encapsulated stem cell suspension in RWV bioreactors [38], optimization of transport phenomena in rotating hollow-fibre bioreactor for artificial liver [74], development of predictive models for oxygen transport and stem cell aggregation within stirred bioreactors [75], scaffold seeding and engineered tissue maturation in perfusion bioreactors [72], and assessment and adjustment of flow-induced shear stress levels inside porous scaffolds in perfused bioreactors [76].

In conclusion, the aim of multiphysics modelling is always trying to understand the biological process, designing *in silico* strategies to improve the desired *in vitro* outcome. In this perspective, the experiments should be designed in parallel with the *in silico* models, in order to realize integration between the experiments and the computational modelling. This approach allows to obtain quantitative information from the experimental process to be applied to the *in silico* model, and vice versa.

1.5 Research Objectives

From the discussion proposed in the previous paragraphs, it is clear that one of the principal focus of regenerative medicine, tissue engineering, and cancer cell biology research is to reach a better understanding on disease development and on biological mechanisms which regulate cellular fate. This improvement requires an enormous quantity of source cells to accelerate the translation from laboratory tissue engineering to clinical practise. Thus, there are biotechnological process optimizations for the standardized mass production of the most promising stem cell sources for autologous implantations.

Whether cell therapy or tissue engineering approaches will be successfully developed, in both cases it is necessary, in this phase of research, to have a large amount of cellular sources available for the realization of scalable in vitro platforms. However, scalability and standardization in cellular manufacturing processes are still major challenges, in particular, when large numbers (10^{10} - 10^{12}) of cells are required. The use of conventional bioreactors is still not sufficient to guarantee a boost towards repeatable and scalable biotechnological procedures, given some existing limitations and drawbacks in their design. In this context, there is an increasing demand for the design of versatile devices optimized to overcome the limitations of conventional bioreactors.

The objectives of this research was the realization of a versatile bioreactor platform for reproducible and scalable bioprocesses in tissue engineering and regenerative medicine. In detail, this platform was developed by the direct integration of in silico multiphysics modelling and the experimental design of a dynamic suspension bioreactor platform. Starting from a CFD optimized configuration of the bioreactor platform [77], the platform was recursively optimized both modifying the bioreactor chamber and implementing new elements such as a monitoring and control system.

In particular, the in silico multiphysics modelling was used for the development and optimization of a versatile suspension bioreactor for 3D cell culture. This bioreactor was conceived to produce dynamic suspension cell culture under tuneable shear stress conditions without the use of moving components. By means of the implementation of a multiphysics model of the bioreactor, taking into account the presence of suspended cells inside the culture chamber (multiphase fluid dynamics model), the in silico platform

was used to support the design and optimization phase of the device. Such model provided a comprehensive analysis of the operating principles of the bioreactor, and permitted the development of *in silico* culture protocols. Indeed, multiphysics simulations were used to set the proper bioreactor conditions according to the experimental application for *in vitro* preliminary biological tests.

The versatile suspension bioreactor is a part of a platform. Originally, the bioreactor chamber is connected to a medium recirculation closed-loop capable of producing cell suspension, which was successively equipped by a home-made on-line monitoring system with sensors for metabolic and nutrient concentration measurements.

The integration of the *in silico* and experimental design facilitated the use of the bioreactor for two different preliminary applications: *i*) dynamic suspension for cancer cell spheroid formation under low shear stress conditions, and *ii*) preliminary feasibility test for free-cell suspension culture of human iPSCs.

1.6 Thesis Outline

The first part of this thesis manuscript will present (Chapter 2) all the design and optimization phase carried out to develop a valuable and usable bioreactor platform. In particular, the integration between computational *in silico* methods with the prototyping of the bioreactor platform is widely described.

The second part will be dealing with two different biological/biotechnological applications. The first application (Chapter 3) is the use of the bioreactor platform for dynamic suspension of cancer cell under low shear stress conditions. The second application (Chapter 4) is the employment of the bioreactor platform in the framework of feasibility study tests for free-cell suspension culture of human iPSCs.

PART I

Chapter 2

Versatile Bioreactor for Reproducible and Scalable Dynamic Suspension

In this chapter, a versatile bioreactor suitable for tuneable (from low to moderate) shear dynamic suspension cell culture is presented. The optimization phase of this device concerned the implementation of a monitoring system to the bioreactor platform, with the implementation of specific sensors, providing real-time information about the metabolic behaviour of cultured cells. The optimization phase of the device was supported by in silico multiphysics modelling, which provided a comprehensive analysis of the operating principles of the bioreactor, and permitted the optimizations of the check valve system.

PART II

Chapter 3

Application to the Culture of Cancer Cells Spheroids

In this chapter, the bioreactor platform was used for the dynamic suspension culture of tumour cells. The experiment design was supported by means of the multiphysics model which provided comprehensive information on the

operating conditions for preliminary in vitro biological tests on human lung carcinoma cell-line.

Chapter 4

Application with human induced Pluripotent Stem Cells: Preliminary Study

In this chapter, the bioreactor platform was tested, in a feasibility study framework, for impeller-free hiPSC suspension culture. This preliminary test phase investigated the effects of the characteristic low shear stress fluid dynamic structures developing inside the bioreactor culture chamber on hiPSC suspended aggregates and free-single cell suspension.

Chapter 5

Discussion and Conclusion

In this chapter, discussion and concluding remarks regarding each section are summarized. Suggestions for future research based on the obtained results and ongoing applications are given.

References

- 1 Mason and Dunnill. Definition of Regenerative Medicine. *Regenerative Medicine*, 3, 1 (2008), 1-5.
- 2 Yu J., Vodyanik M.A., Smuga-Otto K., et al. Induced pluripotent stem cell lines derived from human somatic cells. *Science* (2007).
- 3 Takahashi K., Tanabe K., Ohnuki M. et al. Introduction of pluripotent stem cells from adult human fibroblasts by defined factors. *Cell*, 131, 5 (2007), 861-872.
- 4 Yannas, I.V. *Tissue and Organ regeneration in Adults*. Springer Publishing, 2007.
- 5 Greenwood H.L., THorsteinsdottir H., Perry G., Renihan J., Singer P.A. et al. Regenerative medicine: new opportunities for developing countries. *International Journal of Biotechnology*, 8, 1-2 (2006), 60-77.
- 6 Roco, M.C. Nanotechnology: convergence with modern biology and medicine. *Current opinion in Biotechnology*, 14, 3 (2003), 337-346.
- 7 Zweigerdt, R. Chapter - Large Scale Production of Stem Cells and their Derivatives. In *Engineering of Stem Cells*. Springer, 2009.
- 8 Rosenzweig, A.. Cardiac cell therapy: mixed results form mixed cells. *New England Journal of Medicine*, 355, 12 (2006), 1274-1277.
- 9 Schwartz, R.S. The politics and the promise of stem-cell research. *New England Journal of Medicine*, 355, 12 (2006), 1189-1191.
- 10 Kumar, A. and Starly, B. Large scale industrialized cell expansion: producing the critical raw material for biofabrication processes. *Biofabrication*, 7, 4 (2015), 044103.
- 11 Herch, Raymund E., Boos, Anja M., Quan, Yuan, Bleiziffer, Oliver, Detsch, Rainer, and et al. Cancer research by means of tissue engineering - is there a rationale? *Journal of Cellular and Molecular Medicine*, 17, 10 (2013), 1197-1206.
- 12 Hickman, John A., Graeser, Ralph, de Hoogt, Ronald, Vidic, Suzana, Brito, Catarina, Gutekunst, Matthias, and et al. Three-dimensional models of cancer for pharmacology and cancer cell biology: Capturing tumor complexity in vitro. *Biotechnology Journal*, 9 (2014), 1115-1128.

- 13 McNeisch, J. Embryonic Stem cells in drug discovery. *Nature Reviews*, 3, 1 (2004), 70-80.
- 14 Davila J.V., Cezar G.G., Thiede M., Strom S., Miki T., et. al. Use and application of stem cells in toxicology. *Toxicology Science*, 79, 2 (2004), 214-223.
- 15 Alberts, B. *Molecular Biology of the Cell*, 5th edition. Garland Science, 2008.
- 16 Stem Cell Information. In <http://stemcells.nih.gov/info/basics/Pages/Default.aspx>. 2015.
- 17 Thomson, J. A., Itzkovic-Eldor, J., Shapiro, S. S., Waknitz, M. A., Swiergel, J. J., Marshall, V. S., and et. al. Embryonic stem cell lines derived from human blastocysts. *Science*, 282, 5391 (1998), 1145-1147.
- 18 Cell, Euro Stem. Embryonic stem cell research: an ethical dilemma - WebSite. In <http://www.eurostemcell.org/factsheet/embryonic-stem-cell-research-ethical-dilemma>.
- 19 Parson, A. B. Stem Cell biotech: seeking a piece of the action. *Cell*, 132, 4 (2008), 511-513.
- 20 Murry, C. E., Field, L. J., and Menasche, P. . Cell based cardiac repair: reflections at the 10-year point. *Circulation*, 112, 20 (2005), 3174-3183.
- 21 Conrad, Claudius and Huss, Ralf. Adult stem cell lines in regenerative medicine and reconstructive surgery. *Journal of Surgical Research*, 124, 2 (2005), 201-208.
- 22 Takahashi and Yamanaka. Induction of Pluripotent Stem Cells from Mouse Embryonic and Adult Fibroblast Cultures by Defined Factors. *Cell*, 126 (August 25, 2006), 663-676.
- 23 Yamanaka. A Fresh Look at iPS Cells. *Cell*, 137 (April 03, 2009), 13-17.
- 24 Zhao, Jiang, Sun, Hou, Yang, and Gao. Induced pluripotent stem cells: origins, applications, and future perspectives. *Journal of Zhejiang University-SCIENCE B (Biomedicine & Biotechnology)*, 14 (2013), 1059-1069.
- 25 Zweigerdt, Robert, Olmer, Ruth, Singh, H., Haverich, Axel, and Martin, Ulrich. Scalable expansion of human pluripotent stem cells in suspension culture. *Nature Protocols*, 6, 5 (2011), 689-700.

- 26 Kempf, Henning, Olmer, Ruth, Kropp, Christina, Ruckert, M., Jara-Avaca, M., Robles-Diaz, D., and et al. Controlling expansion and cardiomyogenic differentiation of human pluripotent stem cells in controlled, stirred bioreactors. *Stem Cell Reports*, 3, 6 (2014), 1132-1146.
- 27 Olmer, Ruth, Lange, A., Selzer, S., Kasper, C., Haverich, Axel, Martin, Ulrich, and Zweigerdt, Robert. Suspension culture of human pluripotent stem cells in controlled, stirred bioreactors. *Tissue Engineering Part C Methods*, 18, 10 (2012), 772-784.
- 28 Hong, So Gun, Dunbar, Cynthia E., and Winkler, Thomas. Assessing the risk of genotoxicity in therapeutic development of Induced Pluripotent Stem cells. *Molecular Therapy*, 21, 2 (2013), 272-281.
- 29 Murry and Keller. Differentiation of Embryonic Stem Cells to Clinically Relevant Populations: Lessons from Embryonic Development. *Cell*, 132 (February 22, 2008).
- 30 Ebert and Svendsen. Human stem cells and drug screening: opportunities and challenges. *Nature Reviews Drug Discovery*, 9 (May 2010), 367-372.
- 31 Inoue and Yamanaka. The Use of Induced Pluripotent Stem Cells in Drug Development. *Clinical Pharmacology & Therapeutics*, 89, 5 (May 2011).
- 32 Robinton and Daley. The promise of induced pluripotent stem cells in research and therapy. *Nature*, 481 (May 13, 2012), 295-305.
- 33 Rubin, L. Stem cells and drug discovery: the beginning of a new era? *Cell*, 132, 4 (2008), 549-552.
- 34 dos Santos, F. F., Andrade, P. Z., da Silva, C. L., and Cabral, J. M. Bioreactor design for clinical-grade expansion of stem cells. *Biotechnology Journal*, 8, 6 (2013), 644-654.
- 35 Warnock, J. N. and Al-Rubeai, M. Bioreactor systems for the production of biopharmaceuticals from animal cells. *Applied Biotechnology and Biotechnology*, 45 (2006), 1-12.
- 36 Rodrigues, C. A., Fernandes, T. G., Diogo, M. M., da Silva, C. L., and Cabral, J. M. Stem cell cultivation in bioreactors. *Biotechnology Advances*, 29, 6 (2011), 815-829.
- 37 Amit, M., Chebath, J., Laessky, I., Miropolsky, Y., Peri, M., Blais, I., and et al. Suspension culture of undifferentiated human embryonic and induced pluripotent stem cells. *Stem Cell Review*, 6, 2 (2010), 248-259.

- 38 Consolo, Filippo, Bariani, Christian, Mantalaris, A., Montevecchi, Franco Maria, Redaelli, A., and Morbiducci, Umberto. Computational modelling for the optimization of a cardiogenic 3D bioprocess of encapsulated embryonic stem cells. *Biomechanics and Modelling in Mechanobiology*, 11, 1-2 (2012), 261-277.
- 39 Sen, A., Kallos, M., and Behie, L. Effects of hydrodynamicson cultures of mammalian neural stem cell aggregates in suspension bioreactors. *Industrial and Engineering Chemical Research*, 40, 23 (2001), 5350-5357.
- 40 Cameron, C. M. and Kaufman, D. S. Improved development of embryonic stem cell-derived embryoid bodies by stirred vessel cultivation. *Biotechnology and Bioengineering*, 94, 5 (2006), 938-948.
- 41 Wang, X., Wei, G., Zhao, Y., Yu, X., and Ma, X. Scalable producing bodies by rotary cell culture system and constructing engineered cardiac tissue with ES-derived cardiomyocytes in vitro. *Biotechnology Progress*, 22, 3 (2006), 811-818.
- 42 Siti-Ismail, N., Samadikuchaksaraei, A., Bishop, A. E., Polak, J. M., and Mantalaris, A. Development of a novel three-dimensional, automatable and integrated bioprocess for the differentiation of embryonic stem cells into pulmonary alveolar cells in a rotating vessel bioreactor system. *Tissue Engineering Part C Methods*, 18, 4 (2012), 263-272.
- 43 Hammond, T. G. and Hammond, J. M. Optimized suspension culture: the rotating-wall vessel. *American Journal of Physiology. Renal Physiology*, 281, 1 (2001), F12-25.
- 44 Yu, B., Yu, D., Cao, L., Zhao, X., Long, T., Liu, G., and et al. Simulated microgravity using rotary cell culture system promotes chondrogenesis of human adipose-derived mesenchymal stem cells via the p38 MAPK pathway. *Biochemical and Biophysical Research Communication*, 22;414, 2 (2011), 412-418.
- 45 Tang, Y. J., Li, H., and Hamel, J. Effects of dissolved oxygen and agitation rate in the production of heat-shock protein glycoprotein 96 by MethA tumor cell suspension culture in stirred-tank bioreactors. *Bioprocess and Biosystem Engineering*, 32 (2008), 475-484.
- 46 Rodday, B., Hirschhaeuser, F., Walenta, S., and Mueller-Klieser, W. Semiautomatic growth analysis of multicellular tumor spheroids. *Journal of Biomolecular Screening*, 16, 9 (2011), 1119-1124.

- 47 Mathers, J. P. Laboratory scaleup of cells cultures (0.5-50 liters). *Methods in Cell Biology*, 57 (1998), 219-227.
- 48 Frith, J. E., Thomson, B., and Genever, P. G. Dynamic three-dimensional culture methods enhance mesenchymal stem cell properties and increase therapeutic potential. *Tissue Engineering Part C Methods*, 16, 4 (2010), 735-749.
- 49 Martin, Ivan, Wendt, D., and Heberer, M. . The role of bioreactors in biomedical engineering. *Trends in Biotechnology*, 22, 2 (2004), 80-86.
- 50 Bilodeau, K. and Mantovani, D. Bioreactors for tissue engineering: focus on mechanical constraints. A comparative review. *Biomaterials*, 12, 8 (2006), 2367-2383.
- 51 Massai, Diana, Cerino, Giulia, Gallo , Diego, Pennella , Francesco, Deriu, Marco Antonio, Rodriguez, Andres, and et al. Bioreactors as engineering support to treat cardiac muscle and valvular disease. *Journal of Healthcare Engineering*, 4, 3 (2013), 329-370.
- 52 Frudlay, K. M., Kinney, M. A., and McDevitt, T. C. Hydrodynamic modulation of pluripotent stem cells. *Stem Cell Research Therapies*, 20;3, 6 (2012), 45.
- 53 Godara, P., McFarland, C. D., and Nordon, R. E. Design of bioreactors for mesenchymal stem cell tissue engineering. *Journal of Chemical Technology and Biotechnology*, 83 (2008), 408-420.
- 54 Bu'Lock, John and Bjorn, Kristiansen. *Basic Biotechnology*. Academic Press Inc., London, 1987.
- 55 Ismadi, M. Z., Gupta, P., Fouras, A., Verma, P., Jadhav, S., and Bellare, J. Characterization of a Spinner Flask for induced pluripotent stem cell culture application. *Plos One*, 9, 10 (2014), e106493.
- 56 Cherry, R. S. Animal cells in turbulent fluids: details of the physical stimulus and the biological response. *Biotechnology*, 22, 2 (2004), 80-86.
- 57 Teo, A., Mantalaris, A., and Mayasari, Lim M. Hydrodynamics and bioprocess considerations in designing bioreactors for cardiac tissue engineering. *Journal of regenerative medicine and Tissue Engineering*, 1, 4 (2012).
- 58 Goodwin, T. J., Prewett, T. L., Wolf, D. A., and Spaulding, G. F. Reduced shear stress: a major component in the ability of mammalian

- tissues to form three-dimensional assemblies in simulated microgravity. *Journal of Cellular Biochemistry*, 51, 3 (1993), 301-311.
- 59 Klaus, David M. Clinostats and Bioreactors. *Gravitational and Space Biology Bulletin*, 14, 2 (2001), 55-64.
- 60 Granet, C., Laroche, N., Vico, L., Alexandre, C., and Lafage-Proust, M. H. Rotating-wall vessel promising bioreactors for osteoblastic cell culture: comparison with other 3D conditions. *Journal of Medical and Biological Engineering*, 36, 4 (1998), 513-519.
- 61 Qiu, Q. Q., Ducheyne, P., and Ayyaswamy, P. S. Fabrication, characterization and evaluation of bioceramic hollow microspheres used as microcarriers for 3D bone tissue formation in rotating bioreactors. *Biomaterials*, 20, 11 (1999), 989-1001.
- 62 Turhani, D., Watzinger, E., Weissnbock, M., Cvikl, B., Thrnher, D., Wittwe, G., and et al. Analysis of cell-seeded 3-dimensional bone constructs manufactured in vitro with hydroxyapatite granules obtained from red algae. *Journal of Oral and MAXillofacial Surgery*, 63, 5 (2005), 673-681.
- 63 E, L. L., Zhao, Y. S., Guo, X. M., Wang, C. Y., Jiang, H., Li, J., and et al. Enrichment of cardiomyocytes derived form mouse embryonic stem cells. *The Journal of Heart and Lung Transplantation*, 25, 6 (2006), 664-674.
- 64 Rungarunlert, Sasitorn, Klincumhom, Nuttha, Tharasanit, Theerawat, Techakumphu, Mongkol, Pirity, Melinda K., and Dinnyes, Andras. Slow Turning Lateral Vessel bioreactor improves embryoid body formation and cardiogeninc differentiation of mouse embryonic stem cells. *Cellular Reprogramming*, 15, 5 (2013), 443-458.
- 65 Meijer, G., de Bruijn, J. D., Koole, R., and van Blitterswijk, C. A. Cell-based bone tissue engineering. *PLoS Medicine*, 4 (2007), e9.
- 66 Archer, R. and Williams, D. Why tissue engineering needs process engineering. *Nature Biotechnology*, 23 (2005), 1353-1355.
- 67 Liesbet, Geris. In vivo, In vitro, In silico: Computational tools for product and process design in Tissue Engineering. In *Computational Modelling in Tissue Engineering*. Springer-Verlag, Berlin Heidelberg, 2013.

- 68 Truscello, S., Schrooten, J., and van Oosterwyck, H. A computational tool for the upscaling of regular scaffolds during in vitro perfusion culture. *Tissue Engineering Part C Methods*, 17 (2011), 619-630.
- 69 Bannari, R., Bannari, A., Selma, B., and Proulx, P. Mass transfer and shear in an airlift bioreactor: using a mathematical model to improve reactor design performance. *Chemical Engineering*, 66 (2011), 2057-2067.
- 70 Karim, M. N., Hodge, D., and Simon, L. Data-based modelling and analysis of bioprocesses: some real experiences. *Biotechnology Progress*, 19, 5 (2003), 1591-1605.
- 71 Camacho, E. F. and Bordons, C. *Model predictive control*. Springer-Verlag, London, 1999.
- 72 Raimondi, M. T., Causin, P., Lagana, M., Zunino, P., and Sacco, R. Multiphysics computational modelling in cartilage tissue engineering. In *Computational Modeling in Tissue Engineering*. Springer-Verlag, Berlin Heidelberg, 2012.
- 73 Bjork, J. W., Safonov, Anton M., and Tranquillo, Robert T. Oxygen transport in bioreactor for engineered vascular tissues. In *Computational Modeling in Tissue Engineering*. Springer-Verlag, Berlin Heidelberg, 2012.
- 74 Consolo, F., Fiore, G. B., Truscello, S., Caronna, M., and Morbiducci, U. A computational model for the optimization of transport phenomena in a rotating hollow-fiber bioreactor for artificial liver. *Tissue Eng Part C Methods*, 15, 1 (2009), 41-55.
- 75 Wu, J., Rostami, M. R., Cadavid Olaya, D. P., and Tzanakakis, E. S. Oxygen transport and stem cell aggregation in stirred-suspension bioreactor cultures. *PLoS ONE*, 9, 7 (2014), e102486.
- 76 Cioffi, M., Küffer, J., Ströbel, S., Dubini, G., Martin, I., and Wendt, D. Computational evaluation of oxygen and shear stress distributions in 3D perfusion culture systems: Macro-scale and micro-scale structured model. *Journal of Biomechanics*, 41 (208), 2918-2925.
- 77 Isu, Giuseppe, Massai, Diana, Cerino, Giulia, Bignardi, Cristina, Audenino, Alberto, and Morbiducci, Umberto. A novel perfusion Bioreactor for 3D cell culture in Microgravity Conditions. In *SBC 2013 (Sunriver 2013)*.

- 78 Kemp, P. History of regenerative medicine: looking backwards to move forwards. *Regenerative Medicine*, 1, 5 (2006), 653-669.
- 79 Maherali and Hochedlinger. Guidelines and Techniques for the Generation of Induced Pluripotent Stem Cells. *Cell* (December 4, 2008), 595-605.
- 80 Atala A., Bauer S.B., Soker S., Yoo J.J., Retik A.B. Tissue-engineered autologous bladders for patients needing cytoplasty. *Lancet*, 367, 9518 (2006), 1241-1246.

PART I

Chapter 2

Versatile Bioreactor for Reproducible and Scalable Dynamic Suspension

2.1 Introduction

As previously debated in Chapter 1, suspension culture has recently been employed for the realization of scalable cell expansion and long-term cell viability performance [1,2,3,4]. Suspension culture can be obtained by means of bioreactors. As a matter of fact, bioreactors have been demonstrated to be devices capable of providing automated, repeatable, and scalable cell expansion [2,3,5], spheroid aggregation formation [6,7], cellular differentiation and tissue maturation [8], and 3D cancer models [9].

Nevertheless, most of these bioreactors still suffer from critical issues, limiting the upscaling and the standardization of the expansion bioprocesses. Concerning stirred bioreactors, their performance can be affected by (1) collisions of the cells with the impeller and (2) the onset of turbulent flow, that both can induce non-physiological mechanical and hydrodynamic-shear stresses on the cells and lead to cell damage. Moreover, these unfavourable

conditions can affect cell growth rate and metabolism, interfere with stem cell pluripotency, and limit efficiency and reproducibility of the culture process [5,10,11,12,13]. Rotating bioreactors generate a low-shear stress culture environment, allowing to partially overcome the limitations of stirred tank devices. However, the complexity of the technological solutions adopted for rotation make these devices not easily scalable and unsuitable for continuous medium replacement and real-time monitoring [10].

In this chapter, a versatile bioreactor suitable for tuneable (from low to moderate) shear dynamic suspension cell culture is presented. Adopting simple technological solutions, and avoiding any moving or rotating components, the herein proposed bioreactor permits cell suspension by assuring a well-mixed laminar flow regime, resulting in homogenous oxygen and nutrient transport, as well as a wide range of spatially uniform shear stress conditions. The peculiar geometric features of the bioreactor chamber were previously optimized (patented, [14]) to assure the formation of buoyant vortices within the culture environment, by means of the sole culture medium perfusion. In order to go beyond the typical experimental trial-and-error approach and to reach a deeper understanding of the fluid dynamics developing inside the culture environment, the optimization phase of the device was supported by *in silico* multiphysics modelling [15], which provided a comprehensive analysis of the operating principles of the bioreactor, and permitted the optimizations of the check valve system.

Moreover, the optimization phase of the original version concerned the implementation of a monitoring system: the bioreactor platform was equipped with specific sensors, upstream and downstream the bioreactor chamber, in

order to provide real-time information about the metabolic behaviour of cultured cells. The measured signals were acquired by means of an in house-made acquisition and display software.

2.2 Bioreactor Platform Description

2.2.1 Design Requirements

The bioreactor was designed and developed in order to guarantee suspension conditions with enhanced mass transfer (see Appendix I – Oxygen Transport Computational Model) with tuneable low shear stress. In fact, the design of the device was driven by two main requirements:

- to provide dynamic suspension culture with proper mixing;
- to guarantee a tuneable ultralow-to-moderate shear stress culture environment, adjustable on the basis of culture requirements by simply modifying the bioreactor operating conditions.

The bioreactor was designed to assure full compatibility with good manufacturing practise (GMP) standards, satisfying the following requirements:

- cytocompatibility and corrosion-resistance of all materials in contact with the culture medium;
- ease of sterilization and sterility maintenance;
- ease of use, regarding the ease of assembly under sterile conditions for non-trained users;
- small dimensions, suitable to fit inside standard culture incubators;

- no medium stagnation.

2.2.2 Bioreactor Platform Functioning Principle

The functioning principle of the bioreactor platform is based on the continuous recirculation of the culture medium inside the culture chamber under laminar flow regime, obtained through the modulation of the peristaltic pump-imposed flow rate, in order to produce from ultralow to moderate shear stress dynamic suspension conditions (flow rate working range from 5 to 120 mL/min). In detail, the medium flows through the check valve, driven by the peristaltic pump, and pervades the culture chamber. Successively, the medium passes through the filter and flows out from the lid, moving back to the reservoir in a continuous closed-loop process (Figure 2.1C). The formation of buoyant vortices inside the culture chamber allows the dynamic suspension of the cultured cells/constructs.

2.2.3 Original Architectural Design and Constitutive Elements

As shown in Figure 2.1, the bioreactor combines peculiar geometric features with a continuous recirculation of the culture medium, assured by a closed-loop perfusion circuit, avoiding the use of impellers and/or rotating components. The key constitutive elements of the entire bioreactor platform are (Figure 2.1C):

- a transparent, sealable and sterile culture chamber where cells (free or microcarrier-anchored cells) are suspended in the culture medium during the experiments;

- a closed loop recirculation circuit constituted by a medium reservoir, a peristaltic pump, and oxygen permeable tubes (oxygenation module, further described in Appendix I).

Culture Chamber

The bioreactor culture chamber (Figure 2.1B, external dimensions of 95 mm x 70 mm x 70 mm) consists of: an AISI 316L base; a polycarbonate culture chamber for housing the cells/constructs (priming volume = 75 mL); a polycarbonate lid. The internal wall curvature and shape of the culture chamber were designed and optimized for the generation of toroidal buoyant vortices (axial-symmetry of the culture chamber) for specimen suspension (as detailed in the following). It has been manufactured by material removal by a computer numerical controlled (CNC) milling machine starting from a polycarbonate bar. All the parts of the chamber in contact with the culture medium were designed and realized with round edges, avoiding discontinuities, stagnation points, fissures, interstices, and holes, considered principal spots of microbial contamination.

Suspended cells/constructs are confined inside the culture chamber by means of the presence of (1) an AISI 316L unidirectional check valve (which prevents backflow and guarantees a symmetric flow inlet), and (2) a culture medium-permeable filter (Durapore[®], MerckMillipore, Germany), which prevents accidental outputs of cells.

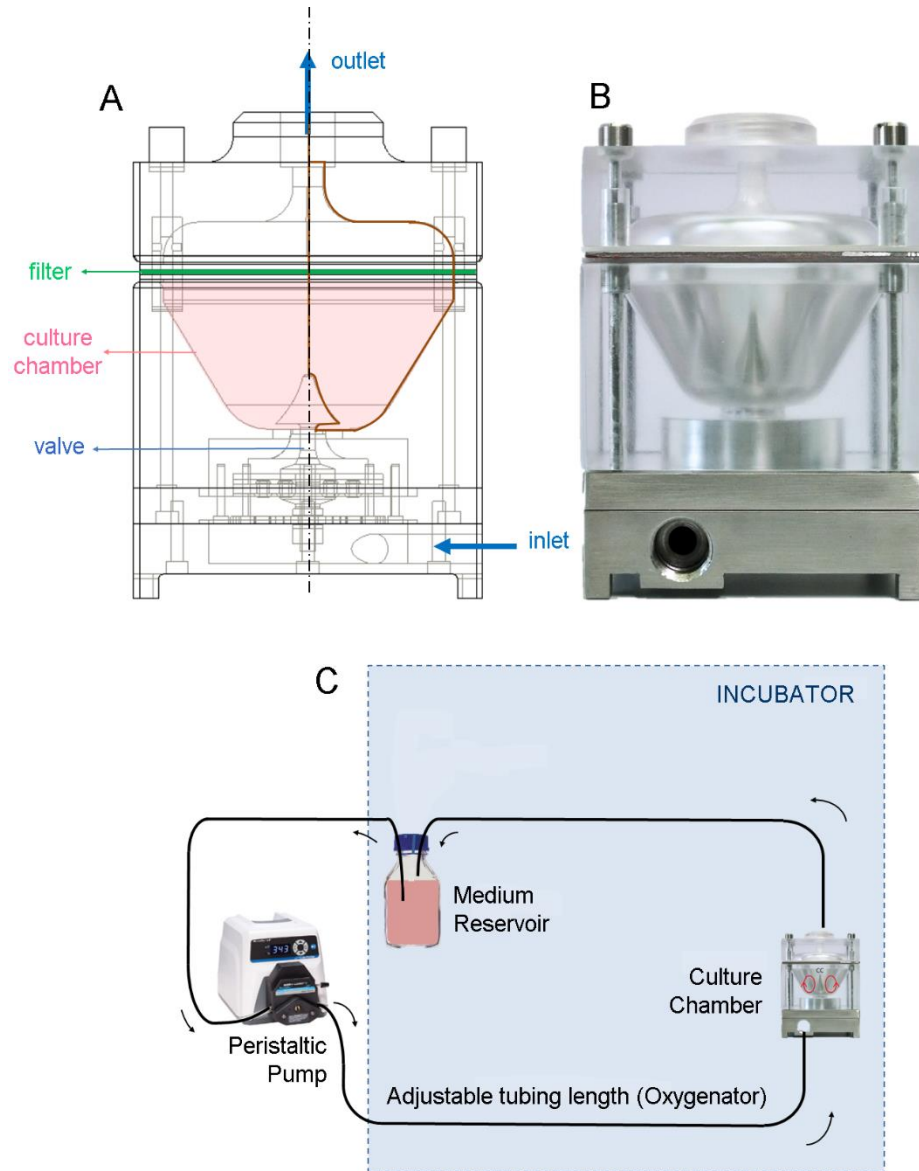


Figure 2.1: (A) Schematic draw of the bioreactor showing its internal components and its axial symmetry (red lines). (B) Picture of the bioreactor. (C) Schematic representation of the set-up of the bioreactor connected to the closed loop perfusion circuit.

Check Valve (original configuration)

The check valve, in its original configuration (the optimized version will be described in detail paragraph 2.3.3), was designed to guarantee the uni-

directionality of the fluid, opening and closing when the pump is activated or switched off, respectively. Taking advantage of the technical drawing of the check valve system shown in Figure 2.2, all the components of the valvular system are made in AISI 316L, excepted the silicone membrane. The culture medium flow produces an overpressure in the valve chamber upstream the silicone membrane, respect to the downstream chamber. The culture medium flows through the check valve only when the trans-valvular pressure drop overcomes the cracking pressure of the valve and produces the deformation of the silicone membrane. This silicone membrane is provided in different thickness (2 or 3 mm) and with a different number of holes (up to six) in order to modulate the proper operating trans-valvular pressure necessary to open the check valve.

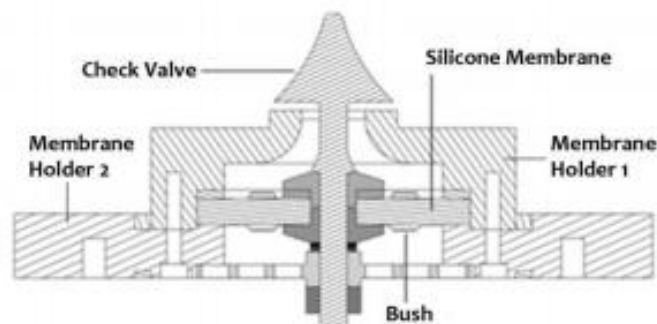


Figure 2.2: Check Valve (original configuration). Technical drawing highlighting its constitutive elements.

Filter System

The poly-vinylidene fluoride filter (PVDF - Durapore^{ff}, MerckMillipore, Germany) was designed with the aim to prevent accidental outputs of cells or constructs during the recirculation of the culture medium (80% porosity and average pore diameter of 5 μm). To ensure rigidity, correct positioning,

and perfect sealing to the filter system, the PVDF membrane is used with three silicone washers and an AISI 316L stainless steel grate. Figure 2.3 illustrates the constitutive components of the filtration system and the assembling procedure to be done under laminar-flow hood.

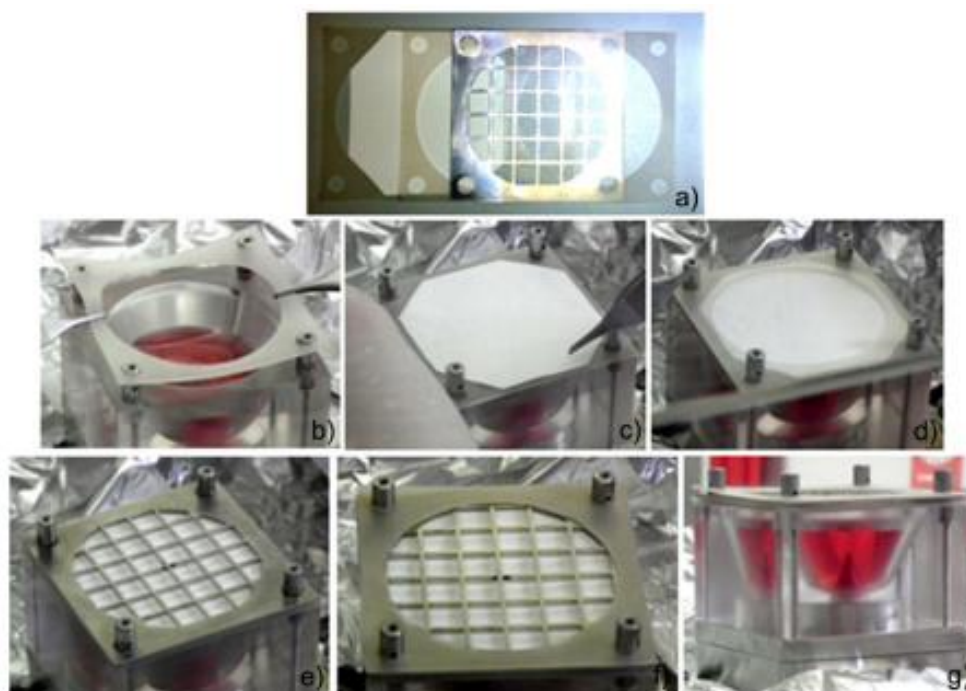


Figure 2.3: Bioreactor filter setup. a) Filter Components, b) insertion of the first silicone washer, c) insertion and positioning of the PVDF filter, d) insertion of the second silicone washer, e) insertion of the AISI 316L stainless steel grate, f) insertion of the third silicone washer, g) completed filter setup.

Closed loop Recirculation Circuit

The bioreactor is part of a closed-loop perfusion circuit for the recirculation of oxygenated culture medium (Figure 2.1C). Such perfusion circuit is composed of a medium reservoir, oxygen-permeable tubes (silicone, peroxyde-cured) with quick-disconnect couplings, and a peristaltic pump (Masterflex

L/S[®], Cole-Parmer, IL, USA), for a total working volume of approximately 200 mL.

In detail, the peristaltic pump was chosen to assure the technical features summarized in Table 2.1.

Table 2.1: Technical features of Masterflex L/S[#] RX-07551-00 pump.

Flow Rate Range	0.006 - 3400 mL/min
VAC	90/260
rpm	0.1 - 600
Speed Control	Precision digital
Operating Temperature	0-40°C
Drive Dimensions	25.4 cm x 21.6 cm x 21.6 cm
Motor	75 W, 1/10 hp

The hydraulic couplings (Figure 2.4) are capable of being quickly connected and disconnected, maintaining sealing and sterility (Table 2.2).



Figure 2.4: Cole-Parmer quick-disconnect couplings.

Table 2.2: Technical features of Cole-Parmer quick-disconnect couplings.

Body Material	acetal
Seal Material	ethylene propylene rubber (EPR)
Spring and latch Material	AISI 316 stainless steel
Max Vacuum	711 mmHg
Max Temperature	71°C
Max pressure at 21 °C	6.8 atm

To guarantee the adequate supply of oxygen within the culture chamber, the perfusion circuit was sized using an analytical oxygen mass balance model in accordance with Orr et al. [16] (largely described in Appendix I). The permeability properties to CO₂, H₂, O₂, and N₂ used for the tubing sizing were provided by the supplier and are summarized in Table 2.3.

Table 2.3: Permeability properties of the platinum-cured silicone pump tubing.

	Permeability x 10¹¹ [cm²/mmHg·s]
CO₂	0.020
H₂	6.58
O₂	7.96
N₂	2.76

During the experimental phase, the culture chamber, the fresh medium reservoir, and a portion of the oxygen-permeable tubes are positioned within the incubator. If the incubator settings are fixed on 95% of humidity, the peristaltic pump is positioned outside the incubator to protect the electrical circuitry from the high levels of humidity, exposing a short portion of the oxygen-permeable tubes to the external environment (Figure 2.5A). If the incubator is completely dedicated to the bioreactor platform, it is possible to set up the incubator culture environment without humidity and place the

entire recirculation circuit, peristaltic pump included, inside the incubator (Figure 2.5B).

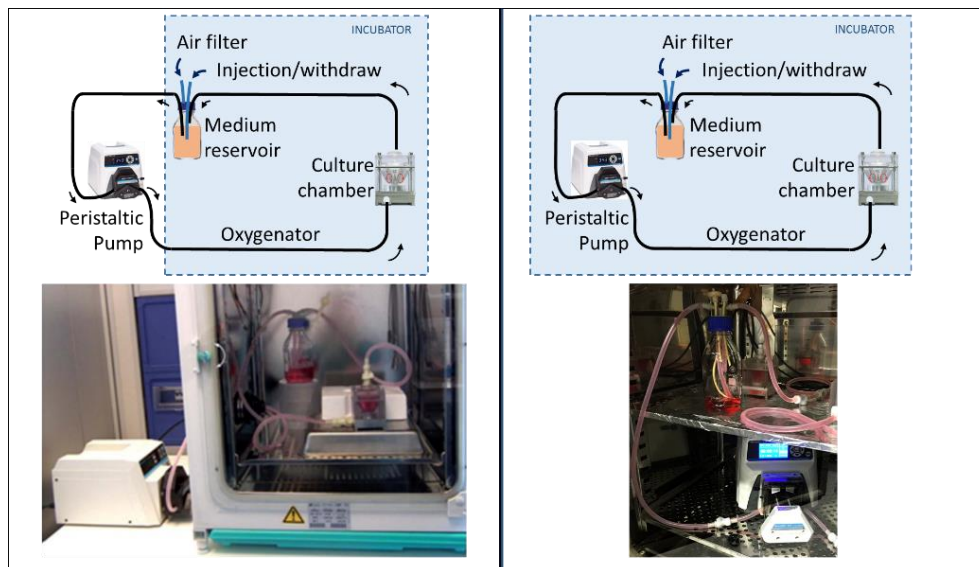


Figure 2.5: Bioreactor setup within the incubator in two possible configurations. Schematic drawings (top) and pictures of the real working system (bottom). The peristaltic pump can be put outside the culture incubator in case of high humidity (left panel) or can be positioned inside the incubator in absence of humidity (right panel).

2.3 In Silico Multiphysics Model-Based Design Optimization

A computational multiphysics approach supported the design and the optimization phases of the device, allowing the identification of (1) the optimal geometry of the culture chamber, and (2) the operating conditions for dynamic suspension cell culture. A massive number of simulations was performed varying cell/construct dimensions (in terms of their diameter) and highly dilute cell inoculation densities, in order to study the sensitivity of the fluid flow within the chamber volume to these culture parameters.

Technically, three different computational studies were accomplished. The first approach was oriented to the identification and definition of the typical fluid dynamics structures generated inside the bioreactor culture chamber varying flow rate conditions: multiphysics simulations were carried out taking into account the concomitant presence and mutual interaction of culture medium and suspended cells. The second was directed to the *in silico* study of alternative culture protocols (*pulsed protocols*) by means of the same multiphysics simulation cited above. This multiphysics simulations gave the possibility to devise *in silico* protocols to be used as user's guidelines for the setup of the bioreactor platform. The third computational approach was intended to the improvement of the check valve performance. After having conceived and designed an innovative kinematic mechanism for the check valve, single phase three-dimensional simulations were carried out to optimize its geometry and assess its efficiency at different flow rates.

2.3.1 Multiphysics Modelling for Fluid Dynamics

Characterization

Methods

Taking advantage of the axial-symmetry of the device (Figure 2.6A), a set of axisymmetric time-dependent numerical simulations was carried out using a customized finite volume technique-based commercial software (FLUENT, ANSYS Inc., PA, USA). The fluid domain was discretized using ICEM CFD software (ANSYS Inc., PA, USA). A mesh cardinality equal to 6.5×10^3 quadrilateral cells was considered. As in previous studies [3,17], the concomitant presence of culture medium and cells was modelled using the Eulerian-

Eulerian Multiphase Model, which allows mixtures of multiple separated yet interacting phases of a continuum to be described.

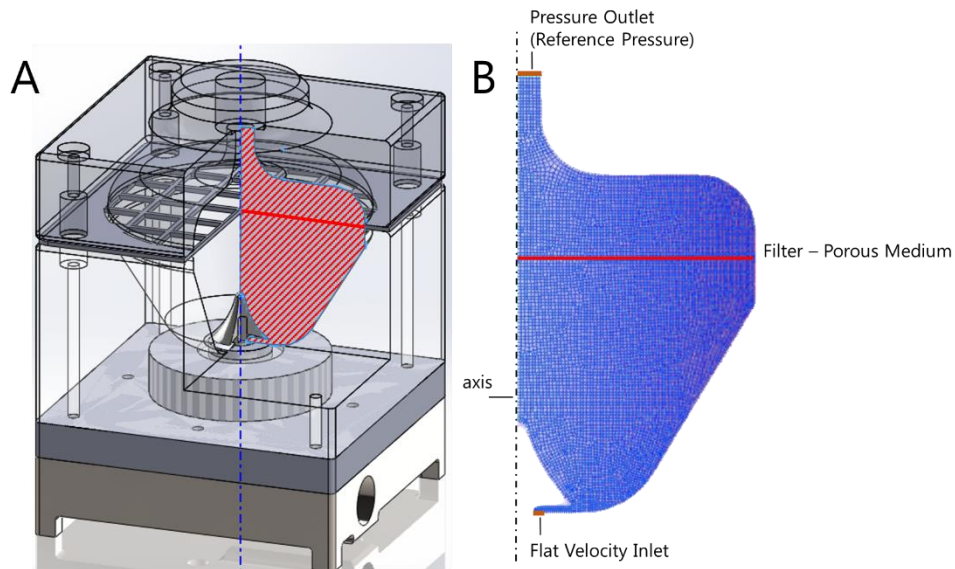


Figure 2.6:3D model of the bioreactor chamber with emphasis on its axial-symmetry (A), axial-symmetric computational domain with boundary conditions (B).

In this model, for each phase the governing equations of motion, the Navier–Stokes equations, were solved by the numerical solver. Subscript q refers to the q -th phase (i.e. primary phase = culture medium and secondary phase = cells/constructs). By neglecting the mass transfer between the two phases, Navier–Stokes equations can be written in the form of eq. 1 and eq. 2.

Continuity equation:

$$\frac{\partial}{\partial t}(VF_q \rho_q) + \nabla \cdot (VF_q \rho_q \vec{v}_q) = 0 \quad \text{eq. 1}$$

Conservation of momentum

$$\begin{aligned} \frac{\partial}{\partial t}(VF_q \rho_q \vec{v}_q) + \nabla \cdot (VF_q \rho_q \vec{v}_q \vec{v}_q) = & -VF_q \nabla P + \nabla \cdot \overline{\overline{\tau}}_q + VF_q \rho_q \vec{g} + \\ & + \sum_{p=1}^n (\vec{R}_{pq}) + (\vec{F}_q + \vec{F}_{lift,q} + \vec{F}_{vm,q}) \end{aligned} \quad \text{eq. 2}$$

where VF_q is the volume fraction, ρ_q the density, and \vec{v}_q is the velocity of the q -th phase. In eq. 2, P is the pressure shared by the two phases, $\overline{\overline{\tau}}_p$ is the stress-strain vector, \vec{F}_q is an external body force, $\vec{F}_{lift,q}$ is a lift force, $\vec{F}_{vm,q}$ is the virtual mass force ($\vec{F}_{lift,q}$ and $\vec{F}_{vm,q}$ were neglected in this model). \vec{R}_{pq} is the interaction force between phases, i.e. the interaction between q -th phase and the generic p -th phase. Within the bioreactor culture chamber, culture medium (primary phase) exerts a drag force to the suspended cells/constructs (particles, p -th phase). For granular secondary phase (such as cellular suspensions), the drag force is expressed as a function of relative cell velocity ($\vec{v}_p - \vec{v}_q$) (eq. 3).

$$\vec{R}_{pq} = K_{pq} (\vec{v}_p - \vec{v}_q) \quad \text{eq. 3}$$

where K_{pq} is a function of Stokes number, Reynolds number (Re), and phase VF, according to Gidaspow and colleagues model [18].

Regarding the calculation of flow-induced mechanical stress, shear stress magnitude was mathematically computed according to eq. 4 :

$$|\tau| = \mu \left| \dot{\gamma} \right| \quad \text{eq. 4}$$

where $\dot{\gamma}$ is the shear rate, related to the second invariant of the deformation tensor $\overline{\overline{D}}$ (eq. 5)

$$\dot{\gamma} = \sqrt{\frac{1}{2} \overline{\overline{D}} \cdot \overline{\overline{D}}} \quad \text{eq. 5}$$

In 3D Cartesian coordinates the shear rate $\dot{\gamma}$ is defined as eq. 6:

$$\dot{\gamma} = \sqrt{\left[\frac{\partial u}{\partial x} \left(\frac{\partial u}{\partial x} + \frac{\partial u}{\partial x} \right) + \frac{\partial u}{\partial y} \left(\frac{\partial u}{\partial y} + \frac{\partial v}{\partial x} \right) + \frac{\partial u}{\partial z} \left(\frac{\partial u}{\partial z} + \frac{\partial w}{\partial x} \right) \right] + \left[\frac{\partial v}{\partial x} \left(\frac{\partial v}{\partial x} + \frac{\partial u}{\partial y} \right) + \frac{\partial v}{\partial y} \left(\frac{\partial v}{\partial y} + \frac{\partial v}{\partial y} \right) + \frac{\partial v}{\partial z} \left(\frac{\partial v}{\partial z} + \frac{\partial w}{\partial y} \right) \right] + \left[\frac{\partial w}{\partial x} \left(\frac{\partial w}{\partial x} + \frac{\partial u}{\partial z} \right) + \frac{\partial w}{\partial y} \left(\frac{\partial w}{\partial y} + \frac{\partial v}{\partial z} \right) + \frac{\partial w}{\partial z} \left(\frac{\partial w}{\partial z} + \frac{\partial w}{\partial z} \right) \right]} \quad \text{eq. 6}$$

where u , v , w are the three Cartesian components of the velocity vector \vec{v}_q .

The culture medium, considered as the primary phase, was assumed to be Newtonian with physical properties (dynamic viscosity = 1×10^{-3} Pa·s, density = 1000 kg/m^3) of culture media typically used in cell culture applications [3]. Suspended cells, considered as the secondary suspended phase, were modelled as non-deformable spherical beads, with a density equal to 1070 kg/m^3

[19] and an average diameter ranging from 10 to 100 μm (i.e. the typical dimension range going from single cell to more complex cell aggregates). Simulations were carried out considering always highly dilute suspension cultures (Stokes numbers greatly lower than 1, VF lower than 1%). In detail, Stokes numbers within the bioreactor culture chamber were calculated for every simulated cell/construct dimensions (10, 25, 50, 100 μm), considering the lowest culture medium velocity inside the chamber when a flow rate of 5 mL/min is imposed (the lowest flow rate in the bioreactor platform working range). Table 2.4 reports the calculated Stokes numbers, which are always largely lower than 1.

Table 2.4: Stokes numbers calculated for different cell/aggregate diameter values.

Diameter (μm)	Stokes Number ($\times 10^{-5}$)
10	1.4
25	8.4
50	33.8
100	135.2

With the hypothesis of high dilution, variations in initial VF do not affect markedly the primary phase flow. In such condition, with the aim to characterize the flow field inside the chamber for different characteristic suspended particle diameter, VF was kept constant varying only cell/construct dimensions.

The presence of the filter was modelled as a porous medium characterized by a value of Darcy hydraulic resistance equal to $96 \times 10^4 \text{ m}^{-2}$ for the culture medium and setting the maximum hydraulic resistance accepted by the solver ($1 \times 10^{20} \text{ m}^{-2}$) for the cells, being the filter impermeable to them. Cell/construct

inoculation was assumed to be uniform in the lower region of the culture chamber. Indeed, the initial VF occupied by the cells was set to be uniform in the lower vessel region (10 mL).

The maximum packing limit was set to 63%, i.e., the packing limit for regularly packed non-deformable spherical beads [3]. Simulations were extended over flow rate values in the range 5 - 120 mL/min, with a simulated culture time equal to 60 mins, which was considered sufficient to fully describe the dynamics of the medium inside the culture chamber. The phase-coupled SIMPLE scheme was used for the pressure-velocity coupling. The Second order upwind and the QUICK formulation were used for the spatial discretization of the momentum and the secondary phase transport, respectively. To solve the equation the phase-coupled SIMPLE scheme was used for the pressure-velocity coupling. The second order upwind and the QUICK formulation were used for the spatial discretization of the momentum and the secondary phase transport, respectively. A time step equal to 0.002 s was set in order to reach the numerical stability. Absolute convergence criterion was applied and convergence was considered achieved for relative residuals below 10^{-6} for Navier-Stokes equations and 10^{-7} for volume fraction residuals. At the inlet the flow rate was imposed by means of a flat velocity profile, and at the outlet a null pressure gauge condition (pressure outlet condition) was set (Figure 2.6). No-slip condition was applied at the walls.

Results and Discussion

The multiphysics simulation setting herein proposed allowed to characterize the flow field inside the culture chamber. Figure 2.7 depicts, in a diagrammatic representation, the typical medium flow structures establishing

inside the bioreactor culture chamber, as a result of the mutual interaction between the medium (primary phase) and the cells/constructs (secondary dispersed particulate phase). In detail, the modulation of flow rate in two different intervals (from 5 to 20 mL/min and from 20 to 120 mL/min) produces different characteristic fluid dynamic structures qualitatively repeated (varying the flow rate inside each range may result in similar flow structures, but with different extent). As shown in Figure 2.7A and 2.7C, in case of flow rate values lower than 20 mL/min, the medium streaming inside the bioreactor culture chamber has not sufficient energy to interact markedly with the side wall of the culture chamber. The interaction between the culture medium stream and the suspended cells/constructs leads to the formation of a dynamic big buoyant vortex located far from the wall of the chamber. This buoyant vortex is surrounded by smaller vortical structures located closer to the wall, which may assure cultured cell/construct suspension and increased mixing and transport inside the culture chamber. Shear stress measured in such flow rate range are typically lower than 1 mPa, generating an *ultralow* shear stress condition (Figure 2.8A). If the flow rate is increased beyond 20 mL/min, the culture medium stream entering the bioreactor culture chamber is attracted to the nearby wall (Coanda effect [20]) and, taking advantage of the peculiar wall curvature, a separation region occurs far from the bottom wall of the chamber Figure 2.7B and 2.7D.

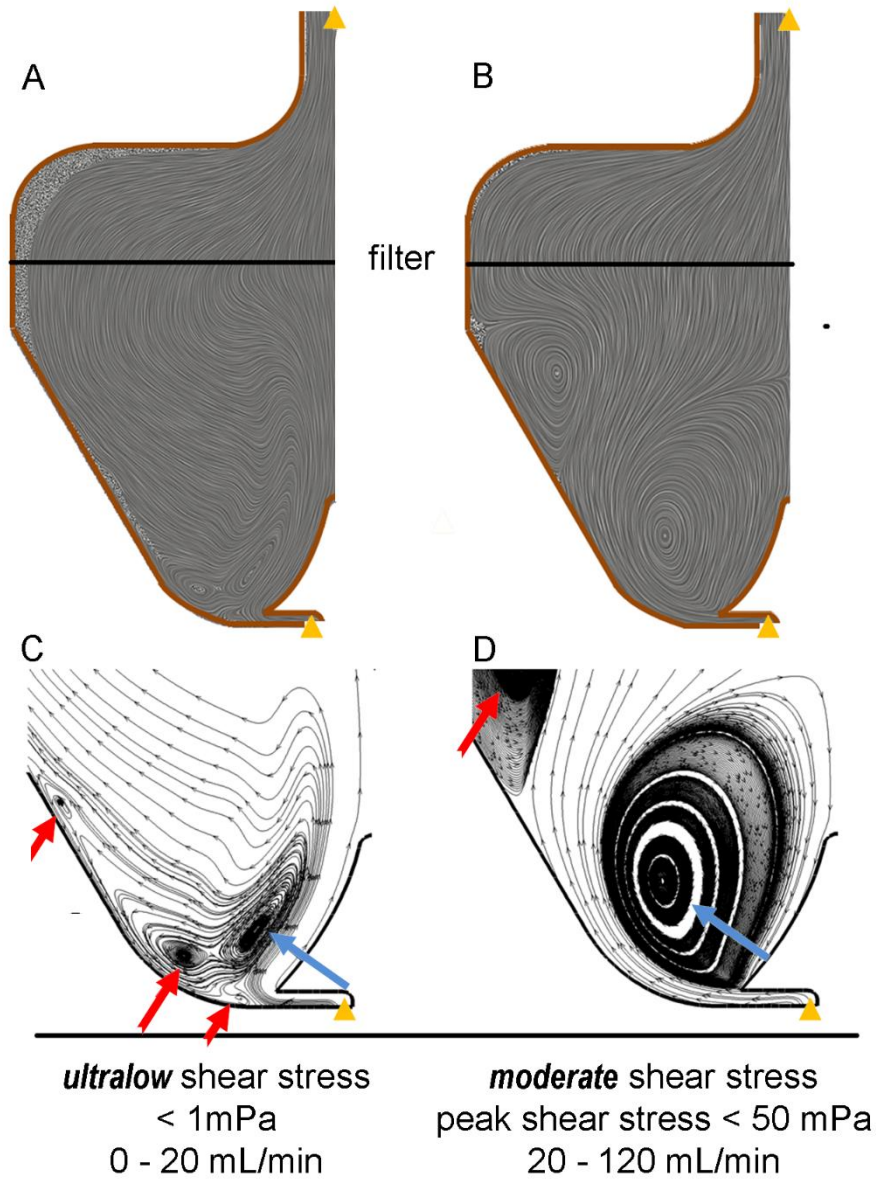


Figure 2.7: Flow field visualization of the mutual interaction between the medium (primary phase) and the cells/constructs (dispersed phase) within the culture chamber for ultralow (A and C) and moderate (B and D) shear stress conditions. Flow field is depicted using both linear integral convolution lines (A and B), and a classical streamline representation (C and D). Red arrows point to the smaller vortical structures, while blue arrows indicate the bigger buoyant vortices.

As a result, a large buoyant vortex of cell/construct suspension is generated. Near the outer wall, a smaller vortex develops, playing a beneficial role, and enhancing mixing and floating construct suspension. Adopting this flow rate range, shear stress levels increase, producing a *moderate* shear stress environment. However, Figure 2.8B-2.8E shows shear stress distributions calculated for four different flow rates inside this *moderate* shear stress range, i.e. 30, 50, 70, 120 mL/min. It can be observed that the distributions are all markedly skewed right and characterized by mean and mode values consistently low. Indeed, mean shear stress value inside the culture chamber vary from approximately 2 to 7 mPa (for 30 and 120 mL/min, respectively), while mode values are lower than 1 mPa for each reported flow rate. The tuneable shear stress values obtained inside this bioreactor chamber are one order of magnitude lower than shear stress values developing within commercial spinner flask bioreactors. In such bioreactors, imposing agitation rates ranging from 15 to 50 rpm, the reached mean shear stress values are from 20 to 120 mPa (with peak values reaching 200 mPa) [21]. Contemporarily, shear stress values generated by the herein proposed bioreactor platform are orders of magnitude lower than the reference shear stress value (250 mPa) considered critical for sensitive cells, such as embryonic stem cells or neonatal rat cardiomyocytes [12]. Furthermore, the fluid dynamics described within the bioreactor culture chamber has a beneficial role on mixing and transport of oxygen and nutrients (oxygen transport model in Appendix I).

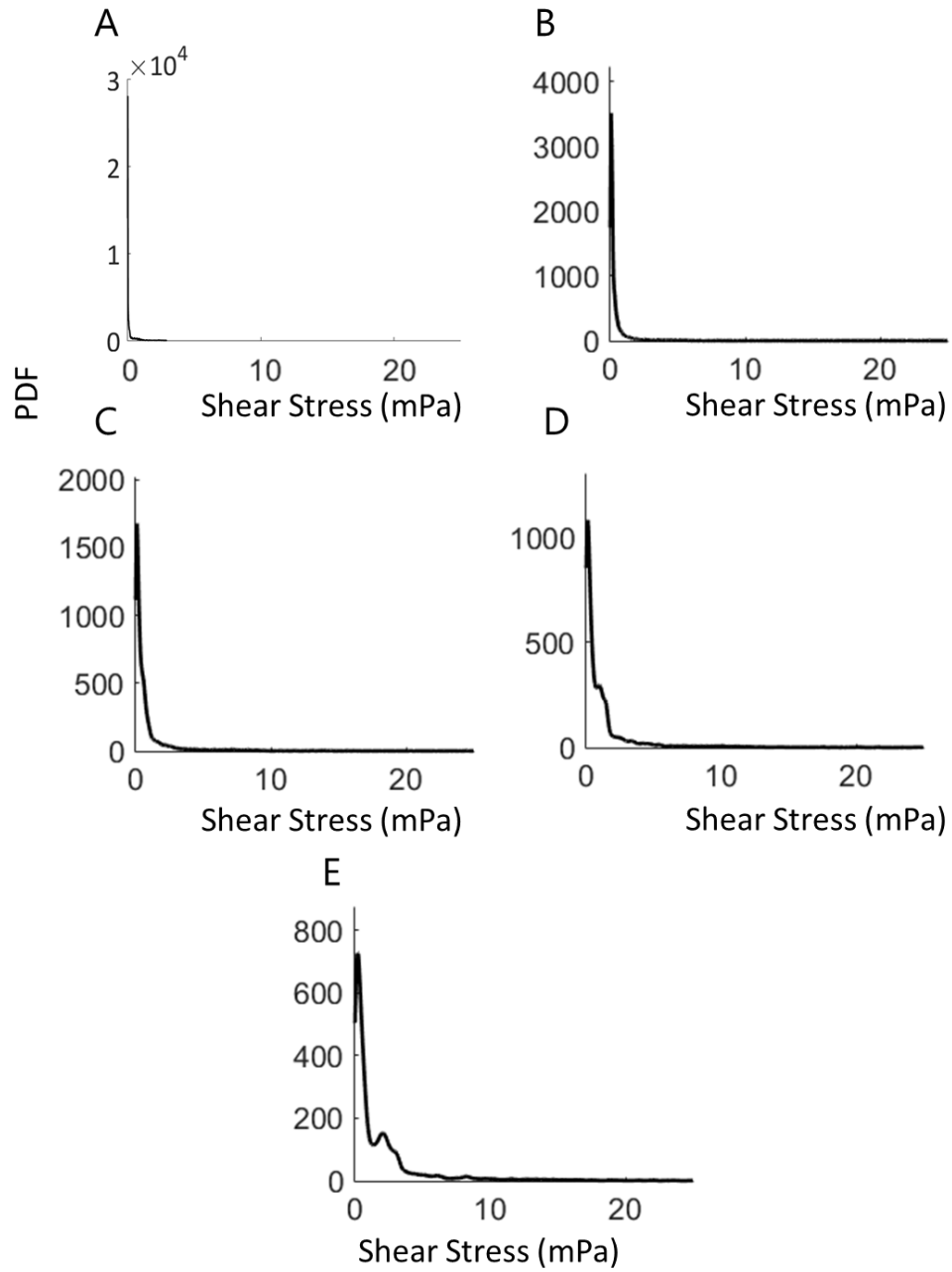


Figure 2.8: PDF of shear stress values inside the bioreactor culture chamber varying the imposed flow rate. (A) 5, (B) 30, (C) 50, (D) 70, and (E) 100 mL/min.

Summarizing, this multiphysics model results allowed to define two main flow conditions in culturing cells/constructs: (1) *ultralow* shear stress condition, obtained working with flow rates below 20 mL/min, and (2) *moderate* shear stress condition, established in flow rate range from 30 to 120 mL/min. Moreover, modelling allowed to optimize the design of the bioreactor platform, in terms of performance for the establishment of dynamic suspension of biological specimens at low shear stress levels.

Some limitations could weaken the presented multiphysics numerical model. A main limitation is that aggregation and disaggregation of the cultured cells/constructs are not considered in the model, since the biological sample size was assumed to be always equal to the initial cell dimension. The primary interest of this model was to assess the fluid dynamics inside the culture chamber at the very early stage of the culture process, in order to ascertain cell/constructs suspension. Therefore, since aggregation, disaggregation, and proliferation phenomena have typical characteristic time of days, they were neglected in the simulations. Another possible limitation is given by the assumption of non-deformable, spheroid suspended cell/constructs. Inhomogeneity of particle size and shape could modify the outcome of the simulation in terms of cell VF distribution inside the culture chamber. In the context of the fluid dynamic characterization proposed, and under high dilution conditions, the effect of irregularly-shaped cell/constructs on culture medium flow field is negligible.

Although the possible limitations could undermine the findings of this study, the information obtained by means of this computational setup demonstrates the potential offered by multiphysics simulation as a tool during the

design phase of a bioreactor platform. The further insight on the fluid dynamics establishing inside the bioreactor culture chamber can be helpful for the formulation of experimental frameworks with a more systematic approach (Chapter 3 – Application to the culture of Cancer Cell Spheroids).

2.3.2 Multiphysics Modelling for in silico Protocol Development

In order to go beyond the experimental trial-and-error approach, the multiphysics model proposed in the previous paragraph (2.3.1) was used to study and develop an alternative functioning mode of the bioreactor platform. As previously explained in paragraph 2.2.2 , the standard functioning principle of the bioreactor platform is the continuous recirculation of the culture medium inside the culture chamber. An alternative functioning mode might be the imposition of a pulsed flow rate, alternating time intervals during which the pump is set to run, with time intervals in which the pump is momentarily stopped. The rationale beyond this alternative functioning mode is the possibility to develop (in silico) a protocol capable of alternating both flow-driven particle suspension and particle free-fall, inside the bioreactor culture chamber (specifically oriented to mammalian cell and aggregate suspension culture). Indeed, when a flow rate is imposed by means of the peristaltic pump, particles inside the bioreactor chamber are dragged and transported in the same conditions described in paragraph 2.3.1 . When the pump is momentarily stopped, suspended particles will experience a free-fall condition, undergoing a null acceleration state. Moreover, this pulsation produces an intermittent moderate shear stress stimulation which, in free-cell suspension culture applications, can be useful in the modulation of cell aggregate dimension without continuously exposing cells to shear stress.

This study was intended to give a tool to estimate the applicability of this protocol of use, with the aim to determine the flow rate *pulsation* shape and frequency, providing a set of operational graphs as guidelines for its future preliminary experimental applications.

Methods

A massive number of simulations was carried out with the same numerical setup proposed in paragraph 2.3.1 . Summarizing, axial-symmetric time-dependant numerical simulations were carried out using a customized finite volume technique-based commercial software (FLUENT, ANSYS Inc., PA, USA). The fluid domain was discretized with 6.5×10^3 quadrilateral cells and the Eulerian-Eulerian multiphase model was implemented to simulate the concomitant presence of culture medium and suspended particles (general way to refer to either cells, or aggregate, or constructs). As in the previous setup (paragraph 2.3.1), highly dilute suspension cultures (Stokes numbers greatly lower than 1, VF lower than 1%) were considered, imposing a VF ranging between $5.4 \times 10^{-3}\%$ and $2.5 \times 10^{-2}\%$. This assumption allows to consider cells as non-deformable spheres transported by the culture medium, without markedly modifying the flow field. Due to high dilution condition, the free-fall phase particle motion, occurring when the pump is momentarily stopped, can be simplified by the formulation of the force balance acting on a single sphere in free-fall. The free-fall terminal velocity \vec{v}_{ff} can be obtained expressing the dynamic balance among Stokes drag force (\vec{F}_d), Archimedes buoyancy force (\vec{F}_b), and particle weight force (\vec{W}) (Figure 2.9).

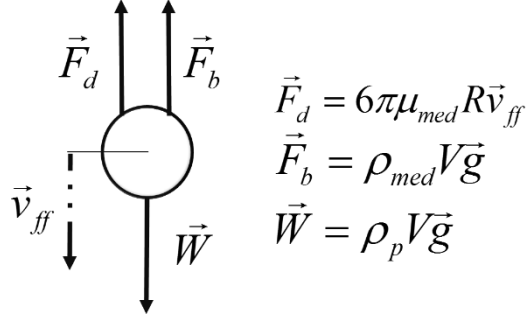


Figure 2.9: Free-body diagram of forces representing the dynamic balance between Stokes drag force, weight force, and Archimedes buoyancy force when a spherical particle reaches the terminal velocity while being in free-fall.

Through the explicitation of the force balance, it is possible to obtain the expression of the terminal velocity \vec{v}_{ff} (eq. 7) as

$$\vec{v}_{ff} = \frac{2(\rho_p - \rho_{med})R^2}{9\mu_{med}} \vec{g} \quad \text{eq. 7}$$

where ρ_p and ρ_{med} are particle and medium density, respectively; μ_{med} is the medium dynamic viscosity; and R is the particle diameter.

In order to characterize the pulsed functioning of the bioreactor platform, the multiphysics model was used to define the pulsed flow rate waveform duration and its duty-cycle. For a square waveform (Figure 2.10B), it is possible to obtain different duty-cycles, modifying the ratio between the time interval when the pump imposes a non-null flow rate (T_{on}), and the time in which the pump is stopped (T_{off}). The duration and duty-cycle of the waveform depends on T_{on} . In fact, according to the value of T_{on} , the flow entering the culture chamber lifts suspended particle cloud to a different height respect to its initial height (Figure 2.10A). The height attained by the particle cloud

was computed by means of the multiphysics model, imposing different durations of non-null flow rate T_{on} . For every simulated T_{on} , considered as an independent variable, T_{off} was expressed (the dependent variable) in function of the terminal velocity v_{ff} (eq. 8) to compute the stop time of the pump necessary to bring back the level of the suspended particle cloud to its initial level:

$$T_{off} = \frac{x_{fall}}{v_{ff}} \quad \text{eq. 8}$$

where x_{fall} is the vertical distance to be covered to restore the initial particle cloud height and v_{ff} is the free-fall terminal velocity.

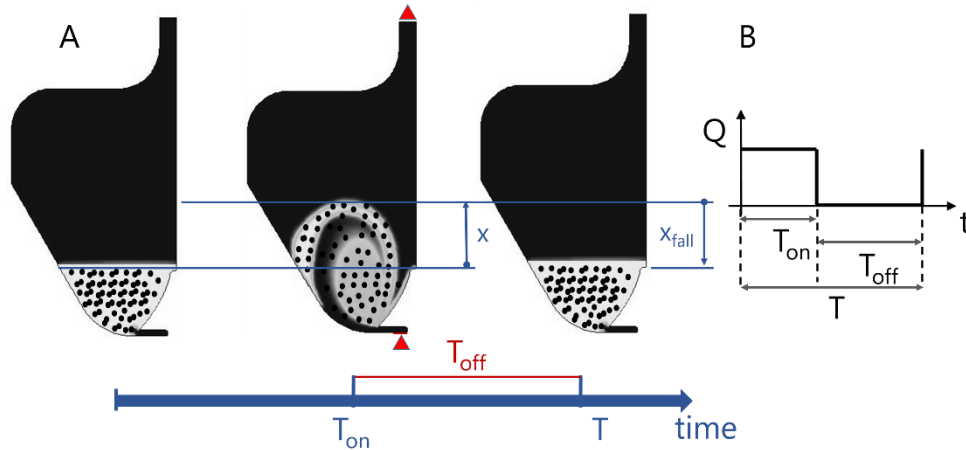


Figure 2.10: Representation of the concept of pulsed functioning mode. (A) The cloud of particles, starting from an initial distribution, is redistributed within the culture chamber when a non-null flow rate is imposed. Stopping the pump will produce the particle free-fall which will bring back the particles to the original distribution (red arrow represents the flow direction). (B) Flow rate square waveform.

In this way, the integration of the multiphysics and the analytical approach led to the definition of the pulsed flow rate square waveforms. As a matter of fact. Starting from homogenous initial distributions of the particle cloud and varying T_{on} as simulated time, the correspondent value of T_{off} was

obtained applying eq. 8. The outcome of the multiphysics simulations was used to calculate the transformation of suspended particle cloud overtime, when the flow rate is non-null. As a result, it was possible to relate T_{on} , T_{off} and the initial suspended particle cloud height in a single graph (*operational graph*), which can be used to determine the couple T_{on}/T_{off} imposing the initial cloud height.

This was done for a total of 40 combinations (summarized in Figure 2.11), modifying flow rate and particle dimensions, and performing a sensitivity test on the initial condition of particle cloud volume (indicated as initial volume homogenously occupied by the particle cloud with an initial constant VF). In order to have a most reliable measure of the particle cloud height, this value was transformed as minimum distance from the filter (according to x coordinate origin in Figure 2.11).

To demonstrate the validity of the integration of numerical and analytical approach, three explanatory examples of the application of operational graphs will be provided. Multiphysics simulations were carried out to simulate three entire pulsed cycles for 10, 25, and 100 μm particles, applying a flow rate of 50 mL/min.

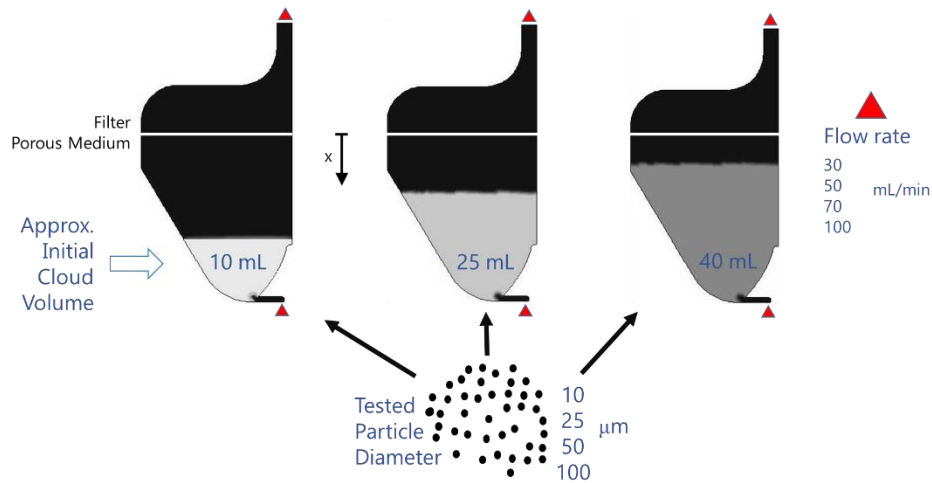


Figure 2.11: Explicative representation of the combination of parameters varied in the multiphysics simulations. x coordinate origin is positioned on the filter to calculate the cloud distance from the filter.

Results and Discussion

In order to unburden the reader and to give a clear and neat description of the results, it was chosen not to show all the 40 graphs obtained as outcome of the simulations, but only a few explanatory examples. Figure 2.12 shows the operational graph as outcome of the multiphysics model. This graph was found imposing a flow rate of 30 mL/min and suspended particles with a diameter of 10 μm . In Figure 2.12, A, B, and C correspond to the three different initial conditions applied for the particle cloud distribution. As expected, the higher is the initial particle cloud distribution, the quicker it will reach the filter, which is located at the maximum reachable height inside the bioreactor culture chamber (being a barrier to cells and constructs). The graphs herein shown are not significantly sensitive respect to the initial particle cloud volume, showing not evident differences in their monotonically increasing shapes, observing the curves respect to the secondary right axis

values.

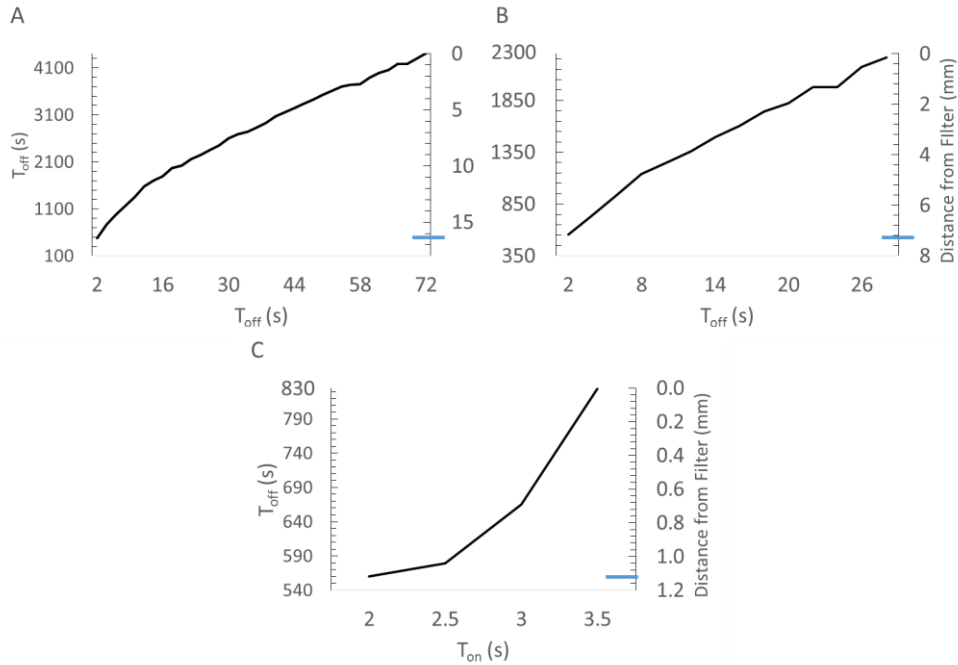


Figure 2.12: Example of operational graph. This graph was obtained for particle diameter equal to $10\ \mu\text{m}$ and flow rate $30\ \text{mL}/\text{min}$. (A) Graph for an initial particle cloud volume equal to $10\ \text{mL}$, (B) $25\ \text{mL}$, and (C) $40\ \text{mL}$. Blue ticks on the right vertical axis represent the initial distance of the particle cloud, which varies according to the initial cloud volume variations.

The chart allows to determine the couple T_{on} and T_{off} necessary to cyclically maintain the particle cloud at a certain distance from the filter. For this particle dimensions ($10\ \mu\text{m}$), there is a huge imbalance between the duration of flow-driven transport and the duration of free-fall. Figure 2.13 shows the outcome of the multiphysics simulation, depicting the suspended particle cloud coloured by VF values, varying the initial condition of particle cloud volume (golden arrow in Figure 2.13). For every instant of simulated time, it is possible to calculate the distance of the particle cloud from the filter (dash-point line in Figure 2.13), but also to determine the variations of the particle cloud height occurring in a specific interval of simulated time.

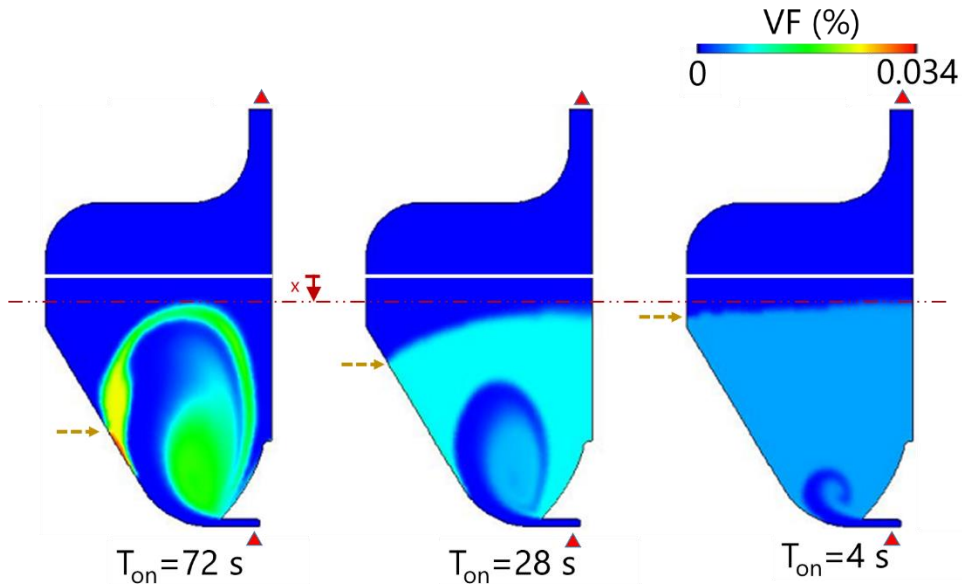


Figure 2.13: Example of outcome of the multiphysics simulation. The golden arrow represents the initial height of the particle cloud, for the three different initial conditions A, B, C. Fixed the height to be reached (red dash-point line), the pump should run for 72 s (A), 28 s (B), and 4s (C). From the operational graph, it is possible to extrapolate the value of T_{off} necessary to bring back the cloud to original level by free-fall motion. Red arrows represent the direction of the imposed flow rate.

For bigger particles, T_{on} and T_{off} have the same order of magnitude. Figure 2.14 shows the operational graphs in form of 3D stem plots for suspended particles with diameter equal to 100 μm . In this case, faster terminal velocity reached by the free-falling particles entails the comparable magnitude of T_{on} and T_{off} , which were calculated with flow rate values ranging from 50 to 100 mL/min. This outcome suggests that, the pulsed functioning mode applied to cell aggregates will result in the development of a pulsatile flow with an imposed flow rate square waveform with a duty cycle closer to unity.

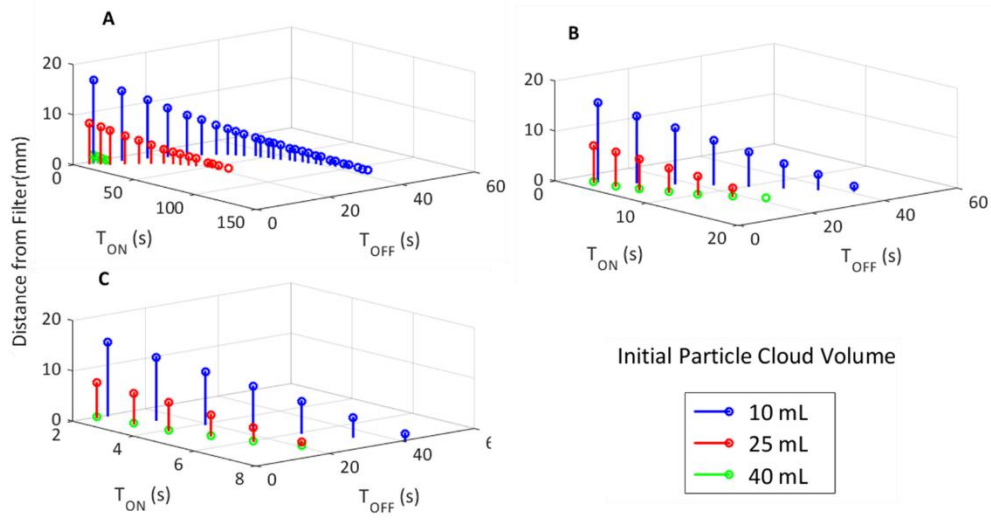


Figure 2.14: Operational graph in form of stem plots for suspended particles of $100\ \mu\text{m}$, varying the flow rate from (A) $50\ \text{mL/min}$, (B) $70\ \text{mL/min}$, and (C) $100\ \text{mL/min}$.

To verify the validity of the integration of the multiphysics model and the analytical calculation of the particle free-fall time, three applications of the operational graphs were simulated for the three entire flow rate waveform cycles. To enforce the clarity of the dissertation, only the results of one of the three applications are herein described. Figure 2.15 shows the application of the pulsed bioreactor platform functioning mode imposing a flow rate equal to $50\ \text{mL/min}$ and inoculating around 4×10^6 suspended particles with a diameter equal to $10\ \mu\text{m}$ (e.g. single cells). Starting from an initial particle cloud distribution volume of $10\ \text{mL}$ with homogenous VF equal to $2.5 \times 10^{-2}\%$ (Figure 2.11), the minimum cloud distance from the filter was brought, after 2 seconds of imposed flow rate, to $16\ \text{mm}$, selected as the initial distance before the imposition of the pulsed cycles (Figure 2.15A). The pulsation waveform was defined by the operational graph, previously obtained and shown

in Figure 2.15A, finding the couple T_{on} and T_{off} necessary to periodically keep the level of the particle cloud at the initial distance of 16 mm.

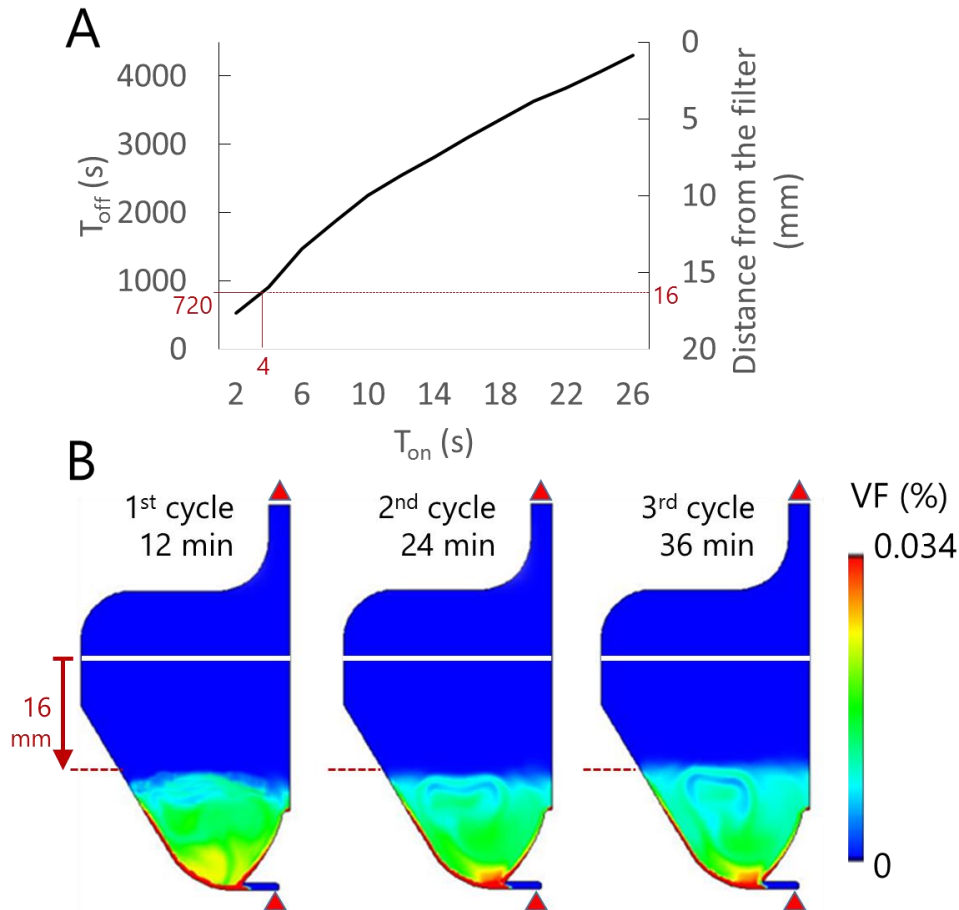


Figure 2.15: Example of application of the pulsed protocol by the application of the operational graphs for suspended particles with diameter of 10 μm and flow rate equal to 50 mL/min. (A) Chosen the minimum distance from the filter of the particle cloud (16 mm), the couple T_{on} / T_{off} is determined ($T_{on} = 4$ s $T_{off} = 720$ s or 12 mins). (B) VF distribution describing the particle cloud at the end of every simulated pulsed cycle.

Figure 2.15B depicts the distribution of the suspended particle cloud in terms of VF profile inside the culture chamber at the end of the three cycles. The alternation of flow-driven transport and free-fall motion, produces a uniformly distributed suspended particle cloud. In detail, it can be observed that

the distance from the filter of the suspension cloud is periodically restored with essentially homogenous VF distributions. In fact, PDF distributions of VF values inside the suspension particle cloud (Figure 2.16A), calculated at 12, 24, 36 mins, present VF mode values varying from $1.5 \times 10^{-2}\%$ (at 12 mins) to $1.15 \times 10^{-2}\%$ (at 36 mins), with mean VF values of $1.71 \times 10^{-2}\%$ (at 12 and 24 mins) and $1.62 \times 10^{-2}\%$ (at 36 mins).

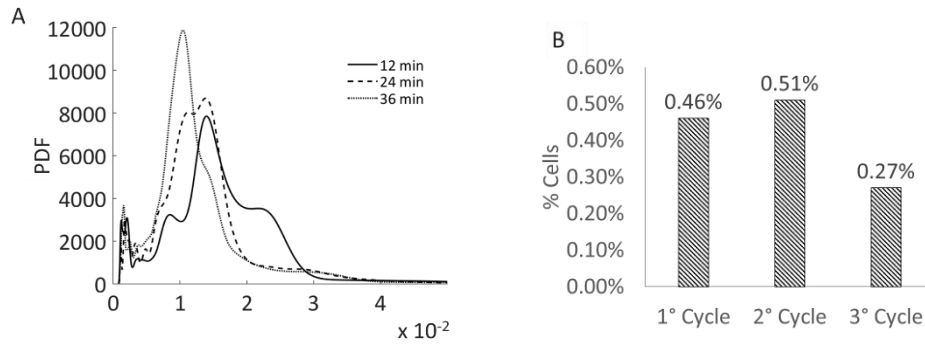


Figure 2.16: (A) Probability density functions (PDF) of VF distribution inside the particle suspended cloud at each cycle end (12, 24, 36 mins). (B) Percentage of the inoculated cell number on the bottom of the bioreactor in of volume equal to $2.6 \mu\text{L}$ at a VF close to $3 \times 10^{-2}\%$.

Higher VF values around $3.1 \times 10^{-2}\%$ were found on the bottom of the bioreactor culture. The trend of this slightly different VF values was investigated calculating the amount of particles packed at $3.1 \times 10^{-2}\%$ respect to the total amount of suspended particle in the cloud. From 0.27 to 0.51% of the total 4×10^6 suspended particles are found in the lower part of the culture chamber occupying a volume of $2.6 \mu\text{L}$, with a trend which do not increases with respect to the cycles (Figure 2.16B).

The multiphysics model herein presented and its application suggested the possibility to investigate the potentiality of the bioreactor platform and to assess its feasibility to be used in alternative culture protocols. Although

the *in silico* approach is affected from some limitations, this study gave an insight on the initial parameter configuration for future preliminary experimental tests involving expensive small molecules, cells, and culture media. Accordingly, it represents a useful tool to reduce the costs during the technical assessment of the device functioning. The data acquired by the multiphysics model herein described must be validated and adapted to the experimental framework, though the model represents a valuable alternative to the traditional trial-and-error method. Indeed, there are some assumption which can influence the outcome of the model, particularly referring to the use of the bioreactor platform for mammalian cell suspension culture. Firstly, this study considered spherical non-deformable suspended particles with constant diameter. In the real applications with mammalian cells or aggregates, suspended particles are characterized by variable diameters and different, sometimes irregular, shapes. In the scope of cell/aggregate transport, with particular attention on free-fall cell/aggregate motion, shape irregularities will invalidate the applicability of Stokes' law for the calculation of the particle terminal velocity. Contemporarily, the inhomogeneity of particle diameters, will determine different timing in the free-fall motion, thus provoking a more complex behaviour of the suspended particle cloud during the cycle evolution. Moreover, this model is useful to describe the very early stage of the culture procedure, giving only indications on the initialization of the experimental process. In fact, the model does not take into account cell aggregation, aggregate disaggregation, and cell proliferation, which may have an impact on the experimental outcome, even if it has typical characteristic time of days (simulated time were in the order of magnitude of minutes).

Although these limitations could weaken the findings of this study, the validity of the proposed process optimization method could be the basis for more complex studies which, validated in vitro, can consistently help the biotechnological experimental work and confer an in silico-based *a priori* knowledge useful to limit the experimentation costs.

2.3.3 In silico Supported Check Valve Optimization

Revised Check Valve System: Concept

The complex assembly and the huge number of elements constituting the original check valve kinematic mechanism entailed some difficulties in the bioreactor chamber handling, producing some lacks in the reproducibility of the symmetric opening of the check valve orifice. Asymmetries in the valve opening were not acceptable given the enormous impact on the cell culture environment homogeneity. As a matter of fact, a new valve kinematics was conceived, designed, realized, tested, and finally implemented in the bioreactor platform. Compared to the original system, the revised architecture of the check valve system does not have any deformable component. As explained in this chapter in section 2.2.3 (Check Valve (original configuration) - page 41) the valve opening was produced through the silicone membrane deformation due to the pressure drop generated across it. However, the minimal deviations from the axis of the elements constituting the check valve system might produce a non-symmetric deformation of the silicone membrane and a consequent asymmetric check valve opening.

As a result, the revision strategy dealt with the necessity to fulfil the following requisites: (1) remove any deformable component, increasing the

rigidity of the system, (2) facilitate the vertical translation degree of freedom, reducing the check valve crack pressure, and (3) guarantee the completely controlled valve opening for all the flow rate functioning range of the bioreactor platform. Figure 2.17 shows a comparison between the original and revised architectures of the check valve system.

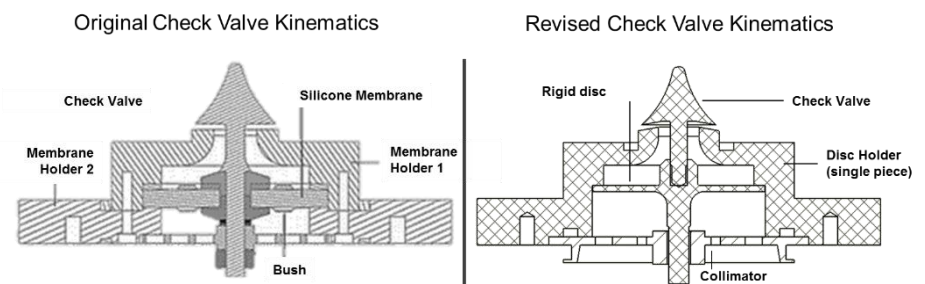


Figure 2.17: Comparison between the original and revised kinematic mechanism of the check valve system visualizing a section of the check valve system both in open position. The number of elements composing the assembly of the revised check valve assembly was consistently reduced.

The kinematic motion of the check valve is governed by the pressure drop generated across a rigid perforated disc (Figure 2.18A). The upwards hydrodynamics lift can be modulated by means of a number of holes: hole dimension and number was optimized to produce a correct valve opening applying the typical flow rate applied for cell culture (optimization widely described in the forthcoming section). The rigid disc can move along a runner, made up by the collimator and the inner cylindrical surface of the disc holder, which permits the vertical translation, but removes all other translational and rotational degree of freedom. The presence of the fixed collimator forces the perfect alignment of the valve to the bioreactor culture chamber axis. To maintain the check valve co-axial also in the closed position, the check valve cap and the bottom part of the bioreactor culture chamber were sloped of 10 degrees (Figure 2.18B).

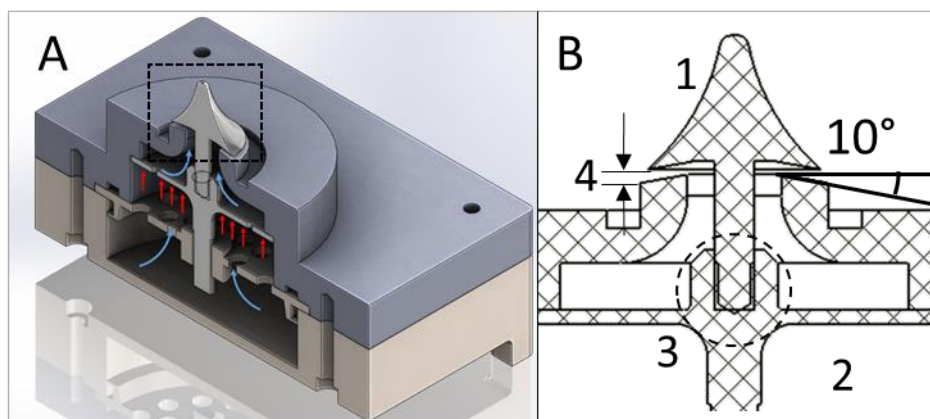


Figure 2.18: A) 3D model of the revised check valve complex. Blue arrows represent the direction of the culture medium flow. From the base to the collimator, the flow reaches the rigid POM disc and the pressure drop across the sliding disc produces a net lift force (red arrows represent the upwards net pressure distribution). B) Detail of the features of the new check valve system. 1. Check valve cap, 2. Check valve disc, 3. Coupling between the check valve cap and check valve disc: thread which allows to adjust the culture chamber inlet gap (4).

The rigid disc and the check valve are coupled to each other by a thread (Figure 2.18B). The possibility to screw the check valve at different levels allows to adjust closure and opening strength, in order to have a precise control of the velocity stream entering the bioreactor chamber (4 in Figure 2.18B).

Methods

In order to obtain the check valve behaviour described above, it was essential to delineate an optimization protocol. Firstly, the constitutive materials of each element of the revised check valve system were chosen (step 1 - Figure 2.19). All the elements constituting the revised check valve system were conceived and designed in POM (selected for its density of about 1400 kg/m^3). Chosen the minimum thickness of the disc and the shafts of the moving components (necessary to calculate the weight of the check valve, opposed to the hydrodynamics lift force), in silico computational simulations were performed

to assess the effect of the holes (diameters and hole number) on the generated hydrodynamics force was investigated (step 2 to step 4 Figure 2.19). A number of simulations investigated the space of combination ranging between 2 to 8 holes and 1 to 3 mm of hole diameter (always equally distributed along a circumference). The process is summarized in the chart illustrated in Figure 2.19.

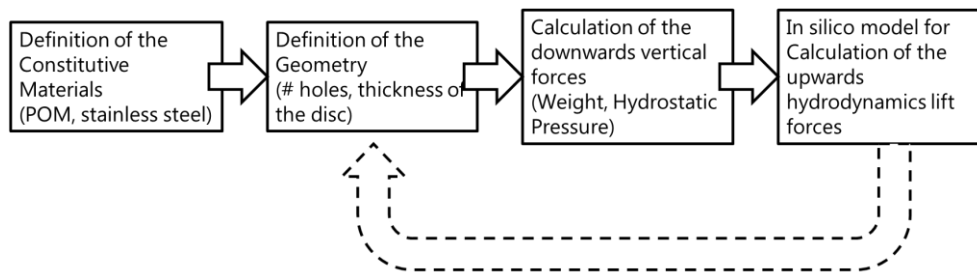


Figure 2.19: Flow chart describing the geometry check valve system optimization process.

Technically, a set of single phase steady-state numerical simulations was developed using a customized immersed boundary-based commercial software (SolidWorks FlowSimulation, Dassault, France). The fluid domain was discretized by means of a hexahedral Cartesian mesh with cardinality equal to approximately 61×10^3 . Since the interest of this computational study was the revised check valve system, the model focused only in the fluid volume shown in Figure 2.20B, considering the bioreactor chamber opened without filter system, nor lid. The position of the rigid disc of the check valve system was kept still and half-open, in order to evaluate the force which is necessary to start the first check valve movement (neither inertial forces, nor fluid resistance). Navier-Stokes equations were solved by the numerical solver considering the culture medium with dynamic viscosity equal to $1 \times 10^{-3} \text{ Pa}\cdot\text{s}$ and density equal to 1000 kg/m^3 [3,17].

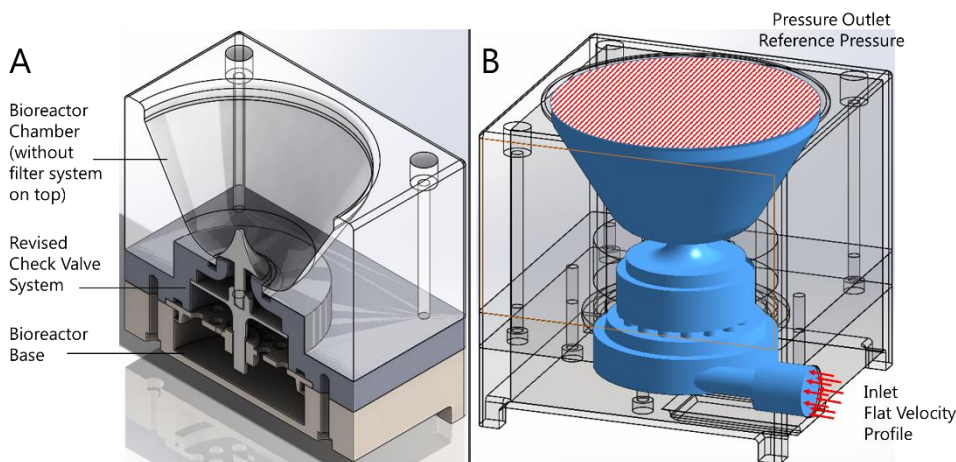


Figure 2.20: Final implementation of the revised check valve system within the bioreactor 3D model (A). This implementation was used for the definition of the computational domain (B) used for the in silico computational optimization of the design.

The inlet flow from the base was imposed by means of a flat velocity profile corresponding to 10 mL/min. The opening on the top of the bioreactor culture chamber was set as reference pressure (null pressure). No-slip condition was set on all the walls of the fluid domain.

The value of hydrodynamics force acting over the check valve and the rigid disc obtained for the different number and dimension of the holes was then used to evaluate the *effective lift force*, calculated as balance between the upwards hydrodynamics force and the downward forces (weight and hydrostatic pressure force, neglecting any friction).

Results

In silico computational modelling allowed to obtain useful information for a preliminary characterization of the revised check valve kinematics. Figure 2.21 depicts a qualitative representation of the flow structures establishing inside the base, across the check valve system, and entering the bioreactor

culture chamber when the disc is perforated with two holes with 1 mm diameter.

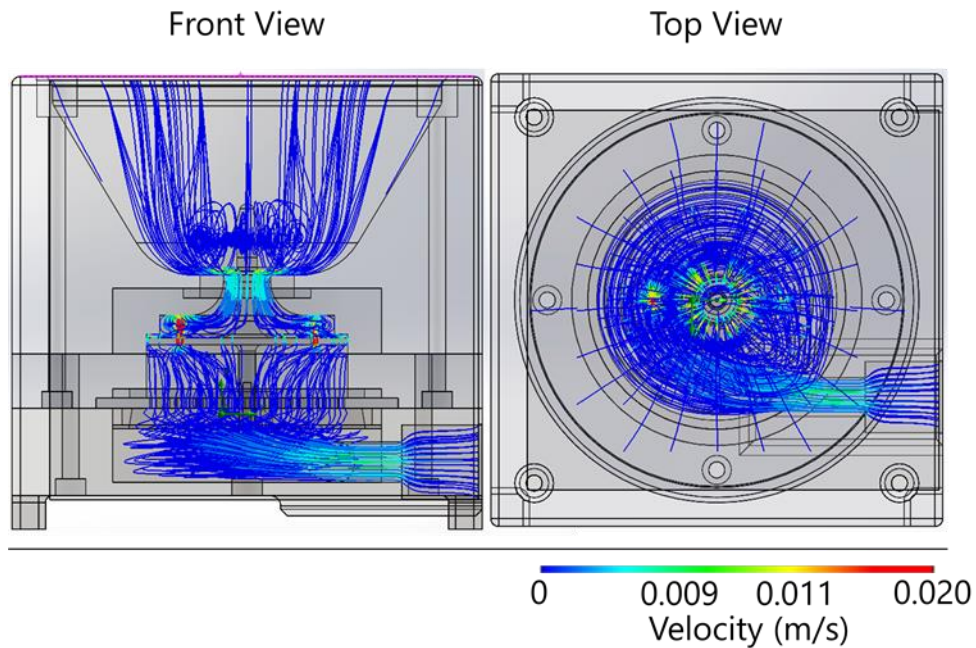


Figure 2.21: Streamline flow structure visualization for the rigid disc configuration with two holes of 1 mm diameter. The medium pervades the base, travels across the check valve system, and enters the bioreactor culture chamber. Front view (left panel) and top view (right panel).

The culture medium pervades the base and, due to the not centred position of the inlet, produces helical structures ascending towards the bioreactor culture chamber (Figure 2.21). Although the presence of the collimator tends to disrupt the helical flow and to collimate the flow structures, the flow-streams reaching the rigid disc of the valve system and passing through the holes are still partially asymmetric (Figure 2.21, left panel). The rigid disc with its two small holes contribute to the symmetrisation of the flow producing a full axial-symmetric flow entering the bioreactor culture chamber (Figure 2.21, right panel).

As final outcome of the optimization, this configuration was found to be the only one which guarantees the check valve opening at low flow rate (i.e. 10 mL/min). Table 2.5 reports the results of the computational simulations in terms of *effective lift force* (i.e. the force capable of starting the valve motion).

Table 2.5: Net lift forces resulting from the computational model outcome. The underlined and bold entry represents the chosen configuration.

No. Holes	Effective Lift Force (mN)		
	Hole Diameter		
	3 mm	2 mm	1 mm
8	-15	-15	-14.9
4	-15	-14.9	-13.9
2	-14.8	-13.9	<u>2.1</u>

This optimization suggested the best configuration which guarantees the check valve opening. Since it was obtained imposing a low flow rate, these hole dimension and number resulting from this optimization process must be considered as a restrictive requirement when all the flow rate functioning range of the bioreactor platform is guaranteed.

2.4 Bioreactor Platform Optimization

2.4.1 Continuous Perfusion Feeding Circuit

Within any batch culture device (such as RWV or stirred bioreactors), exhausted culture medium must be periodically replaced to restore the original nutrient and small-molecule concentrations (e.g. glucose, glutamine, grow factors, etc.) and deplete metabolites content (e.g. lactate, ammonia, indirectly restoring pH) within the culture medium. In general, the medium exchange is performed manually by means of *batch feeding*: the medium is

periodically replenished, e.g. every day, or after having ascertained that nutrient/metabolite concentrations or pH are out of a certain tolerance range. Stirred flask bioreactors are typically suitable for the implementation of a *perfusion feeding circuit*. In detail, perfusion feeding allows to continuously perfuse the culture vessel with fresh medium and contemporarily remove exhausted medium to waste, allowing to maintain a quasi-steady culture environment [22].

In order to avoid manual medium exchange in the herein proposed suspension bioreactor, the original system described in paragraph 2.2.3 was modified with the implementation of a secondary perfusion circuit for continuous perfusion feeding to the existing bioreactor platform.

The continuous medium renewal is achieved preserving the initial total quantity of culture medium present in the main closed-loop recirculation circuit: an amount of medium is extracted from the closed-loop and contemporarily the same amount is injected in the same circuit (Figure 2.22). The medium extraction point is located along the return tube of the closed-loop recirculation circuit, just before the medium reservoir, while the fresh medium injection occurs directly into the reservoir through a specific port created on its cap. For the continuous and automatic medium exchange, a multi-channel computer controllable peristaltic pump was chosen (Ismatec Reglo Digital). Based on previous studies carried out on continuous perfusion feeding for stirred bioreactors [22], it was decided to choose a pump with a flow rate range of 0.01 – 68 mL/min.

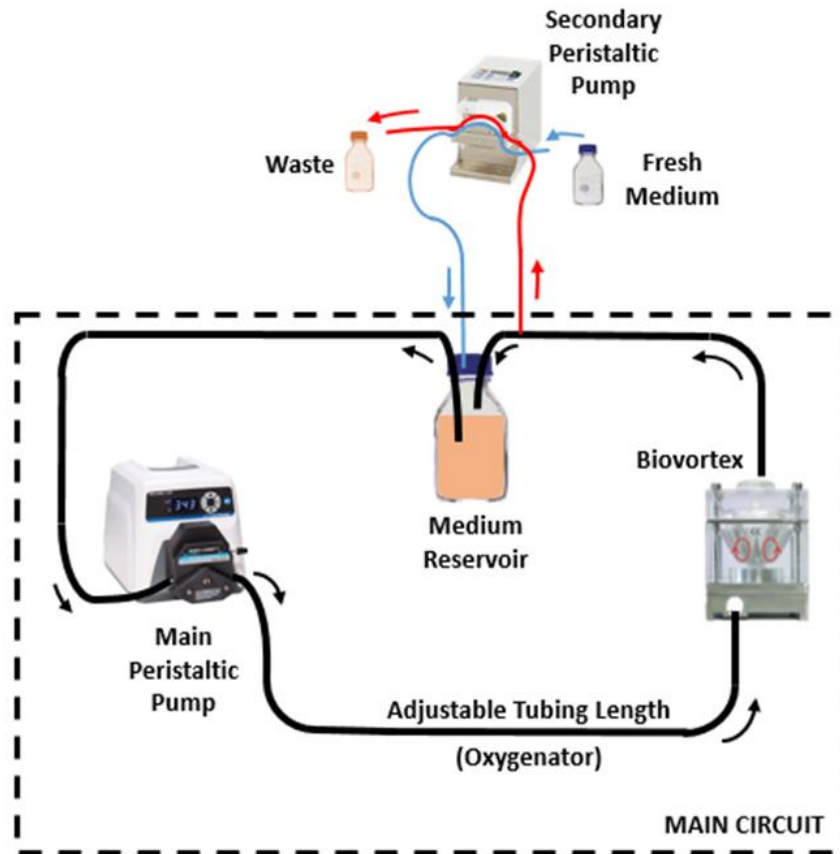


Figure 2.22: Schematic illustration of the modified closed-loop recirculation circuit. The circuit inside the dashed-line box is the original closed-loop recirculation circuit. The continuous perfusion feeding secondary circuit consists of a new tube for fresh medium injection (blue line), a new tube for medium withdraw (red line), a computer-controllable multi-channel peristaltic pump, and two bottles for fresh medium and waste.

The shunt, in correspondence of the extraction point, was made by means of a three-way stopcock (Figure 2.23). It pulls out the medium from the main circuit to the waste reservoir, furthermore it allows to close the output towards the waste reservoir, maintaining seal during disconnecting of the secondary perfusion circuit.

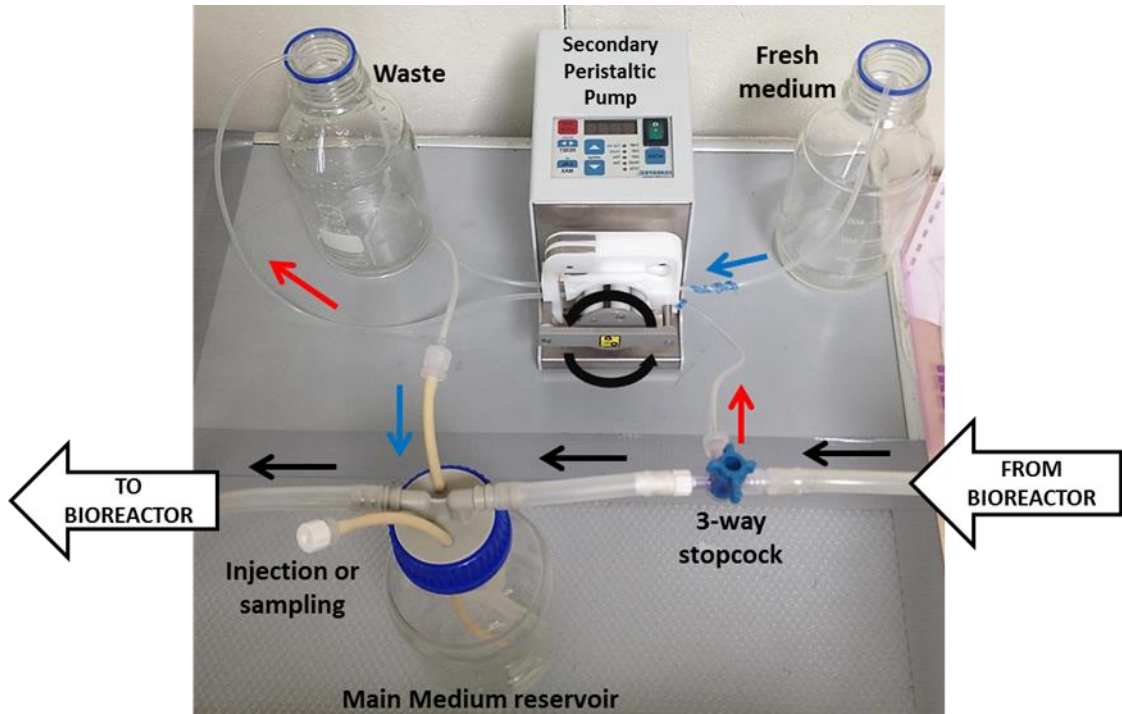


Figure 2.23: Preliminary setup of the continuous perfusion feeding circuit. Red arrows indicate the flow towards the waste bottle. Blue arrows indicate the flow of the fresh medium towards the main reservoir. Horizontal black arrows indicate the flow direction in the closed-loop perfusion loop.

2.4.2 .Control and Monitoring System

The implementation of an automated monitoring, together with a control system, is essential for controlled and reproducible culture conditions. In particular, monitoring of pH and dissolved oxygen (DO) inside the culture medium is useful to quantitatively evaluate the metabolic cell behaviour, hence giving a more objective support on the control of the developing culture. Especially in stem cell culture application, pH level is extremely important, given the sensitivity of this cellular source in response to decimal variations of pH levels which affect proliferation and differentiation [12].

On the basis of these considerations, the original configuration of the bioreactor platform was provided by a control and monitoring system capable of continuously monitor pH and DO variations within the culture medium over time, giving the possibility to interactively set the pumps to adjust the signal in an acceptable range. Figure 2.24 depicts a concept chart of the developed control and monitoring system, which was physically embedded in a control-box, connected to a dedicated computer and communicating with a purpose-built software developed in Labview (Appendix II). In detail, measured signals are collected by the monitoring unit, which analogically and digitally processes pH and DO to be shown on the user interface.

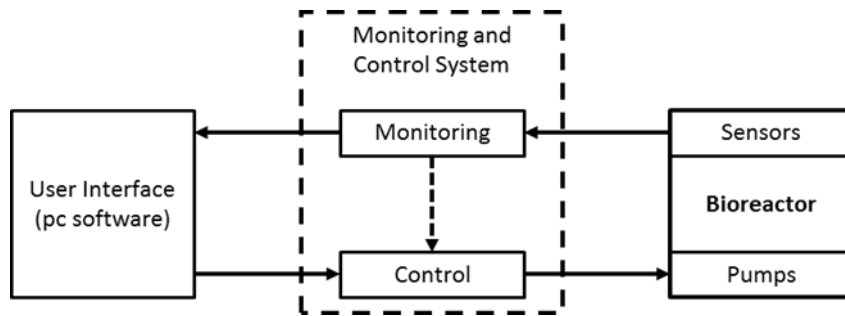


Figure 2.24: Concept chart of the control and monitoring system. Monitoring unit gets the signals from the sensors. These signals (after processing) are showed through the user interface. The user, through the interface, can directly act on control unit to set the pump flow rates in order to adjust pH or DO signals overtime. The dashed arrow represents the future aim to perform an automated control based on monitoring feedback signals.

A developed user-friendly interface allows to control the pumps in order to modify the flow rate in response to pH and DO variation overtime. The software was designed considering the possibility to implement a control algorithm for the automatic adjustment of pump flow rates and to regulate fresh medium automatic replenishment.

Due to the small dimensions of the bioreactor culture chamber, it was impractical to locate the probe points directly inside the culture chamber

without affecting the fluid dynamics features of the device. It was decided to add two separate sensing points integrated in the closed-loop recirculation circuit (Figure 2.25).

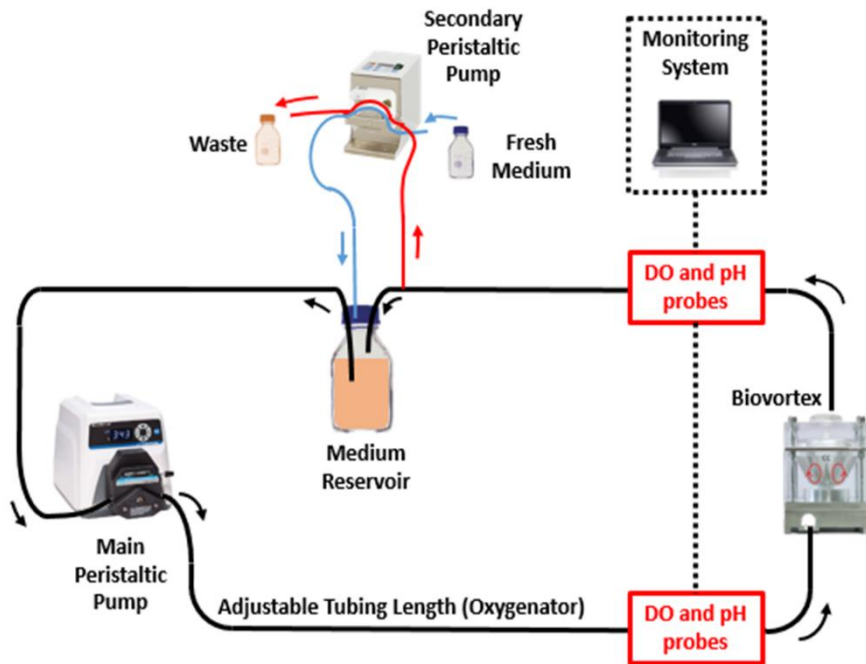


Figure 2.25: Schematic illustration of the complete system (left panel). Red boxes represent the sensing points integrated within the closed-loop recirculation circuit exactly downstream and upstream the bioreactor culture chamber. The signals obtained by the sensor are processed and displayed in the monitoring system software.

The position of the two sensing locations derives from the necessity to obtain information of the metabolic behaviour of the cells inside the bioreactor culture chamber, applying a differential balance between the two different sensing points. To accomplish this objective, two sensing flow chambers were added inside the closed-loop recirculation circuit. Each sensing flow chamber was equipped with DO and pH probes. The sensors were chosen in order to guarantee full compatibility with GMP guidelines and to permit sterilization

in autoclave. The detailed description of sensors and the relative signal conditioner developed for signal processing, as well as the sensor calibration procedure implemented in the control and monitoring software is provided Appendix II.

Sensing Flow Chamber

The pH and DO probes were positioned in the sensing points by means of purpose-built sensing flow chambers directly connected to the closed-loop recirculation circuit of the bioreactor platform (Figure 2.26, Figure 2.27). The sensing flow chamber was designed according to the following requirements:

- *Minimum filling volume*

The calculated filling volume of the chamber is equal to about 17 mL.

- *Autoclavable materials*

Fitting and probe holders were realized in acetal (polyoxymethylene – POM), while the chamber is in polycarbonate (PC). Seals are in ethylene propylene rubber. (EPR)

- *Usability*

Few components easy to assemble.

- *Hydraulic seal*

The seal is guaranteed by the use of o-rings properly chosen.

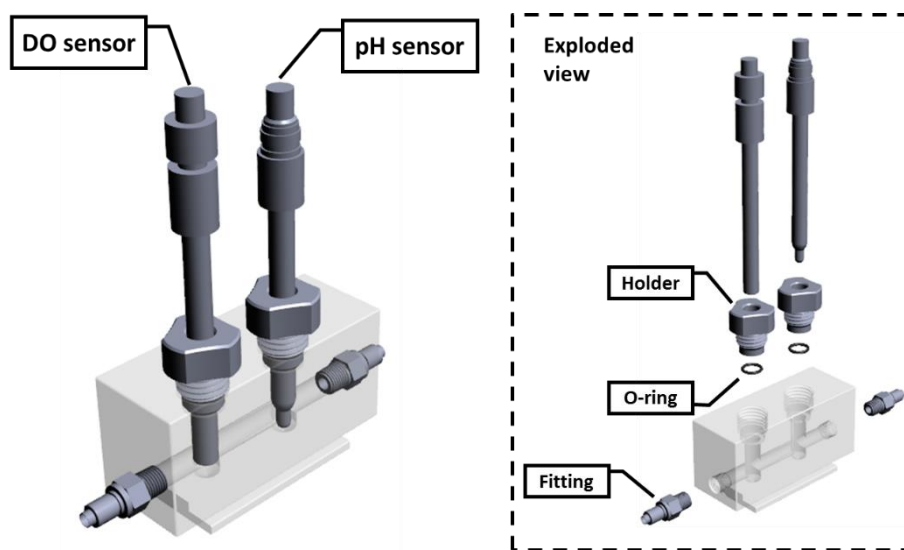


Figure 2.26: Sensing flow chamber 3D model. Left panel, the assembled flow chamber including sensors. Right panel, the exploded view with all the components (holders, o-rings, fittings, sensors).

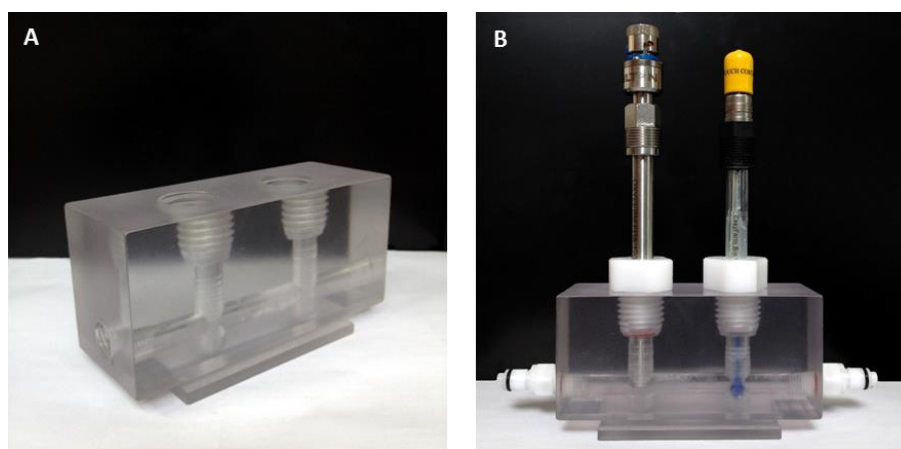


Figure 2.27: Sensing flow chamber. A) Main body in transparent polycarbonate, B) final configuration with installed fittings, holders and sensors.

The main body of the sensing flow chamber and the probe holders were realized by material removal of raw bars by CNC milling. The choice of transparent polycarbonate as main body material was in response of two additional requirements: transparency allows to *i)* evaluate the depth of insertion of the sensors and *ii)* the possible presence of air bubbles into the channel

of the flow chamber. Indeed, in order to provide the most reliable and accurate measurement, it is important to evaluate the position of the most sensitive parts of the sensors, without the presence of air bubbles.

The performance of the flow chamber was characterized placing the pH and DO sensors (described in Appendix II) in the sensing chamber and connected within the complete bioreactor platform (Figure 2.28).



Figure 2.28: Final bioreactor platform configuration. 1, Culture chamber. 2, Downstream sensing flow chamber. 3, Upstream sensing flow chamber. 4, pH and DO sensors. 5, Support. 6, Reservoirs. 7, closed loop recirculation pump. 8, continuous perfusion feeding secondary pump.

The hydraulic circuit was filled with tap water (not to damage the pH sensor glass with distilled water). The flow rate was modified from 30 to 100 mL/min and pH and DO signals were acquired and saved for characterization. The pH sensor was characterized by a very steady signal for all applied

flow rate, since the presence of flow structures around the probe tip did not affect the ionic exchange and consequently the pH signal (Figure 2.29).

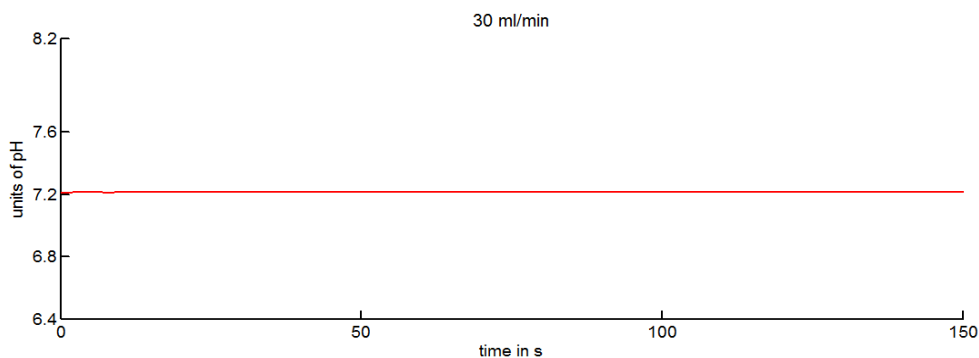


Figure 2.29: pH signal over time with an imposed flow rate of 30 mL/min.

As regards to DO measurement, it was noticed an oscillating behavior of the signal with different frequencies varying the imposed flow rate. In order to characterize the DO signal, it was decided to perform the measurement at different flowrates: 30, 40, 50, 70 and 100 mL/min. All acquired signals were filtered using a first-order lowpass digital Butterworth filter with a cutoff frequency of 0.0085 Hz and by processing the input samples in both the forward and reverse directions (Figure 2.30).

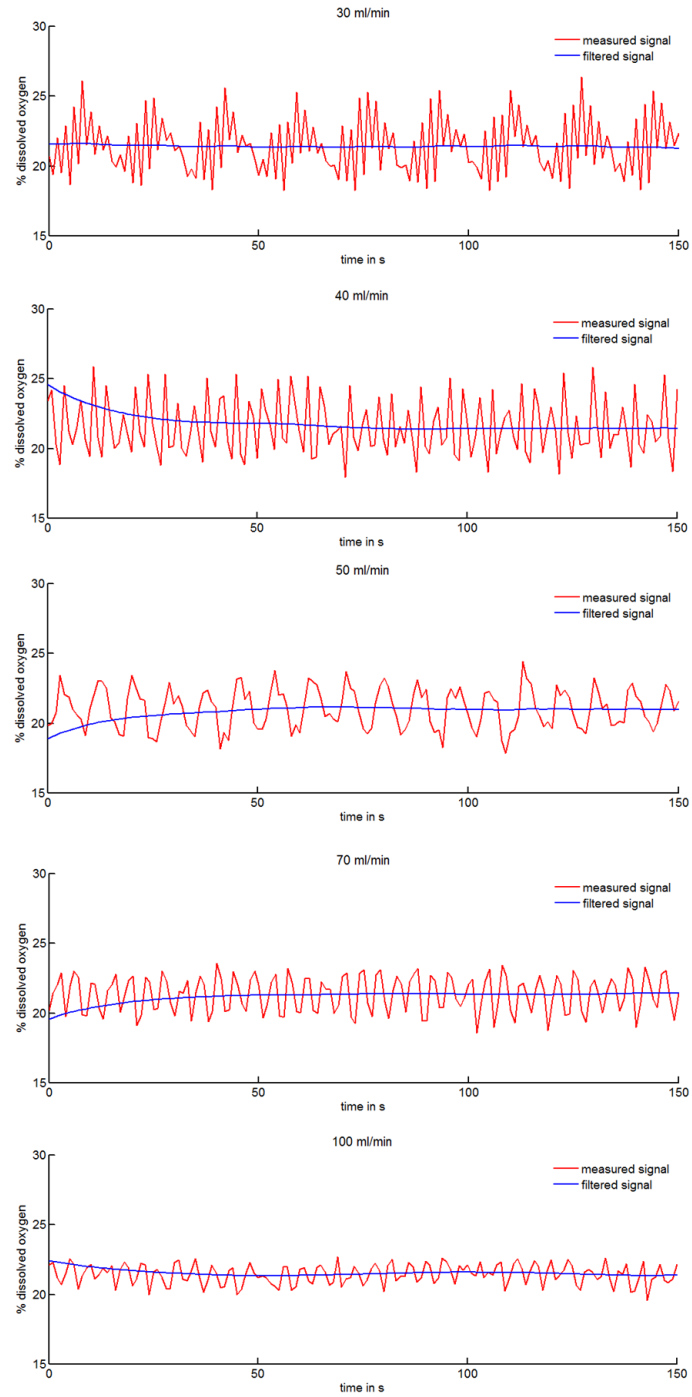


Figure 2.30: DO measurement (red) and filtered signals varying imposed flow rate values.

The results of the DO signal acquisitions and post-processing is shown. It can be seen that the oscillating trend of the signal disappears increasing the flowrate over 30ml/min. In addition, it is evident that the amplitude of the measured signals gradually decreases from 30 to 100 mL/min, however the value of the filtered signals settles around 21%.

References

- 1 Amit, M., Chebath, J., Laessky, I., Miropolsky, Y., Peri, M., Blais, I., and et al. Suspension culture of undifferentiated human embryonic and induced pluripotent stem cells. *Stem Cell Review*, 6, 2 (2010), 248-259.
- 2 Zweigerdt, Robert, Olmer, Ruth, Singh, H., Haverich , Axel, and Martin, Ulrich. Scalable expansion of human pluripotent stem cells in suspension culture. *Nature Protocols*, 6, 5 (2011), 689-700.
- 3 Consolo , Filippo, Bariani, Christian, Mantalaris, A., Montevecchi, Franco Maria, Redaelli, A., and Morbiducci, Umberto. Computational modelling for the optimization of a cardiogenic 3D bioprocess of encapsulated embryonic stem cells. *Biomechanics and Modelling in Mechanobiology*, 11, 1-2 (2012), 261-277.
- 4 Olmer, Ruth, Lange, A., Selzer, S., Kasper, C., Haverich, Axel, Martin, Ulrich, and Zweigerdt, Robert. Suspension culture of human pluripotent stem cells in controlled, stirred bioreactors. *Tissue Engineering Part C Methods*, 18, 10 (2012), 772-784.
- 5 Zweigerdt, R. Chapter - Large Scale Production of Stem Cells and their Derivatives. In *Engineering of Stem Cells*. Springer, 2009.
- 6 Cameron, C. M. and Kaufman, D. S. Improved development of embryonic stem cell-derived embryoid bodies by stirred vessel cultivation. *Biotechnology and Bioengineering*, 94, 5 (2006), 938-948.
- 7 Rungarunlert, Sasitorn, Klincumhom, Nuttha, Tharasanit, Theerawat, Techakumphu, Mongkol, Purity, Melinda K., and Dinnyes, Andras. Slow Turning Lateral Vessel bioreactor improves embryoid body formation and cardiogeninc differentiation of mouse embryonic stem cells. *Cellular Reprogramming*, 15, 5 (2013), 443-458.
- 8 Kempf, Henning, Olmer, Ruth, Kropp, Christina, Ruckert, M., Jara-Avaca, M., Robles-Diaz, D., and et al. Controlling expansion and cardiomyogenic differentiation of human pluripotent stem cells in controlled, stirred bioreactors. *Stem Cell Reports*, 3, 6 (2014), 1132-1146.
- 9 Hickman, John A., Graeser, Ralph, de Hoogt, Ronald, Vidic, Suzana, Brito, Catarina, Gutekunst, Matthias, and et al. Three-dimensional models of cancer for pharmacology and cancer cell biology: Capturing tumor complexity in vitro. *Biotechnology Journal*, 9 (2014), 1115-1128.

- 10 Rodrigues, C. A., Fernandes, T. G., Diogo, M. M., da Silva, C. L., and Cabral, J. M. Stem cell cultivation in bioreactors. *Biotechnology Advances*, 29, 6 (2011), 815-829.
- 11 Cherry, R. S. Animal cells in turbulent fluids: details of the physical stimulus and the biological response. *Biotechnology*, 22, 2 (2004), 80-86.
- 12 Teo, A., Mantalaris, A., and Mayasari, Lim M. Hydrodynamics and bioprocess considerations in designing bioreactors for cardiac tissue engineering. *Journal of regenerative medicine and Tissue Engineering*, 1, 4 (2012).
- 13 King, J. A. and Miller, W. M. Bioreactor development for stem cell expansion and controlled differentiation. *Current Opinion in Chemical Biology*, 11, 4 (2007), 394-398.
- 14 Falvo D'Urso Labate, G. U., Massai, D. N., Pennella, F., and et al. Microgravity generating device. Patent, WO2012157007A1 (2012).
- 15 Isu, Giuseppe, Massai, Diana, Cerino, Giulia, Bignardi, Cristina, Audenino, Alberto, and Morbiducci, Umberto. A novel perfusion Bioreactor for 3D cell culture in Microgravity Conditions. In *SBC 2013 (Sunriver 2013)*.
- 16 Orr, D. E. and Burg, K. J. Design of a modular bioreactor to incorporate both perfusion flow and hydrostatic compression for tissue engineering applications. *Annals of Biomedical Engineering*, 36, 7 (2008), 1228-1241.
- 17 Consolo, F., Fiore, G. B., Truscillo, S., Caronna, M., and Morbiducci, U. A computational model for the optimization of transport phenomena in a rotating hollow-fiber bioreactor for artificial liver. *Tissue Eng Part C Methods*, 15, 1 (2009), 41-55.
- 18 Gidaspow, D., Bezburuah, R., and Ding, J. Hydrodynamics of circulating fluidized beds, kinetic theory approach. (1992), 75-82.
- 19 Eckmann, L., Freshney, M., Wright, E.G., Sproul, A., Wilkie, N., and Pragnell, I. B. A novel in vitro assay for murin haematopoietic stem cells. *British Journal of Cancer Supplement*, 9 (1988), 36-40.
- 20 Coanda, H. Procédé de propulsion dans un fluide. National République Française Patent (1932).

- 21 Ismadi, M. Z., Gupta, P., Fouras, A., Verma, P., Jadhav, S., and Bellare, J. Characterization of a Spinner Flask for induced pluripotent stem cell culture application. *Plos One*, 9, 10 (2014), e106493.
- 22 Olmer, Kropp, and Zweigerdt. Impact of Feeding Strategies on Expansion of Human Pluripotent Stem Cells in Stirred Tank Bioreactors Using mTeSR™1 (2014).

Appendix I

Sizing of the Closed-loop Recirculation Circuit

The oxygenation of the cultured cells/constructs is one of the critical aspects to be taken into account while designing a bioreactor platform. It is essential to avoid problems of poor oxygenation, which can cause inhomogeneous construct growth or even cell death, with a correct optimization of an oxygenator system.

In the bioreactor platform described in Chapter 2, the oxygenator is an oxygen-permeable tubing system which length can be adjusted according to the oxygen supply requirements needed during cell culture. This dimensioning was done, according to Orr and colleagues [1], simplifying the recirculation circuit identifying three separate domains where oxygen exchange occurs (Figure AI.1 - compartmental approach). This compartmental approach allowed to consider each domain of the bioreactor platform independently. Therefore, the dissolved oxygen partial pressure exiting from the bioreactor culture chamber compartment is the inlet condition for the oxygenator, and the oxygen partial pressure exiting the oxygenator becomes the inlet condition for the following compartment.

As depicted in Figure AI.1, the first domain is the bioreactor culture chamber, where the content of oxygen inside the medium is depleted by the cellular phase metabolism, with the production of carbon dioxide. The second domain is the oxygenator, i.e. oxygen-permeable tubing, where gas exchange is optimized between the culture medium flowing inside the tube and the air atmosphere of the incubator. The third and last domain is the medium res-

ervoir, where the culture medium undergoes a medium exchange at the medium free-surface in its air headspace. Since gas exchange through the free-surface of the reservoir headspace is consistently slower (diffusion limited transport) than gas exchange occurring inside the oxygenator (convection-diffusion transport), only the gas exchange inside the oxygenator compartment was considered.

The gas content inside the culture medium can be expressed either in terms of dissolved oxygen concentration or partial pressure, given the liquid-gas balance expressed by Henry's law. The oxygen partial pressure in the external atmosphere (incubator) was considered constant (gas phase presents a constant oxygen partial pressure equal to 159 mmHg, due to 21% of atmospheric oxygen). Along the oxygenator tube, dissolved oxygen pressure increases over length assuming oxygen mass transfer across the membrane of the permeable tube. The bioreactor culture chamber was considered as a black-box compartment, where oxygen is volumetrically depleted by the homogeneously distributed cellular phase which occupies the control volume (culture chamber volume).

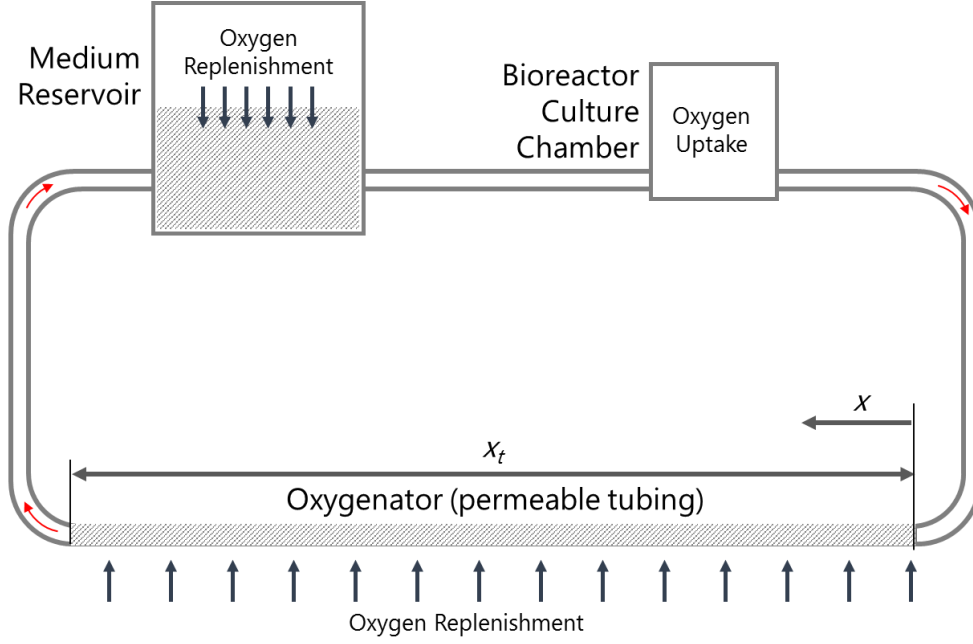


Figure AI.1: Simplified bioreactor platform recirculation circuit. Oxygenation is up-taken by cells inside the bioreactor culture chamber and can be replenished inside the oxygenator tubing or inside the medium reservoir.

Regarding the oxygenator compartment, an integral mass balance for the oxygen species was written in order to define the oxygen-permeable length necessary to restore dissolved oxygen partial pressure to the 98% of saturation within the culture medium. Assuming a steady-state situation (accumulation equal to zero), the mass balance expressed for oxygen species can be written as eq.AI. 1.

$$\left(\frac{Q}{H} pO_2(x) + N_{avg} \right) - \left(\frac{Q}{H} pO_2(x + \Delta x) \right) = 0 \quad \text{eq.AI. 1}$$

where pO_2 is the oxygen partial pressure of dissolved oxygen within the culture medium (according to Henry's law), Q is the flow rate delivered by the pump, and H is oxygen solubility within the culture medium at 37°C. N_{avg} is the average oxygen flow through the oxygen-permeable membrane of the tube. Laminar flow within the tubes was verified up to a flow rate equal

to 400 mL/min (Re=1337), flow rate largely beyond the working flow rate range of the bioreactor platform. In laminar flow conditions, the velocity profile of the medium inside the tubes can be considered parabolic (fully-developed profile of Hagen-Poiseuille law). As a consequence, it is possible to apply the “theory of the two films” (Figure AI.2).

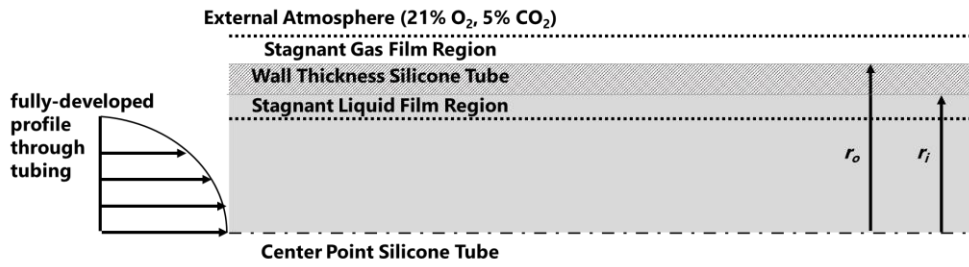


Figure AI.2: Oxygen transport physical model through the wall of the silicone tube: the “theory of two films”.

The no-slip condition at the wall determines a zone of stagnant fluid near the wall at the liquid side of the membrane (i.e. in the inner part of the tube). The same condition can be considered at the external side of the tube, the incubator side. The “theory of the two films” permits to express the oxygen gas-liquid balance across a permeable membrane in terms of average oxygen flux as reported in eq.AI. 2 assuming no oxygen gradients at each cross-section inside the tube:

$$N_{avg} = K_{OL} W \Delta x_t (pO_2' - pO_2(x)) \quad \text{eq.AI. 2}$$

where the net oxygen flux is formalized as a function of the oxygen partial pressure difference across the membrane ($pO_2' - pO_2(x)$), the gas-exchange area of the membrane $W \Delta x_t$, and the overall mass transfer coefficient K_{OL} . Such coefficient, is a function of the mass transfer coefficient liquid-side, solid

side, and of the tube wall permeability. It is usually reported in its inverse form, representing the resistance to mass transfer eq.AI. 3:

$$\frac{1}{K_{OL}} = \frac{H}{k_i} + \frac{t_m W_i}{\rho_{STP} P_m W} + \frac{RTW_i}{K_o W_o} \quad \text{eq.AI. 3}$$

where:

- W_i , W_o represent the inner and outer tubing circumference, respectively;
- W is the logarithmic-averaged circumference of the tube;
- ρ_{STP} is the gas density at standard pressure conditions (0°C and 1 atm);
- R is the gas constant;
- T is the incubator temperature;
- P_m is the silicone tube oxygen permeability;
- t_m is the thickness of the tube;
- k_i is the mass transfer coefficient of the inner layer (liquid side);
- k_o is the mass transfer coefficient of the outer layer (gas side).

The three summations in eq.AI. 3 can be attributed to each layer of the “theory of the two films” depicted in Figure AI.2. In fact, this model describes the oxygen flux across the permeable membrane as the superimposition of three separate ideal mass transport resistances: stagnant gas and liquid film, and membrane mass transport resistance. In detail, membrane resistance depends on the permeability P_m of silicone tube membrane, its thickness t_m , mass properties of oxygen ρ_{STP} , and gas-exchange surface W .

k_i and k_o mass transport coefficients depend on the fluid dynamics at the two sides of the membrane. Mass transport coefficients can be expressed as function of adimensional Sherwood number (eq.AI. 4), which is as well correlated with Reynolds number (eq.AI. 5):

$$Sh = \frac{k_i L}{D_i} \quad \text{eq.AI. 4}$$

$$Sh = 0.43 + 0.53 Re^{0.5} Sc^{0.31} \quad \text{eq.AI. 5}$$

$$Sc = \frac{\mu}{\rho D_i} \quad \text{eq.AI. 6}$$

where L is the characteristic length, D_i is the oxygen diffusivity within the gas or the liquid, Sc is the adimensional Schmidt number (eq.AI. 6), and the coefficients 0.43 and 0.53 are valid only under fully-developed laminar flow regime. In this case study, the gas side can be considered static air. This implies that at the gas side, mass transport is driven by natural diffusion, and Sherwood number is always equal to 0.43 for every flow rate imposed by the pump of the bioreactor platform. For the liquid side (inside the tube), Sherwood number depends on Reynolds number and must be re-computed for each imposed flow rate.

Combining eq.AI. 1 and eq.AI. 2, it is possible to reformulate eq.AI. 1 in a differential form. (eq.AI. 7):

$$\frac{dp_{O_2}}{dt} = \frac{K_{OL} WH (p_{O_2}' - p_{O_2}(x))}{Q} \quad \text{eq.AI. 7}$$

which integrated allows to explicitate $p_{O_2}(x)$ (eq.AI. 8):

$$pO_2(x) = pO_2' - (pO_2' - pO_{2o}) e^{-\frac{K_{ol}WH}{Q}x} \quad \text{eq.AI. 8}$$

where pO_{2o} is the value of oxygen partial pressure entering the oxygenator tubing system, and contemporarily exiting from the bioreactor culture chamber compartment. Eq.AI. 8 shows that dissolved oxygen partial pressure increases exponentially while the tubing length increases.

Taking advantage on the compartmental approach, the value of pO_{2o} can be calculated considering the bioreactor culture chamber domain. Inside the culture chamber, the same continuous flow Q which travels within the tubing system perfuses the cellular phase, which is constantly supplied by the dissolved oxygen within the culture medium. Cellular metabolism produces a metabolic oxygen volumetric consumption Γ , which may produce a drop in oxygen partial pressure (schematized in Figure AI.3). The volumetric consumption kinetics Γ can be experimentally determined, hypothesized, or obtained from literature for each specific cell type to be cultured, and depends on the inoculated cell density within the bioreactor culture chamber (eq.AI. 9):

$$\Gamma = \frac{N_{cell}\gamma_{cell}}{V_{med}} \quad \text{eq.AI. 9}$$

where N_{cell} is the number of cells inoculated in the bioreactor chamber, γ_{cell} is the cell type-specific metabolic molar consumption rate.

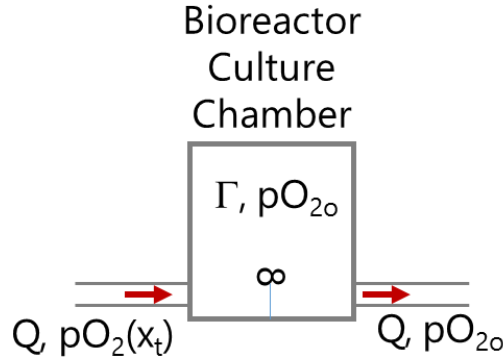


Figure AI.3: Schematic of the bioreactor chamber compartment. The amount of dissolved oxygen within the medium is homogenously consumed with a consumption kinetics Γ .

Accordingly, oxygen partial pressure exiting from the bioreactor culture chamber can be expressed as in eq.AI. 10:

$$pO_{2o} = pO_2(x_t) - \frac{N_{cell}\gamma_{cell}H}{V_{med}Q} \quad \text{eq.AI. 10.}$$

Known the oxygen depletion occurring inside the culture chamber, it is possible to combine eq.AI. 8 and eq.AI. 10 in order to explicitate the required tubing length (eq.AI. 11) to restore a specific dissolved oxygen partial pressure entering the bioreactor culture chamber $pO_2(x_t)$ (design goal).

$$x_t = -\frac{Q}{K_{OL}WH} \ln \frac{pO_2' - pO_2(x_t)}{pO_2' - pO_{2o}} \quad \text{eq.AI. 11}$$

All the parameters required as input for the model are summarized in Table AI. 1 and This model must be applied during the setup procedure of an experimental framework, in order to provide good oxygen supply to the suspended cells. As a matter of fact, the cell type metabolic features must be an a-priori knowledge or must be hypothesized before starting the dynamic culture with the bioreactor platform.

Table AI.2.

Table AI. 1: Model parameters.	
Fluid Dynamics Parameters	
H (mmHg/ μ M)	0.74
pO_2' (mmHg)	150
$pO_2(x_i)$ (mmHg)	147
t_m (cm)	0.159
W_i (cm)	1.995
W_o (cm)	2.991
W (cm)	2.459
ρ_{STP} (mol/cm ³)	4.46 x10 ⁻⁵
R(mmHg/(mM K))	6.24 x10 ⁻²
T(K)	310
P_m (cm ² /mmHg s)	7.96 x10 ⁻⁸
d_i (cm)	0.635
d_o (cm)	0.952
ρ ((g/cm ³))	1
μ (g/cm s)	0.001
$D_{o2/air}$ (cm ² /s)	0.21
$D_{o2/medium}$ (cm ² /s)	2.18 x10 ⁻⁵
Sh_{air}	0.43
k_o (cm/s)	0.094

This model must be applied during the setup procedure of an experimental framework, in order to provide good oxygen supply to the suspended cells. As a matter of fact, the cell type metabolic features must be an a-priori knowledge or must be hypothesized before starting the dynamic culture with the bioreactor platform.

Table AI.2: Overall mass transfer coefficients varying the flow rate.

Q (mL/min)	$K_{OL} \times 10^{-6}$ (mM cm/mmHg s)	$1/K_{OL} \times 10^6$ (mmHg s/mM cm)
400	2.38	0.42
300	2.06	0.48
200	1.69	0.59
100	1.20	0.84
90	1.13	0.88
80	1.07	0.94
70	1.00	1.00
60	0.93	1.08
50	0.85	1.18
40	0.76	1.32
30	0.67	1.52
1	0.13	7.89

In the following, as an explanatory example, it is described the approach adopted for the tubing sizing made up for the preliminary cell culture experiments with human induced pluripotent stem cells (h-iPSC), which will be illustrated in Chapter 4. Table AI.3 lists the characteristic metabolic parameters of h-iPSCs. This parameters were extrapolated from previous dynamic suspension culture studies carried out with conventional bioreactors [2]. Starting from the data included in the work of Olmer and colleagues [2], the number of cells considered for the tubing sizing was increased of 10 folds in order to contemplate the worst case of oxygen consumption given by high proliferation rates.

Table AI.3: Metabolic Parameters for h-iPSCs.

Consumption Model Parameters	
N_{cell}^1	300×10^6 [2]
γ_{cell} (mol/cell s)	2.40×10^{-17} [2]
V_{med} (cm ³)	50

As a result, considering the metabolic data listed in Table AI.3 it was possible to obtain the tubing length necessary to restore the dissolved oxygen partial pressure within the culture medium, varying the flow rate from 1 to 400 mL/min (Table AI.4).

Table AI.4: Tube length obtained at different flow rates.

Q (mL/min)	x_t (cm)
400	8.92
300	10.29
200	12.56
100	17.64
90	18.56
80	19.65
70	20.96
60	22.57
50	24.62
40	27.30
30	31.27
1	90.08

Oxygen Transport Computational Model

In order to predict the oxygen delivery inside the bioreactor culture chamber, the diffusion/convection transport equation for dissolved oxygen within the

¹ The number of hypothesized inoculated cells was extracted from the work of Olmer and colleagues [2] which deals with the expansion of induced pluripotent stem cells in dynamic suspension culture, and considering cell number after a 10 fold expansion.

medium flowing inside the culture chamber was solved. This equation was written in the form

$$\frac{\partial}{\partial t}(\rho Y_{O_2}) + \nabla \cdot (\rho \vec{v} Y_{O_2}) = \rho D_{O_2} \nabla^2 Y_{O_2} \quad \text{eq.AI 12}$$

where Y_{O_2} represents the dissolved oxygen mass fraction (i.e. the mass of the species per unit of mass of the culture medium in which is dissolved), D_{O_2} is the oxygen diffusivity within the culture medium ($2.55 \times 10^{-9} \text{ m}^2/\text{s}$). The diffusion/convection equation for dissolved oxygen is coupled with the Navier-Stokes equations for the culture medium by the presence of \vec{v} which is the velocity field of the culture medium within the culture chamber (eq. 1 and eq. 2 - Chapter 2) expressed for the culture medium. It was chosen to calculate a mixing condition, imposing a constant inlet of oxygen saturated culture medium ($pO_2 = 159 \text{ mmHg}$) within the initially anoxic culture medium filling the culture chamber (0 mmHg of dissolved oxygen as initial condition within the culture chamber). This configuration allows to calculate the so called 'blend time', i.e. the time to achieve a predefined level of homogeneity of a tracer in a mixing vessel. Simulations were performed with Fluent (ANSYS Inc., PA, USA). The simulated time was 840 s (14 mins), time necessary to fill the 90% of the bioreactor culture chamber with 159 mmHg of dissolved oxygen. The Second Order Upwind formulation was used to solve the momentum and oxygen transport equation. A flow rate equal to 40 mL/min was imposed by means of a flat velocity profile at the inlet port.

Figure AI.4 shows the evolution of dissolved oxygen partial pressure during the filling phase. It is possible to evaluate that in the extreme situation of fully anoxic culture medium inside the culture chamber, after around 14 mins dissolved oxygen partial pressure is replenished in about the 90% of the

culture chamber volume. This type of study is useful to emphasize the capability of the bioreactor of mixing nutrients and dissolved gasses, in particular dissolved oxygen, homogenizing the concentrations within the culture chamber. The same model can be replicated for every dissolved species within the culture medium (e.g. nutrients). In fact, since Peclet number (i.e. the ratio between convective and diffusive transport) is largely higher than unity (order of magnitude between 10^2 and 10^3 for the species diffused within the culture medium), mass transport is controlled by convection and these outcome may be generalized to all the dissolved nutrients inside the medium.

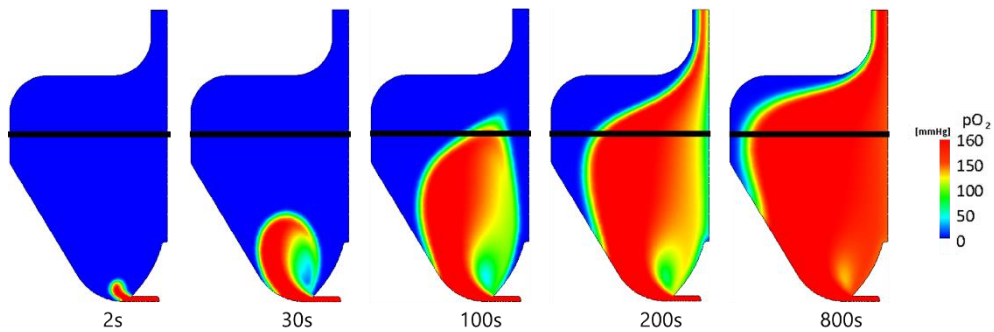


Figure AI.4: Contour plot of the oxygen partial pressure over time. In 800 s the 90 % of the culture chamber is completely saturated of oxygen.

References

- 1 Orr, D. E. and Burg, K. J. Design of a modular bioreactor to incorporate both perfusion flow and hydrostatic compression for tissue engineering applications. *Annals of Biomedical Engineering*, 36, 7 (2008), 1228-1241.
- 2 Olmer, Ruth, Lange, A., Selzer, S., Kasper, C., Haverich, Axel, Martin, Ulrich, and Zweigerdt, Robert. Suspension culture of human pluripotent stem cells in controlled, stirred bioreactors. *Tissue Engineering Part C Methods*, 18, 10 (2012), 772-784.

Appendix II

Sensors and Conditioning Circuit for Monitoring System

In this Appendix paragraph, the main components of the devised monitoring system are described. In detail, the sensors and their operating principles are treated, discussing the acquisition circuitry and hardware.

pH Sensor

For the purpose of pH measurement, it was opted for glass *combined pH electrodes* (EasyFerm Bio VP 120, Hamilton, Hamilton, Bonaduz, Figure AII.1) which are much easier to handle than two separate electrodes and are largely used for FDA approved biotechnological applications. In a combination electrode the measuring electrode is concentrically surrounded by the reference electrode (Figure AII.2).



Figure AII.1: EasyFerm Bio VP 120 pH sensor (Hamilton).

The aim of *the measuring electrode* is to determine the pH value, i.e. the concentration of active hydrogen ions (H^+) in the aqueous solution. The pH sensitive part of the measuring electrode is its tip, where the *glass membrane* is located. The glass electrode is partly filled with a buffer solution of potassium chloride (KCl), normally having a pH value of 7. A silver wire, coated

with silver chloride (Ag/AgCl) is inserted into the glass electrode right down into the inner buffer and serves as a conducting electrode. The Ag/AgCl wire is connected to one terminal of a pH meter or, as in this case study, to the data acquisition system (Figure AII.2).

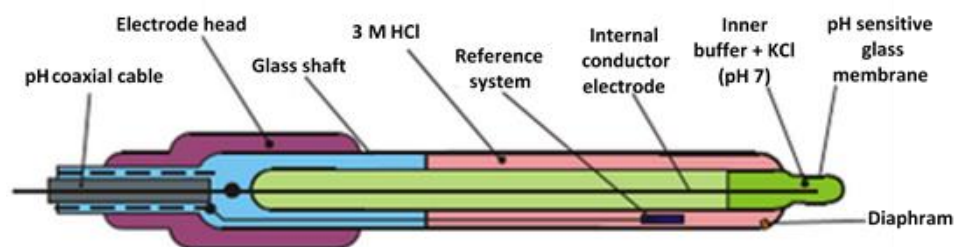


Figure AII.2: Construction of the combined electrodes. Green parts represent the measuring electrode volume, white, blue, and pink are parts of the reference electrode volume.

The glass membrane is made of special hydrogen ion sensitive glass and is fused to the measuring electrode shaft. When the membrane comes into contact with an aqueous solution, it forms a thin gel layer between the glass surface and the solution. As the inner side of the glass membrane is in contact with the inner buffer, a gel layer is also formed on the inside of the glass membrane. A continuous exchange of H^+ ions in the gel layers and H^+ ions of the solutions takes place on both sides of the membrane. This ion exchange is controlled by the H^+ ion concentration of both solutions. If the hydrogen ion concentration of each solution is identical on both sides of the glass membrane, the ion exchange stops after an equilibrium has been reached between the H^+ ions in the solutions and the H^+ ions in the gel layers. Therefore, both sides of the membrane glass have the same potential and the potential difference is 0 mV. To be able to measure the membrane potential, the membrane itself has to be conductive. This is achieved by the mobility of the alkaline ions in the membrane glass (Li^+ ions). Without the gel layer there can be no pH measurement. Therefore a measuring electrode needs to be hydrated. The

reference electrode provides a well-defined and stable reference potential to the potential acquired from the pH electrode. The data acquisition system acquires directly the differential potential between the measuring and reference electrodes as a function of pH value of the culture medium in which the probe is immersed, which is high enough to avoid preconditioning and amplification stages. Theoretically, the voltage changes linearly with a sensitivity of 56.16 mV/pH at 20°C. The voltage produced by the measuring chain can only be measured by an instrument having such a high internal resistance that it does not draw a current from the chain. To perform a correct measurement, the pH transmitter should have an internal resistance of at least 10 GΩ. The reason of this is the high electrical resistance of the glass electrode which is mainly determined by the resistance of the glass membrane (between 10 MΩ and 1000 MΩ at 25 °C) [1]. In detail, Table AII.1 lists the product specifications of the selected pH probe, including geometrical characteristics.

Table AII.1: EasyFerm BIO VP 120 pH sensor (Hamilton). Specifications.

pH Sensor Specifications	
Autoclavable	Yes
Probe Type	Combined Electrode
Measurement Principle	pH potential, with reference
Membrane Shape	Cylindrical
Diaphragms	1
Diameter	12 mm
Shaft length	120 mm
Output	Voltage
Measuring Range	0-12
Pressure Range	0 – 6 bar
Sensitivity	57 to 59 mV/pH at 25°C
Zero Point	0 ± 20 mV

Dissolved Oxygen (DO) Sensor

In order to measure the dissolved oxygen partial pressure within the culture medium, a DO sensor based on the Clark's principle was implemented in bioreactor platform (OxyFerm FDA 120 – Hamilton, Bonaduz). The Clark sensor is a polarographic oxygen sensor which consists of two electrodes, a *silver/ silver-chloride anode* and a *platinum cathode* which are both immersed into half-saturated KCl-electrolyte (Figure AII.3). The electrolyte chamber is separated from the culture medium by an O₂ permeable membrane. Oxygen molecules from the sample solution diffuse through the membrane into the electrolyte. The platinum cathode is completely insulated by a glass cylinder and only the tiny tip is exposed to the electrolyte. The dissolved oxygen is reduced at the surface of the cathode, while at the Ag/AgCl anode an oxidation produces 4 electrons which, flowing from the anode to the cathode, represent the measuring signal proportional to oxygen partial pressure in the culture medium.

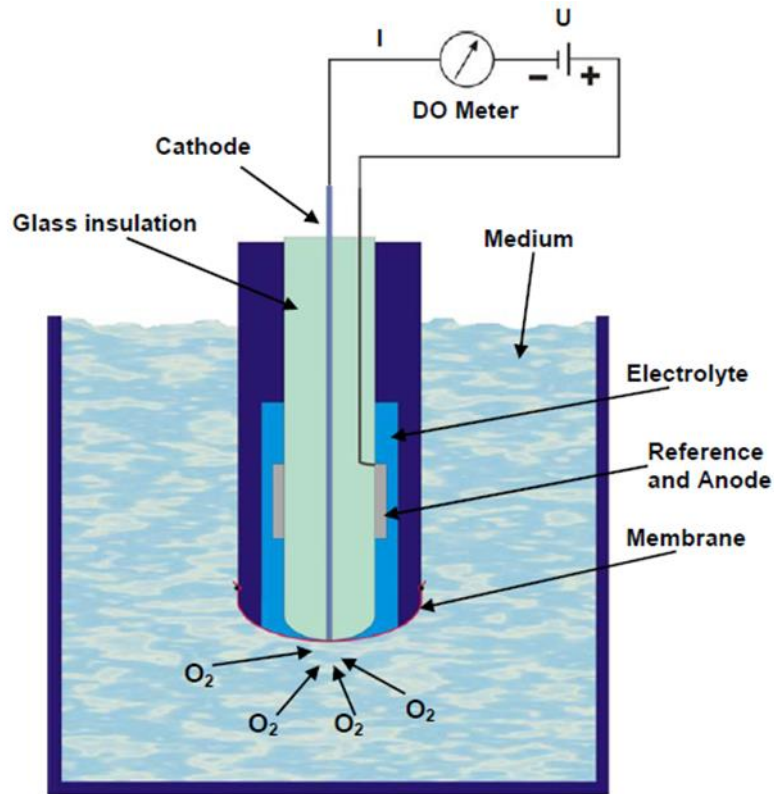


Figure AII.3: Illustration of Clark's dissolved oxygen sensor.

To start this reaction, it is necessary to polarize the electrodes with a constant polarization voltage. For Pt- Ag/AgCl electrode combination lies between -600 and 750 mV. It produces a very low current output signal which must be preconditioned and amplified.

Table AII.2, the main specifications of the selected DO sensor are listed. This sensor produces a very low current output signal which must be preconditioned and amplified.

Table AII.2: OxyFerm FDA 120 DO sensor (Hamilton). Specifications.

pH Sensor Specifications	
Autoclavable	Yes
Probe Type	Clark Electrode
Stabilizing Time	2h
Membrane Shape	Cylindrical
Diameter	12 mm
Shaft length	120 mm
Output	Current
Measuring Range	10 ppb -40 ppm of DO
Flow	min. 0.03 m/s
Current Output	40 to 80 nA at 25°C
Polarization Voltage	-670 ± 50 mV

Amplification and Current/Voltage circuit

The output signal produced by the dissolved oxygen sensor is a current signal with amplitude order of magnitude around nano-amperes. A signal conditioning circuit was designed, in order to amplify and convert the signal from current to tension before sending it to the DAQ. Contemporarily, this sensor must be polarized to produce a readable and stable signal. According to this issues, the same circuit was designed to provide the polarization voltage to the probe. The amplification circuit (Figure AII.4) was designed to produce a voltage signal ranging from 0 (0 mmHg) to 1.7 V (159 mmHg, 21% oxygen). The polarization voltage was obtained by means of a simple voltage divider to drop the supply voltage to -670 mV, as required. This voltage is connected to the sensor cathode through a buffer amplifier, implemented to stabilize the voltage signal. The sensor anode is contemporarily connected to the negative input of an operational amplifier (op amp) to be amplified and converted to a voltage signal. The op amp output is finally sent to the DAQ.

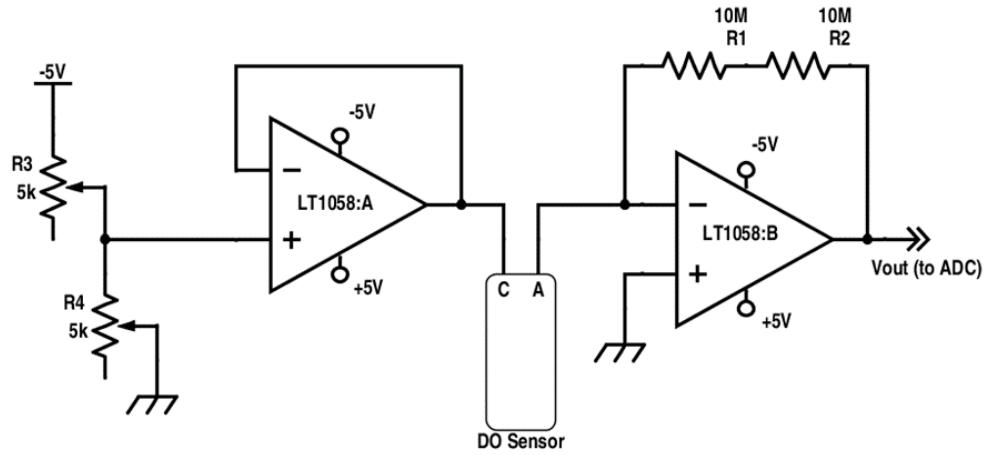


Figure AII.4: Main functional diagram of the amplification/polarization circuit.

To realize this circuit, high precision op amps were needed, because of their very low bias current. The selected op amp (LT1058, Linear Technologies, Milpitas, USA) had a maximum bias current of 50 pA, and it was implemented in an integrated circuit containing four op amps used for all the stages schematized in Figure AII.4.

The final circuit was in-house realized on a printed circuit board. Taking advantage of the numbering in Figure AII.5 the printed circuit was constituted of an integrated circuit LT1058 with four op amps (1), a positive voltage regulator with fixed output voltage of 5V (2), trimmers (3), capacitors (4), 10 M Ω resistors (5), negative voltage regulator with fixed output voltage of -5V(6), supply voltage of 12V (7), sensor connection (8), and output ADC (9).

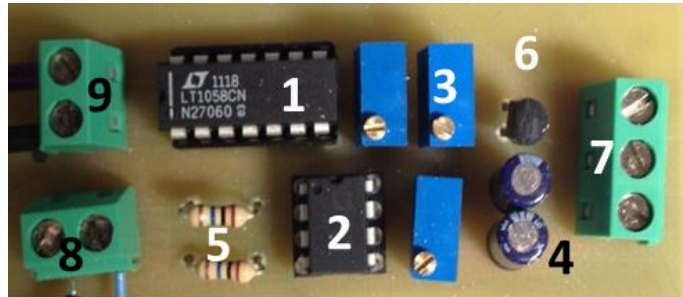


Figure AII.5: realized amplification/polarization circuit.

Monitoring System Characterization

To ensure the proper functioning of the monitoring system, the realized system was previously characterized. In detail, it was verified the stability and robustness of the measurements done with the pH and DO sensors verifying the repeatability of the signals obtained with measurement buffers. To accomplish this goal, a characterization procedure was designed, and the schematic is shown in Figure AII.6.

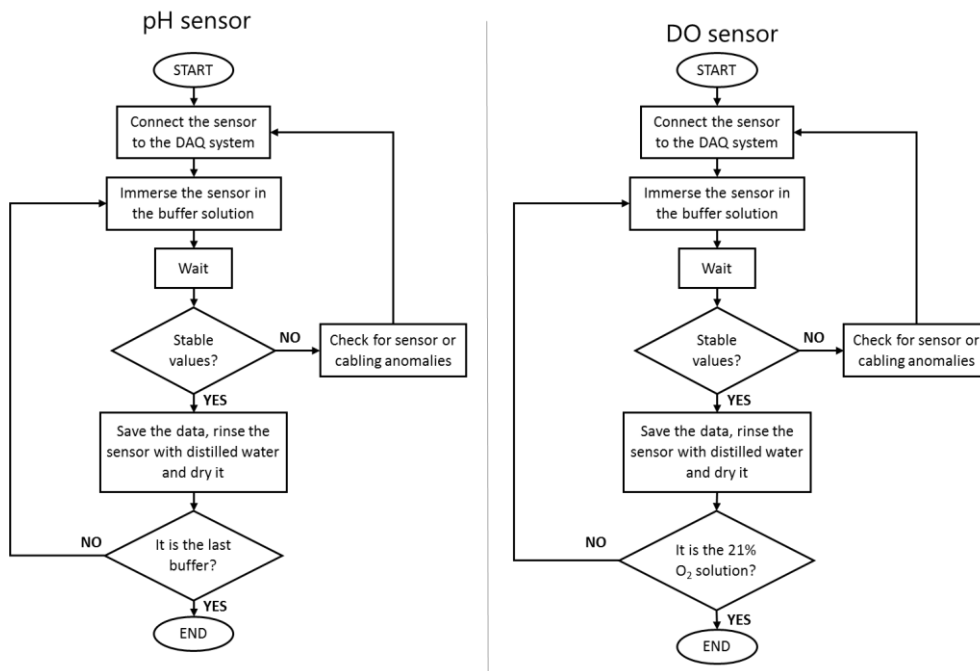


Figure AII.6: Schematic of the characterization procedure for the pH and DO sensors.

pH sensor Characterization

During the characterization procedure, when stable values of the acquired voltage signal were reached, 10 consecutive measurements were stored. Then, the software automatically calculated the average and the standard deviation of the 10 measured values. Repeating this for each pH buffer solution (for pH 4, 7, and 9), at the end of the characterization process, three voltage values were obtained. The procedure was repeated 4 times and the result of this characterization are listed in Table AII.3 and shown in Figure AII.7.

Table AII.3: Mean values and standard deviations of the output voltages from 4 tests

Voltage Values (mV)						
pH buffer	#1	#2	#3	#4	mean	st.dev.
4	173.39	178.8	174.04	164.49	172.70	5.99
7	-2.23	-1.04	-0.09	-8.69	-3.01	3.88
9	-111.51	-106.74	-100.36	-104.96	-105.90	4.61

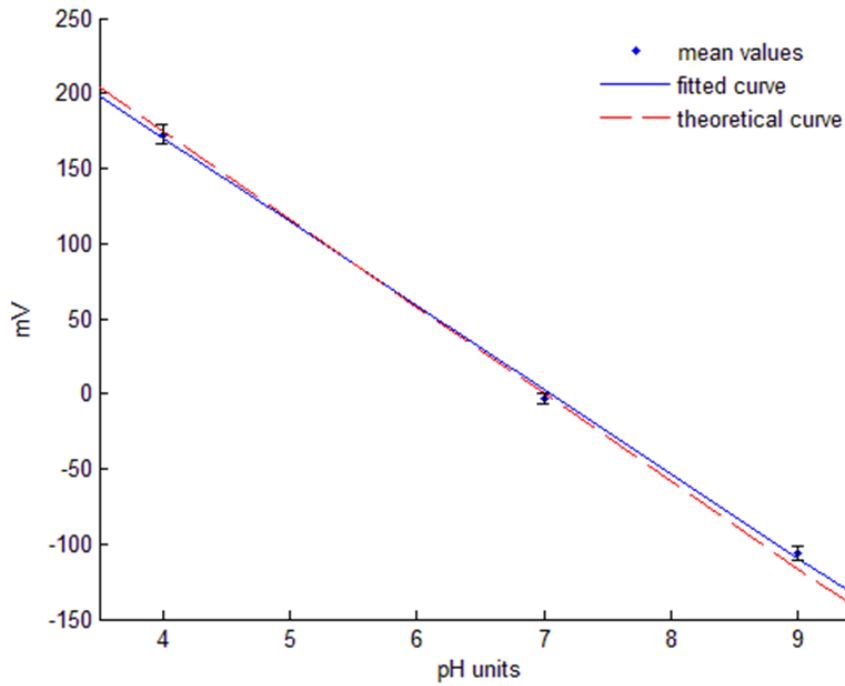


Figure AII.7: Calibration curve obtained after the characterization process.

It must be specified that, since the pH measurement is temperature dependent, the temperature influence was taken into consideration. In particular, the slope increases with the rise in temperature of the measured solution. If the calibration temperature and working temperature (37 fC) are different, then a temperature compensation is necessary. This temperature compensation is automatically performed by setting in the software the temperature solution during calibration.

DO sensor Characterization

The first characterization of the DO measurement was done using a two-point calibration. The characterization could be performed both in air and liquid (e.g. water, culture medium, etc.). The maximum oxygen mass percentage dissolvable in the culture medium is given by the environmental oxygen percentage (21%). Therefore, it was defined to consider 21% as maximum DO percentage. To expose the probe tip to 0% DO, a on purpose prepared 2% w/w bisulphite solution was used. To have a measure of the 21% DO, the sample solution was constantly aerated by environmental air to be saturated.

Since the zero current of this sensor is negligibly small, the characterization was carried out with only one point (21%), simulating the calibration phase in the bioreactor platform when, for cytotoxicity reasons, the bisulphite solution cannot be use during cell culture procedures. The results of this characterization are presented in Table AII.4 and depicted in .

Table AII.4: Mean values and standard deviations of the output voltages from 4 tests.

Voltage Values (V)						
DO buffer	#1	#2	#3	#4	mean	st.dev.
21%	1.72	1.76	1.76	1.83	1.77	0.045

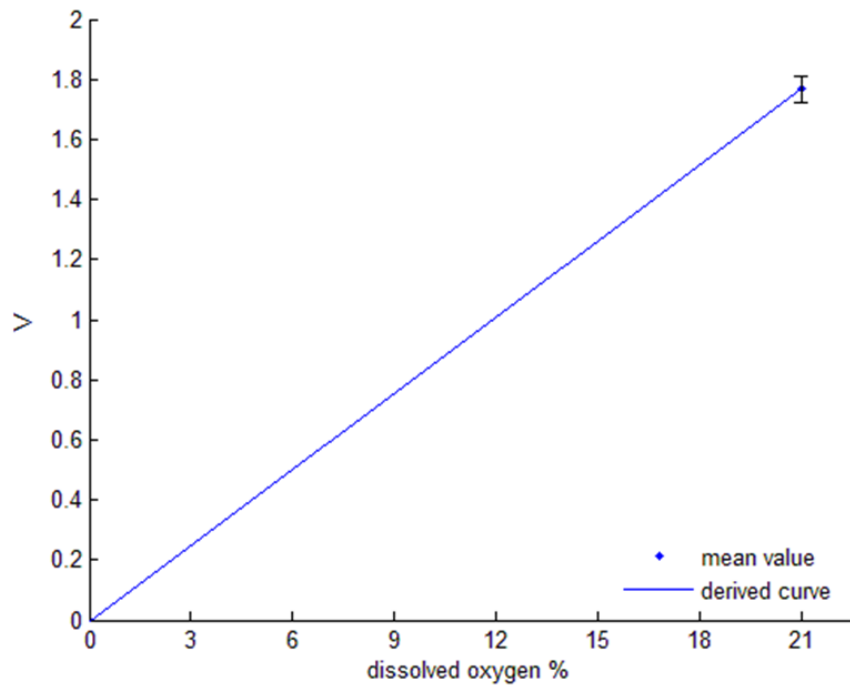


Figure AII.8: Calibration curve obtained after the DO sensor characterization.

Monitoring and Control System: Control Unit

Recalling Figure 24 of chapter 2, the monitoring and control system integrates the possibility to continuously acquire the signals from the sensors and interactively control the pump actions through a control software. This system is embedded in the control unit shown in Figure AII.9.

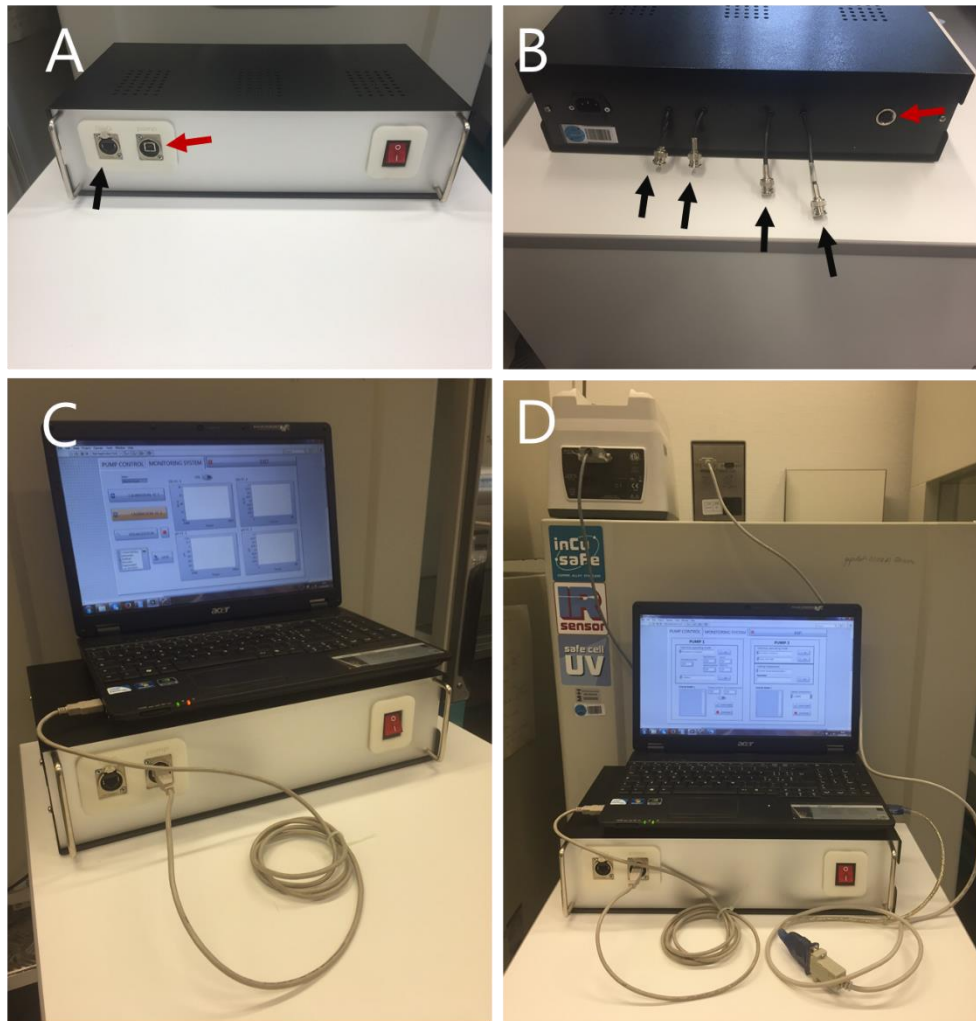


Figure AII.9: Control Unit: (A) Front and (B) rear panels. Black arrows point the connections for the monitoring system, while the red arrows indicate the connections to the pumps. Control unit connected to the dedicated PC for the control of the continuous perfusion feeding circuit (C), and entire control system connected to the pumps (D).

The control unit is connected to a dedicated PC and communicates through an in-house designed monitor and control software. In the current version of the software it is possible to interactively control the pumps for the main recirculation and the continuous perfusion feeding circuits of the bioreactor platform. The software was realized in order to allow the possibility to implement automatic algorithms for the control of the continuous perfusion feeding in response to unwanted variations of pH or DO signals.

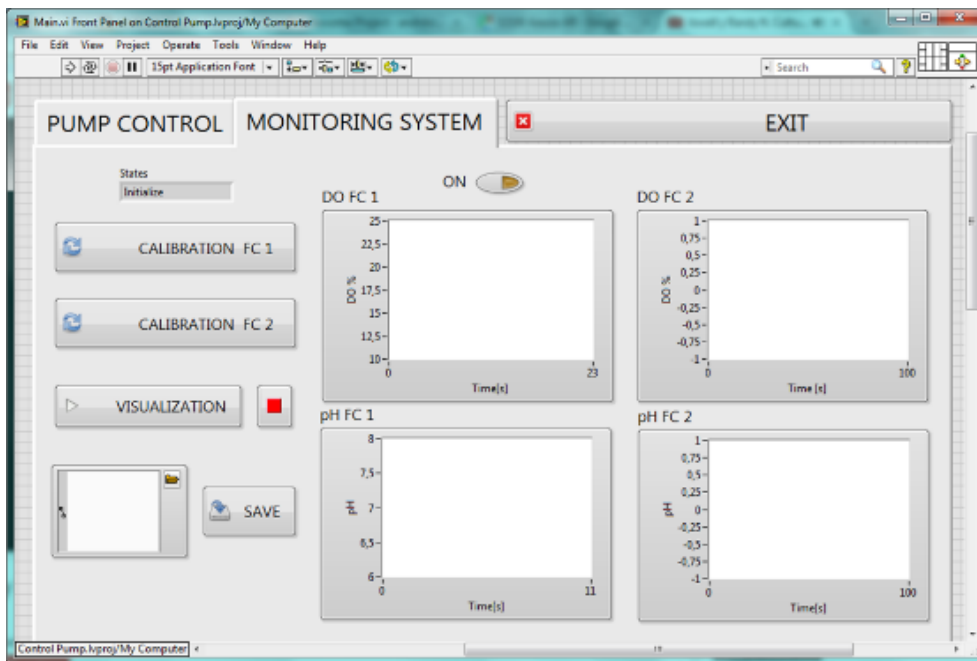
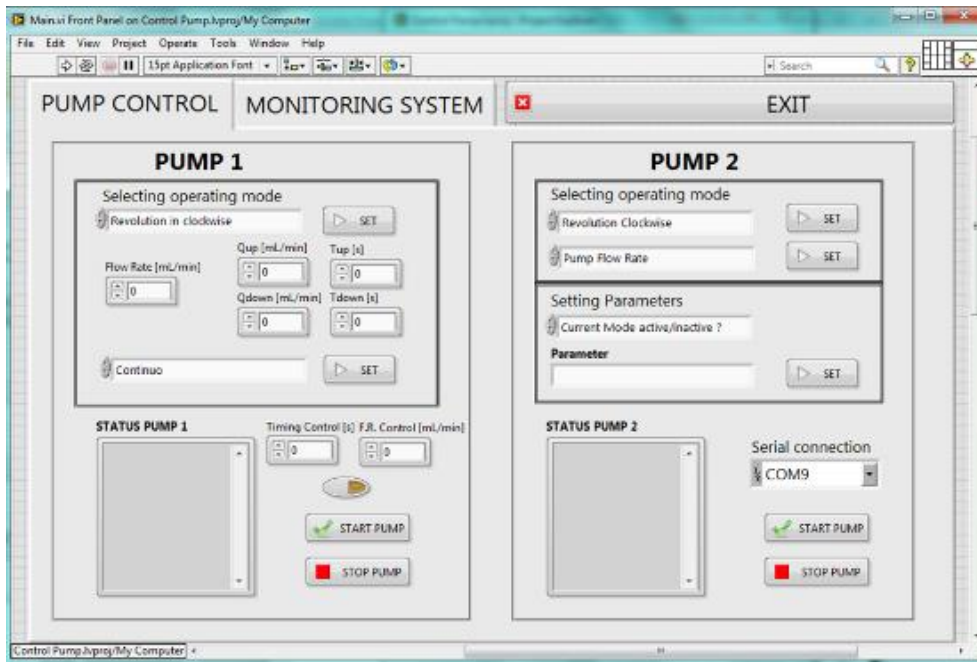


Figure AII.10: Screenshot of the realized control unit software. (top) View of the monitoring system window, and (bottom) the control system window with its dialog blocks.

Since this feature is totally cell culture-dependent, in the scope of the preliminary experiments presented in this thesis it was decided to consider

this feature without implementing any algorithm. Figure AII.10 shows a screenshot of the realized control unit software.

References

- 1 HAMILTON. pH Measurement Guide.

PART II

Chapter 3

Application to the Culture of Cancer Cell Spheroids

This chapter is the transcription of the paper “*A versatile bioreactor for Dynamic Suspension Cell Culture. Application to the Culture of Cancer Cell Spheroids*” submitted to PlosONE, and already accepted under major review. This paper described the bioreactor platform and its application to cancer cell spheroid culture. For this reason, a few parts of this chapter may repeat some general concepts about the bioreactor platform which were already reported in Chapter 2.

3.1 Introduction

The large scale production of cells is a mandatory step to set up economically viable in vitro experimental models for basic research, disease modelling and drug testing, and to definitely translate tissue engineering and regenerative medicine strategies to the clinical practice, for therapeutic applications. However, scalability and standardization in cellular manufacturing processes are still major challenges. In particular, when large numbers (10^{10} - 10^{12}) of

cells are required, conventional two-dimensional (2D) culture strategies, mainly based on manual, extremely space- and labour-intensive interventions, are practically and financially unsustainable [1-5].

In a scaling-up perspective and inspired by the manufacturing processes of therapeutics in biopharmaceutical industry [6,7], three-dimensional (3D) suspension culture has demonstrated to be an advantageous alternative to monolayer techniques for large-scale expansion of cells [4,5,8,9]. In detail, suspension methods have been widely adopted: (1) for scalable and controlled expansion of stem cells [10-14] and cancer cells [15-17]; (2) for guiding stem cell differentiation [13,18-21]; (3) for the production of cellular spheroids and tissue-like constructs [22-24]. The provision of a 3D suspension culture environment, mimicking the microenvironment of the cellular niche, has proven to be beneficial, promoting cell survival and retaining cell functional properties *in vitro* [9,25,26]. Moreover, when suspension is obtained by dynamic mixing of the culture medium, (1) the formation of gradients in, e.g., temperature, pH, dissolved oxygen, nutrients/metabolites is prevented, (2) the transport of oxygen and nutrients is increased, and (3) the sedimentation of cultured cells/constructs is avoided, thus going beyond the intrinsic limitations of static culture systems [4,7,9,28].

Nowadays, dynamic suspension culture for scalable production and differentiation of cells is mostly performed by stirred tank and rotating bioreactors [2,4]. Such devices are designed for providing a 3D homogenous culture environment and for enabling monitoring and control of culture parameters, leading to more reproducible, robust and cost-effective processes [5,28,29,30]. However, most of these bioreactors still suffer from critical issues, limiting

the upscaling and the standardization of the expansion bioprocesses. Concerning stirred tank bioreactors, their performance can be affected by (1) collisions of the cells with the impeller and (2) the onset of turbulent flow, that both can induce non-physiological mechanical and hydrodynamic-shear stresses on the cells and lead to cell damage. Moreover, these unfavourable conditions can affect cell growth rate and metabolism, interfere with stem cell pluripotency, and limit efficiency and reproducibility of the culture process [4,9,27,29,31,32]. Rotating bioreactors generate a low-shear stress culture environment, allowing to partially overcome the limitations of stirred tank devices. However, the complexity of the technological solutions adopted for rotation make these devices not easily scalable and unsuitable for continuous medium replacement and real-time monitoring [4].

We present here a versatile bioreactor suitable for tuneable shear dynamic suspension cell culture. In detail, by adopting simple technological solutions and avoiding rotating components, the proposed bioreactor enables cell suspension by assuring a laminar mixing flow regime, thus guaranteeing oxygen and nutrient transport and ultimately homogeneous culture environment under a wide range of shear stress conditions.

In order to go beyond the experimental trial-and-error approach and to reach a deeper understanding of the fluid dynamics developing inside the culture environment [33,34], the design phase of the device was supported by *in silico* multiphysics modelling, providing a comprehensive analysis of the operating principles of the bioreactor. Moreover, findings from the multiphysics simulations served as criteria to set the proper bioreactor operating conditions for preliminary *in vitro* tests. In particular, this first study was focused

on assessing the suitability of the bioreactor as ultralow shear dynamic suspension device for cancer cell spheroid culture. To this purpose, the Calu-3 human lung carcinoma cell line was subjected to ultralow shear dynamic suspension provided by the device. Our results indicate that this approach preserves cancer cell growth in vitro, including spheroid formation, and suggest the suitability of the proposed bioreactor for investigation on functional properties and for expansion of different cell types.

3.2 Materials and Methods

3.2.1 Dynamic Suspension Bioreactor

The design of the device (Figure 3.1A) was driven by two main requirements: (1) to provide dynamic suspension culture with proper mixing; (2) to guarantee a tuneable ultralow-to-moderate shear stress culture environment, adjustable on the basis of culture requirements by simply modifying operating conditions. These objectives were achieved combining the peculiar geometric features of the bioreactor culture chamber with the continuous recirculation of the culture medium, assured by a closed-loop perfusion circuit, avoiding the use of impellers and/or rotational components. This combination promotes the establishment of buoyant vortices within the culture chamber, that maintain cells/constructs in dynamic suspension, minimizing their sedimentation.

The bioreactor (Figure 3.1B, external dimensions of 95 mm x 70 mm x 70 mm) consists of: an AISI 316L base; a polycarbonate culture chamber for housing the cells/constructs (chamber volume = 75 mL); a polycarbonate lid. The internal wall curvature and shape of the culture chamber were designed

and optimized for the generation of buoyant vortices for specimen suspension (as detailed in the following). Suspended cells/constructs are confined inside the culture chamber by means of the presence of (1) an AISI 316L unidirectional check valve (which prevents backflow and guarantees a symmetric flow inlet), and (2) a culture medium-permeable filter (Duraporeff, MerckMillipore, Germany), which prevents accidental outputs of cells. The bioreactor is part of a closed loop perfusion circuit for the recirculation of oxygenated culture medium (Figure 3.1C). Such perfusion circuit is composed of a medium reservoir, oxygen-permeable tubes with quick-disconnect couplings, and a peristaltic pump (Masterflex L/Sff, Cole-Parmer, IL, USA), for a total working volume of approximately 200 mL. To guarantee the adequate supply of oxygen within the culture chamber, the perfusion circuit was sized using an analytical oxygen mass balance model in accordance with Orr et al. [35].

The functioning principle of the bioreactor is based on the continuous recirculation of the culture medium inside the culture chamber under laminar flow regime, obtained through the modulation of the perfusion circuit flow rate, in order to produce from ultralow to moderate shear stress dynamic suspension conditions. In detail, the medium flows through the check valve, driven by the peristaltic pump against the static pressure gradient, and pervades the culture chamber. Successively, the medium passes through the filter and flows out from the lid, moving back to the reservoir in a continuous closed-loop process. The formation of buoyant vortices inside the culture chamber allows the dynamic suspension of the cultured cells/constructs.

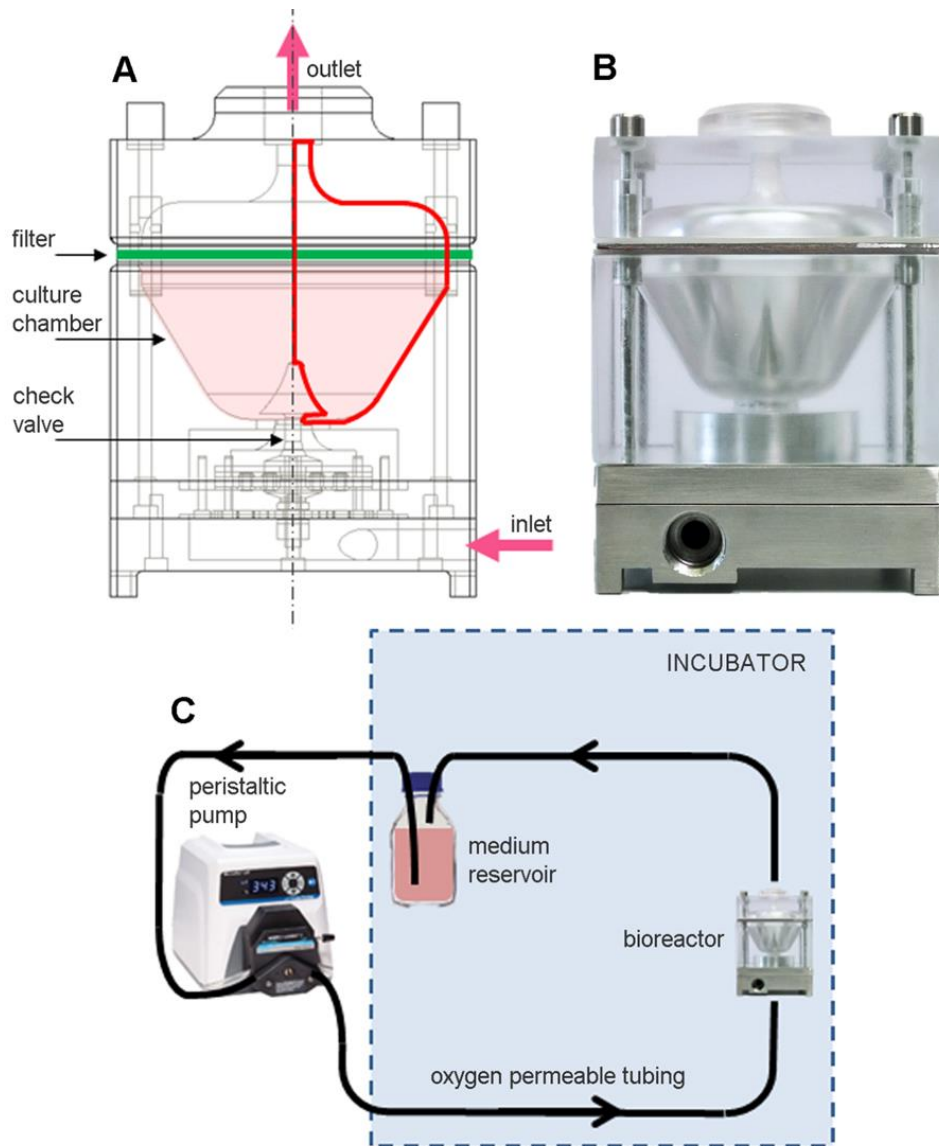


Figure 3.1: Dynamic suspension bioreactor. (A) Schematic draw of the bioreactor showing its internal components and its axial symmetry (red lines). (B) Picture of the bioreactor. (C) Schematic representation of the set-up of the bioreactor connected to the closed loop perfusion circuit.

3.2.2 Computational model

A computational multiphysics approach supported the design and the optimization phases of the device, allowing the identification of (1) the optimal

geometry of the culture chamber, and (2) the operating conditions for dynamic suspension cell culture. A massive number of simulations was performed varying cell/construct dimensions (in terms of their diameter) and highly dilute cell inoculation densities, in order to study the sensitivity of the fluid flow within the chamber volume to these culture parameters.

Technically, taking advantage of the axial-symmetry of the device (Figure 3.1A), a set of axisymmetric time-dependent numerical simulations was carried out using a customized finite volume technique-based commercial software (FLUENT, ANSYS Inc., PA, USA). The fluid domain was discretized using ICEM CFD software (ANSYS Inc., PA, USA). A mesh cardinality equal to 6.5×10^3 quadrilateral cells was considered. As in previous studies [20,36], the concomitant presence of culture medium and cells was modelled using the

Eulerian–Eulerian Multiphase Model, which allows mixtures of multiple separated yet interacting phases of a continuum to be described. For each phase the governing equations of motion, the Navier–Stokes equations, were solved by the numerical solver. The culture medium, considered as the primary phase, was assumed to be Newtonian with physical properties (dynamic viscosity = 1×10^{-3} Pa·s, density = 1000 kg/m³) of culture media typically used in cell culture applications [20]. Suspended cells, considered as the secondary immersed phase, were modelled as non-deformable spherical beads. In the explanatory example reported in this work, a density equal to 1070 kg/m³ [37] and an average diameter equal to 20 μm (i.e. the measured diameter of Calu-3 cancer cells) were considered. The presence of the filter was modelled as a porous medium characterized by a value of Darcy hydraulic resistance

equal to $96 \times 10^4 \text{ m}^{-2}$ for the culture medium and setting the maximum hydraulic resistance accepted by the solver ($1 \times 10^{20} \text{ m}^{-2}$) for the cells, having the filter an average pore size of $5 \mu\text{m}$, thus being impermeable to them. Cell inoculation was assumed to be uniform in the lower region of the culture chamber. This assumption was translated into the computational framework prescribing, as initial condition, a uniform volume fraction (VF) occupied by the cells (the secondary phase) in the lower vessel region (10 mL, in the explanatory example using Calu-3 cell line). Simulations were carried out considering always highly dilute suspension cultures (Stokes numbers greatly lower than 1, VF lower than 1%), for which variations in initial VF do not affect markedly the primary phase flow field. As an indicative limit value for sedimentation, a value of VF higher than 20% was considered, corresponding to approximately one third of the maximum packing limit of 63%, i.e., the packing limit for non-deformable spherical beads regularly packed [20]. Simulations were extended over flow rate values in the range 5 - 120 mL/min, with a simulated culture time equal to 60 min, which was considered sufficient to fully describe the dynamics of the medium inside the culture chamber. The phase-coupled SIMPLE scheme was used for the pressure-velocity coupling. The Second order upwind and the QUICK formulation were used for the spatial discretization of the momentum and the secondary phase transport, respectively.

3.2.3 *In vitro* cell culture

The performance of the bioreactor was explanatory tested in the ultralow shear stress dynamic culture frame (imposing a flow rate of 5 mL/min), as identified from the *in silico* analogue of the *in vitro* experiment (see Results). The Non Small Cell Lung Cancer (NSCLC) cell line Calu-3 (American Type

Culture Collection, ATCC, VA, USA) was selected and the results of the dynamic culture were compared to a static suspension culture control. More in detail, cells were grown in complete medium Dulbecco's Modified Eagle Medium (DMEM, Sigma Aldrich, MO, USA) added with 10% Fetal Bovine Serum (FBS), 1% Penicillin/Streptomycin (P/S) and 1% Non-Essential Amino Acids (NEAA, Sigma Aldrich, MO, USA), and maintained under standard cell culture conditions at 37°C in a water-saturated atmosphere of 5% CO₂ in air. Following expansion in cell culture flasks, 9x10⁶ Calu-3 cells (1.92 x 10⁵cell/mL) were inoculated within the culture chamber and cultured for 5 days in dynamic suspension with complete growth medium. The bioreactor was operated at a flow rate of 5 mL/min. In parallel, Calu-3 cells were seeded at the same density on low attachment culture flasks (Corning Inc., NY, USA) and used as control, representing a model of static suspension culture. After 5 days, dynamic and static suspended cultured cells were rescued from the bioreactor and from the low attachment culture flask, respectively, re-suspended in fresh growth medium and analyzed by inverted microscope (Olympus CK40, Japan). Three independent static and dynamic suspension cultures were carried out.

3.2.4 Assessment of *In vitro* cell culture

Calu-3 cells were collected and processed for Transmission Electron Microscopy (TEM) analysis and for immunocytochemistry. For TEM analysis, Calu-3 cells rescued from the bioreactor and from the low attachment culture flask were fixed in Karnovsky solution (4% formaldehyde, 5% glutaraldehyde). Samples were postfixated in 1% osmium tetroxide and dehydrated by

increasing concentration of alcohol. Then, samples were washed with propylene oxide and embedded in epoxy resin. Sections of 0.5 μm thickness were stained with methylene blue and safranin to morphologically select the field of interest. Subsequently, ultrathin sections were collected on a 300-mesh copper grid and, after staining with uranyl acetate and lead citrate, were qualitatively examined under TEM (Philips EM 208S, The Netherlands). To evaluate the fraction of cells in active cell cycle and the presence of reversible DNA double strand breaks, cells were fixed with 4% paraformaldehyde and cytocentrifuged on a glass slide to obtain a density of 105 cells per spot. Cell spots were stained by anti-Ki67 (Ki67, mouse monoclonal, DAKO, Italy) and anti-gamma histone H2AX (γH2AX , rabbit polyclonal, Bethyl Laboratories, TX, USA) antibodies and revealed by DAB (3,3'-diaminobenzidine) Peroxidase (HRP) Substrate Kit reaction (DAKO, Italy). The quantitative assessment of the fraction of Ki67 and γH2AX positive cells was carried out by computing the number of positive nuclei over a total of 900-2000 nuclei counted on each analyzed sample. Data were analyzed using the one-way ANOVA test. Results were considered statistically significant when $p < 0.05$.

3.3 Results

3.3.1 Flow dynamics within the bioreactor culture chamber

Multiphysics numerical simulations allowed to characterize the flow field inside the culture chamber. Figure 3.2 depicts diagrammatic representations of the typical medium flow structures establishing inside the culture chamber, resulting from the mutual interaction between the medium (primary phase) and the cells/constructs (dispersed phase), depending on the imposed flow

rate. In detail, in case of flow rate values lower than 20 mL/min (Figure 3.2A and 3.2C), the medium streaming into the culture chamber through the valve has not sufficient energy to interact markedly with the side wall of the culture chamber. The balance between hydrodynamic and gravitational forces leads to the formation of a dynamic big buoyant vortex located far from the wall of the chamber. This buoyant vortex is surrounded by smaller vortical structures located closer to the wall, which assure the suspension of the cultured cells and increase mixing and transport.

As an example, Figure 3.3 shows the time evolution of the VF occupied by suspended cells inside the culture chamber, obtained simulating the presence of 9×10^6 inoculated cells (initial VF = 0.48%) and imposing a flow rate value of 5 mL/min (ultralow shear stress condition, similarly to the experimental *in vitro* test). It can be observed that cultured cells are maintained mostly uniformly distributed in the bottom part of the culture chamber. In detail, after a transient of about 5 min, the 95.3% of the inoculated cells are suspended at an average VF value of approximately 0.33%, which is close to the initial VF value (0.48%), with the peak of probability density function (PDF) value equal to 2.5, corresponding to VF values between 0 and 0.5% (Figure 3.4A). At the bottom of the culture chamber, a small volume of about 194 μL is characterized by a VF value around 6%, which dynamically involves only the 2% of the inoculated cells. This packing value is more than three times lower than the threshold value of sedimentation we set (20%) and about ten times lower than the maximum packing limit of 63%. Notably, when a flow rate lower than 20 mL/min is adopted, the distribution of shear stress values experienced by the cells within the culture chamber reveals that the highest shear stress levels are lower than 1 mPa (Figure 3.4B), with mean

and median values close to 1×10^{-2} mPa (the so called ultralow shear stress condition).

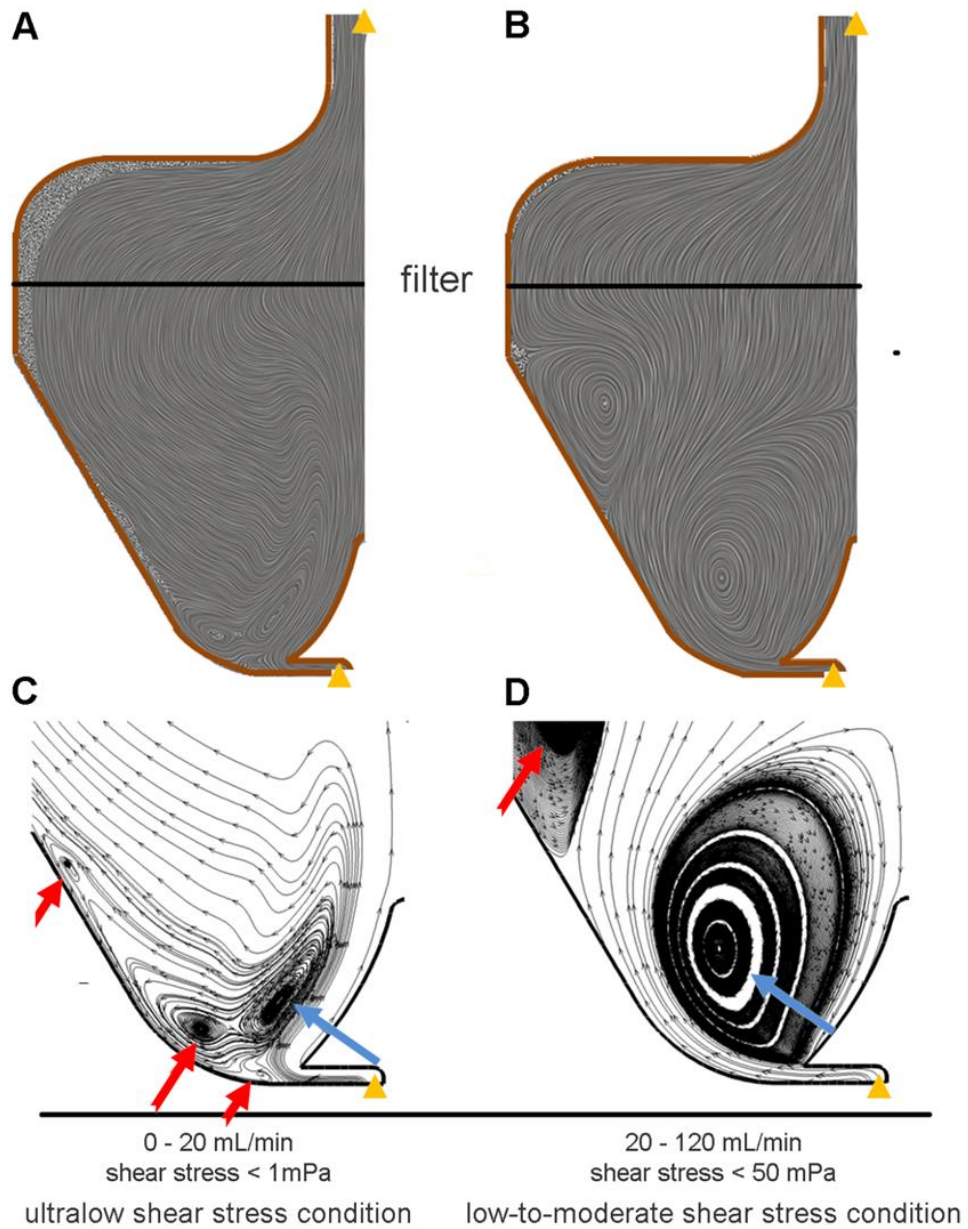


Figure 3.2: Flow field within the bioreactor. Flow field visualization of the mutual interaction between the medium (primary phase) and the cells/constructs (dispersed phase) within the culture chamber for ultralow (A and C) and moderate (B and D) shear stress conditions. Flow field is depicted using both linear integral convolution lines (A and B), and a classical streamline representation (C and D).

Increasing the flow rate beyond 20 mL/min promotes the occurrence of Coanda effect [38] within the culture chamber: the jet entering the culture chamber is attracted to the nearby wall and, due to the peculiar wall curvature, a separation region occurs far from the bottom wall of the chamber. As a result, a large clockwise buoyant vortex (Figure 3.2B and 3.2D), which counterbalances the gravitational force and thus maintains cells/constructs in suspension, is generated. Near the outer wall, a further smaller vortex develops, which can play the beneficial role of enhancing the mixing and the suspension of floating constructs (Figure 3.2D). Adopting such a flow rate range (30-120 mL/min), skewed right shear stress distributions were obtained, with mean values ranging from 2 to around 7 mPa, with peak shear stress values within the culture chamber lower than 50 mPa.

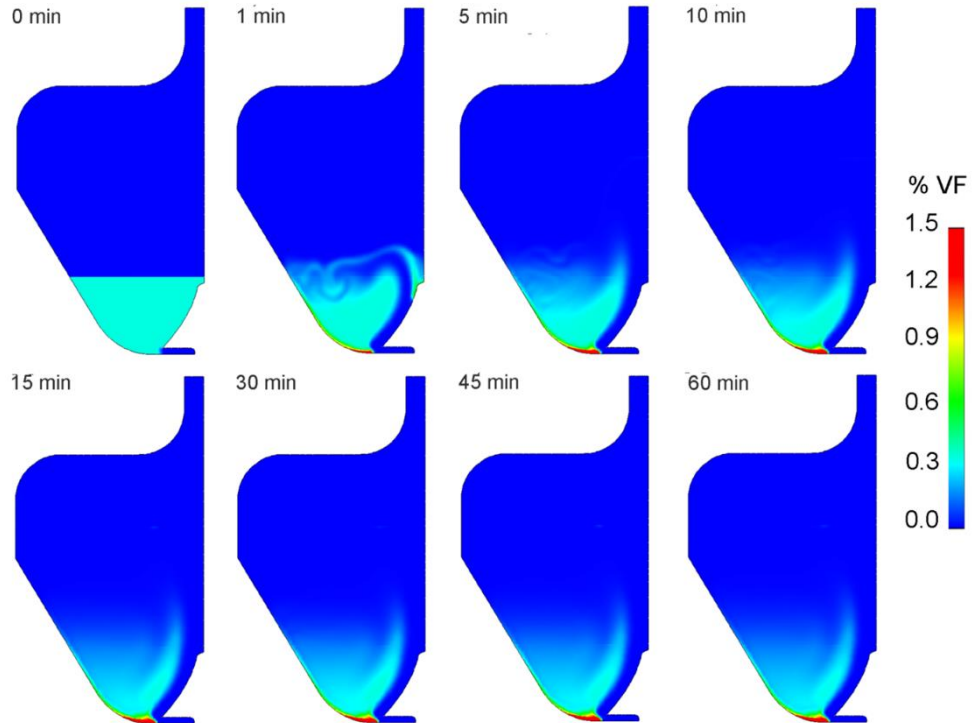


Figure 3.3: Temporal evolution of the volume fraction. Temporal evolution of the VF distribution inside the culture chamber during 60 min of simulated time, with imposed 5 mL/min and 9×10^6 inoculated cells.

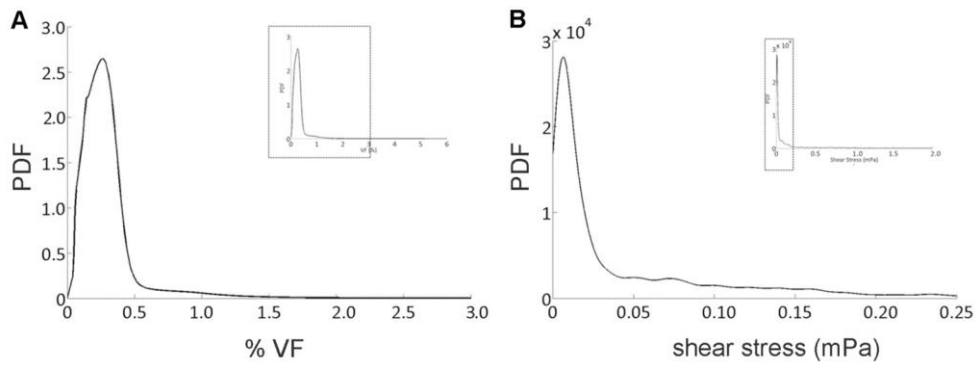


Figure 3.4: Probability density functions of volume fraction and shear stresses. Probability density function (PDF) of cell VF (A), and of shear stresses values (B) experienced by the cellular phase within the culture chamber after 60 min, with imposed 5 mL/min and 9×10^6 inoculated cells.

3.3.2 *In vitro* culture outcome

After 5 days of suspension culture, cells were rescued from the low attachment culture flask (static suspension) and from the bioreactor culture chamber (dynamic suspension). Firstly, they were morphologically analyzed: observed by phase contrast microscopy, Calu-3 cultured under static suspension show individual cells or very small clusters (Figure 3.5A), while cells cultured within the bioreactor under dynamic suspension clearly show the formation of spheroids (Figure 3.5B).

Moreover, ultrastructural analysis by TEM allows to observe that Calu-3 from static suspension are partially connected by weak and tiny adherence junctions (Figure 3.7A and 3.7B), with morphological alterations (Figure 3.6). Conversely, the clusters harvested from the bioreactor culture chamber are composed by several cells and are characterized by the typical morphological features of Calu-3, such as prominent nucleoli and membranes microvilli (Figure 3.7C), with well-developed adherence junctions (Figure 3.7D).

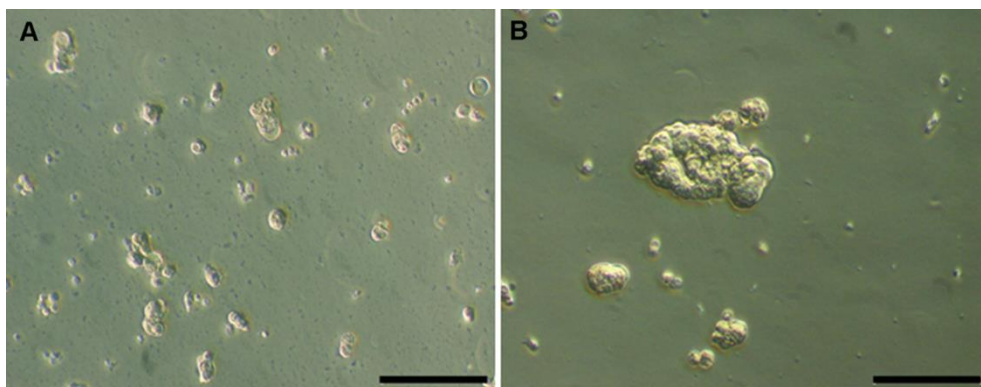


Figure 3.5: Morphological comparison by phase contrast microscopy. After 5 days of suspension culture, (A) Calu-3 cells cultured in static suspension show individual cells or very small clusters, (B) Calu-3 cells cultured under dynamic suspension show the formation of spheroids. Scale bars 200 μ m.

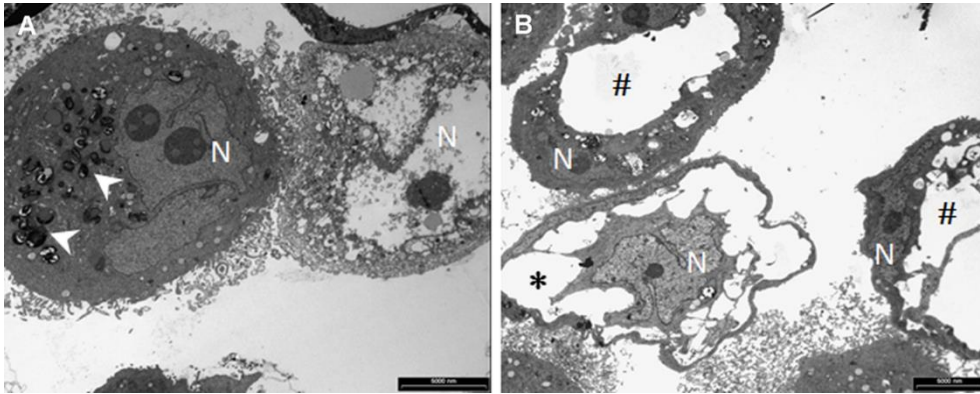


Figure 3.6: Morphological alterations of Calu-3 cells cultured under static suspension. The TEM images of Calu-3 cells cultured under static suspension conditions show A) the presence of both several autophagosomes (white arrowheads) in a cell with preserved ultrastructure and severe depletion of cytoplasmic and nuclear (N) structures in a nearby cell; B) the partial loss of cytoplasmic organelles (*) together with the formation of large vacuoles (#). Scale bars 5 µm.

These observations are supported by the assessment of Ki67 immunostaining, which indicates that the fraction of cycling Calu-3 cells is significantly higher (1.58-fold increase) when cultured in dynamic rather than in static suspension conditions (Figure 3.8A). Furthermore, from the quantification of the DNA double strand breaks, it is possible to note a downward trend (1.5-fold reduction, even if not statistically significant) in the fraction of γ H2AX_{pos} for Calu-3 cells cultured within the bioreactor compared to the cells cultured under static suspension (Figure 3.8B).

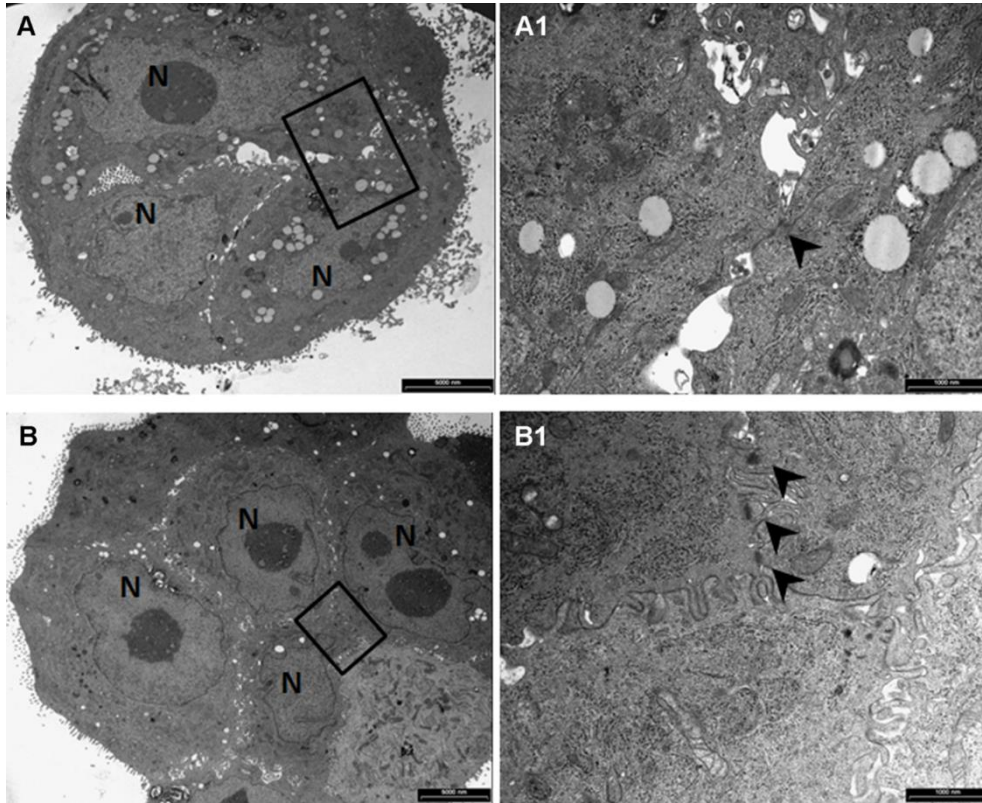


Figure 3.7: Ultrastructural comparison by TEM. The TEM images show (A) a small cluster (3 cells) of Calu-3 cells grown in static suspension and (C) a larger spheroid (9 cells) of Calu-3 cells cultured within the bioreactor, harvested both after 5 days of suspension culture. Prominent nucleoli (N: nuclei), cytoplasmic structures and longitudinally and transversally oriented microvilli are characteristic features of NSCLC cell line Calu-3. High magnification views of areas included in black rectangles in panels A and C shown, respectively, (B) a single tiny adherence junction (arrowhead) among cells cultured under static suspension, and (D) several well-developed adherence junctions (arrowheads) developed by Calu-3 cultured within the bioreactor. Scale bars: A and C = 5 μm ; B and D = 1 μm .

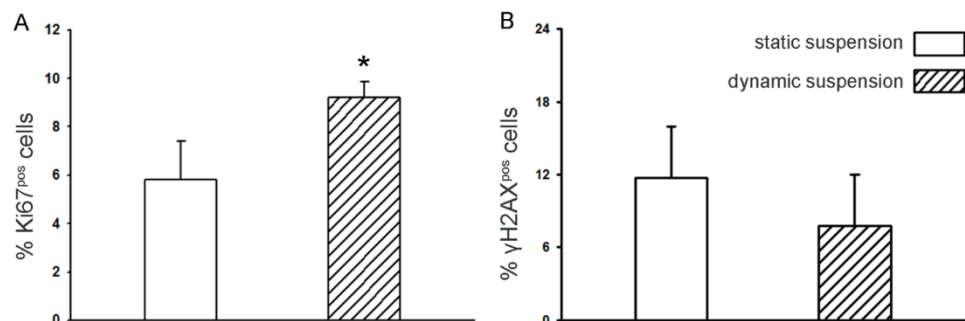


Figure 3.8: Quantitative comparison of cycling cells and double DNA strand breaks. (A) Bar graph of the measurement of Ki67 positive cells, showing the fraction of cycling Calu-3 cells after static and dynamic suspension culture (*: $p < 0.05$ vs static suspension). (B) Bar graph of the measurement of γ H2AX positive cells, quantifying the double DNA strand breaks in Calu-3 cells harvested from static and dynamic suspension culture.

3.4 Discussion and Conclusion

In this study, a versatile bioreactor for culturing cells in dynamic suspension is presented. Due to the combination of the peculiar shape of the culture vessel with the continuous recirculation of the culture medium within a closed-loop perfusion circuit, this bioreactor enables laminar dynamic suspension culture at tuneable ultralow-to-moderate shear stress values. Avoiding the use of impellers and/or rotational components, the presented device overcomes some major limitations of the current dynamic suspension methods. In fact, it is well established that within the stirred systems (e.g., spinner flasks, stirred tank bioreactors) (1) the interaction of cells with the moving components, and (2) the complex fluid dynamics, characterized by turbulence and/or detrimental shear stresses, could lead to cell damage and consequent low expansion efficiency and limited bioprocess reproducibility [4,9,27,29,31,32]. Differently, rotating bioreactors provide laminar, low-shear stress culture environments, but the complex technological solutions needed to impart rotation make them not easily scalable and unsuitable for continuous medium replacement and real-time monitoring [4]. In this context, an

impeller-free dynamic suspension bioreactor, characterized by laminar, ultralow-to-moderate shear flow within the culture vessel and based on simple technological solutions, has been (1) designed, (2) characterized and optimized by means of computational multiphysics, (3) prototyped, and (4) experimentally tested for dynamic suspension cell culture.

More in detail, multiphysics modelling allowed to optimize the design of the device in terms of its performance in establishing dynamic suspension of biological specimens at low shear stress levels. By selecting the operating flow rate and exploiting the geometric features of the culture chamber, the device enables to provide dynamic cell suspension conditions at different shear stress levels, from ultralow (less than 1 mPa) to moderate (less than 50 mPa) values. The computational modelling allowed to define two main flow conditions for culturing cells: (1) the ultralow shear stress condition, obtained working with flow rates in a range up to 20 mL/min (Figure 3.2A); and (2) the low-to-moderate shear stress condition, which can be established working with flow rates in the range 20 - 120 mL/min, characterized by the formation of larger suspension buoyant vortices (Figure 3.2C). Adopting flow rates under 20 mL/min, shear stress values lower than 1 mPa develop within the culture chamber (ultralow shear stress condition, Figure 3.4B), while increasing the flow rates up to 120 mL/min, skewed right shear stress distributions are obtained, with mean values ranging from 2 to around 7 mPa (low-to-moderate shear stress condition). The (tuneable) shear stress values produced by this dynamic suspension bioreactor are (1) one order of magnitude lower than the shear stress values normally developing within a commercial spinner flask where, imposing agitation rates ranging from 15 to 50 rpm, mean shear stress values ranging from 20 to around 120 mPa are reached (with peak values

reaching 200 mPa) [39], and (2) some orders of magnitude lower than the reference shear stress value considered critical (250 mPa) for sensitive cells like human embryonic stem cells or neonatal rat cardiomyocytes [32].

Furthermore, the presence of laminar, dynamic vortex structures within the culture chamber promotes nutrient mixing and transport, as well as cell transport during dynamic suspension.

Lung tumour-derived epithelial cell line (Calu-3) was selected for the preliminary test under ultralow shear stress conditions because of the property to form multicellular spheroids, typically used for investigation of lung cancer biology and ontogeny of epithelial tissues *in vivo* [40]. The biological findings coming from the culture of Calu-3 cancer cells in ultralow shear stress dynamic suspension confirm that with the use of the presented device (1) suspension is ensured (no sedimentation was observed), (2) the formation of functional 3D cell aggregates with active intercellular connection is promoted (Figure 3.5 and 3.7), and (3) a culture environment is established that, in comparison to the static suspension control, increases the cycling cell number and reduces the double strand DNA damage (Figure 3.8).

Some limitations could weaken the potential of the presented bioreactor in 3D culturing cells in suspension. As the bioreactor is at a prototypal stage, the operating flow rates are currently manually set through the peristaltic pump of the perfusion circuit. However, a control system for process automation can be easily integrated in the loop. Moreover, direct sampling and/or monitoring are currently not feasible during bioreactor functioning. In the future, the perfusion circuit will be equipped with specific sensors, upstream

and downstream the bioreactor chamber, in order to provide real-time information about the metabolic behaviour of cultured cells. Concerning the computational multiphysics approach, a main limitation is that the aggregation and disaggregation of the cultured cells/constructs are not considered in the model, since the biological sample size was assumed to be always equal to the initial cell dimension (20 μm). This choice was dictated by a primary interest in assessing the fluid dynamics inside the culture chamber at the very early stage of the culture process, when it is fundamental to ascertain the suspension/sedimentation of the cells, and giving indications on the initialization of the experimental procedure. Therefore, since aggregation and disaggregation phenomena have typical characteristic time of days, they were neglected in the simulation provided in this paper. Moreover, cell growth has not been included in the numerical model since it was assumed that for the time interval considered for the simulation, the cell growth could be neglected.

Although these limitations could weaken the findings of this study, the herein presented combination of outputs of the *in vitro* experiment and the corresponding *in silico* simulation has demonstrated the potential of the device in culturing cells in 3D dynamic suspension at low shear stresses. In particular, the *a priori* knowledge (from simulations) on the flow environment inside the bioreactor culture chamber employed for culturing Calu-3 cells in dynamic suspension allowed to obtain a more favourable condition to cancer cells aggregation than the static suspension control.

In conclusion, here we proposed a suspension bioreactor design, conceived to create a unique fluid dynamic environment inside the culture chamber avoiding any moving component. By adopting simple technological solutions,

the presented versatile bioreactor allows to culture specimens of different dimensions in laminar, dynamic suspension over a range of shear stress conditions, finally allowing to overcome major limitations of the current dynamic suspension devices [4,9,27,29,31,32].

In the future, such a device could be considered to be used: (1) as model system, for investigating the influence of dynamic suspension conditions on different types of cells/constructs; (2) as aggregation system, for culturing and investigating cell clusters; (3) as expansion and differentiation system, e.g., for expansion and differentiation of stem cells, for which non-physiological shear stress values can affect maintenance of pluripotency and interfere with lineage-specific differentiation, thus providing a low-shear culture condition that could significantly increase the bioprocess efficiency and reproducibility.

Acknowledgments

This work was carried out in collaboration with prof. Federico Quaini's group of Università degli Studi di Parma.

References

- 1 Lee J, Cuddihy MJ, Kotov NA. Three-dimensional cell culture matrices: state of the art. *Tissue Eng Part B Rev.* 2008;14(1): 61-86.
- 2 Godara P, McFarland CD, Nordon RE. Design of bioreactors for mesenchymal stem cell tissue engineering. *J Chem Technol Biotechnol.* 2008;83: 408-420.
- 3 Maherali N, Hochedlinger K. Guidelines and techniques for the generation of induced pluripotent stem cells. *Cell Stem Cell.* 2008;4;3(6): 595-605.
- 4 Rodrigues CA, Fernandes TG, Diogo MM, da Silva CL, Cabral JM. Stem cell cultivation in bioreactors. *Biotechnol Adv.* 2011;29(6): 815-29.
- 5 Kumar A, Starly B. Large scale industrialized cell expansion: producing the critical raw material for biofabrication processes. *Biofabrication.* 2015;7(4): 044103.
- 6 Warnock JN, Al-Rubeai M. Bioreactor systems for the production of biopharmaceuticals from animal cells. *Biotechnol Appl Biochem.* 2006;45: 1-12.
- 7 dos Santos FF, Andrade PZ, da Silva CL, Cabral JM. Bioreactor design for clinical-grade expansion of stem cells. *Biotechnol J.* 2013;8(6): 644-54.
- 8 King JA, Miller WM. Bioreactor Development for Stem Cell Expansion and Controlled Differentiation. *Curr Opin Chem Biol.* 2007;11(4): 394-398.
- 9 Zweigerdt R. Large scale production of stem cells and their derivatives. *Adv Biochem Eng Biotechnol.* 2009;114: 201-35.
- 10 Baghbaderani BA, Behie LA, Sen A, Mukhida K, Hong M, Mendez I. Expansion of human neural precursor cells in large-scale bioreactors for the treatment of neurodegenerative disorders. *Biotechnol Prog.* 2008;24(4): 859-70.
- 11 Amit M, Chebath J, Margulets V, Laevsky I, Miropolsky Y, Shariki K, et al. Suspension culture of undifferentiated human embryonic and induced pluripotent stem cells. *Stem Cell Rev.* 2010;6(2): 248-59.
- 12 Olmer R, Lange A, Selzer S, Kasper C, Haverich A, Martin U, Zweigerdt R. Suspension culture of human pluripotent stem cells in controlled, stirred bioreactors. *Tissue Eng Part C Methods.* 2012;18(10): 772-84.
- 13 Kempf H, Olmer R, Kropp C, Rückert M, Jara-Avaca M, Robles-Diaz D et al. Controlling expansion and cardiomyogenic differentiation of human

- pluripotent stem cells in scalable suspension culture. *Stem Cell Reports*. 2014;3(6): 1132-46.
- 14 Zweigerdt R, Olmer R, Singh H, Haverich A, Martin U. Scalable expansion of human pluripotent stem cells in suspension culture. *Nat Protoc*. 2011;6(5): 689-700.
 - 15 Youn BS, Sen A, Behie LA, Girgis-Gabardo A, Hassell JA. Scale-up of breast cancer stem cell aggregate cultures to suspension bioreactors. *Biotechnol Prog*. 2006;22;3: 801-10.
 - 16 Thouas GA, Sheridan J, Hourigan K. A bioreactor model of mouse tumor progression. *J Biomed Biotechnol*. 2007;9: 32754.
 - 17 Hickman JA, Graeser R, de Hoogt R, Vidic S, Brito C, Gutekunst M, van der Kuip H. Three-dimensional models of cancer for pharmacology and cancer cell biology: capturing tumor complexity in vitro/ex vivo. *Biotechnol J*. 2014;9(9): 1115-28.
 - 18 Yu B, Yu D, Cao L, Zhao X, Long T, Liu G, Tang T, Zhu Z. Simulated microgravity using a rotary cell culture system promotes chondrogenesis of human adipose-derived mesenchymal stem cells via the p38 MAPK pathway. *Biochem Biophys Res Commun*. 2011; 22,414(2): 412-8.
 - 19 Siti-Ismail N, Samadikuchaksaraei A, Bishop AE, Polak JM, Mantalaris A. Development of a novel three-dimensional, automatable and integrated bioprocess for the differentiation of embryonic stem cells into pulmonary alveolar cells in a rotating vessel bioreactor system. *Tissue Eng Part C Methods*. 2012;18(4): 263-72.
 - 20 Consolo F, Bariani C, Mantalaris A, Montevicchi F, Redaelli A, Morbiducci U. Computational modeling for the optimization of a cardiogenic 3D bioprocess of encapsulated embryonic stem cells. *Biomech Model Mechanobiol*. 2012.;11(1-2): 261-77.
 - 21 Dahlmann J, Kensah G, Kempf H, Skvorc D, Gawol A, Elliott DA, Dräger G, Zweigerdt R, Martin U, Gruh I. The use of agarose microwells for scalable embryoid body formation and cardiac differentiation of human and murine pluripotent stem cells. *Biomaterials*. 2013;34(10): 2463-71.
 - 22 Akins RE, Boyce RA, Madonna ML, Schroedl NA, Gonda SR, McLaughlin TA, Hartzell CR. Cardiac organogenesis in vitro: reestablishment of three-dimensional tissue architecture by dissociated neonatal rat ventricular cells. *Tissue Eng*. 1999;5(2): 103-18.
 - 23 Sikavitsas VI, Bancroft GN, Mikos AG. Formation of three-dimensional cell/polymer constructs for bone tissue engineering in a spinner flask and a rotating wall vessel bioreactor. *J Biomed Mater Res*. 2002;62(1): 136-48.

- 24 Hwang YS, Cho J, Tay F, Heng JY, Ho R, Kazarian SG, Williams DR, Boccaccini AR, Polak JM, Mantalaris A. The use of murine embryonic stem cells, alginate encapsulation, and rotary microgravity bioreactor in bone tissue engineering. *Biomaterials*. 2009;30(4): 499-507.
- 25 Mathers JP. Laboratory scaleup of cell cultures (0.5–50 liters). *Methods Cell Biol*. 1998;57: 219-227
- 26 Frith JE, Thomson B, Genever PG. Dynamic three-dimensional culture methods enhance mesenchymal stem cell properties and increase therapeutic potential. *Tissue Eng Part C Methods*. 2010;16(4): 735-49.
- 27 Cherry RS. Animal cells in turbulent fluids: details of the physical stimulus and the biological response. *Biotechnol Adv*. 1993;11(2): 279-99.
- 28 Martin I, Wendt D, Heberer M. The role of bioreactors in tissue engineering. *Trends Biotechnol*. 2004;22(2): 80-6.
- 29 King JA and Miller WM. Bioreactor development for stem cell expansion and controlled differentiation. *Curr Opin Chem Biol*. 2007;11(4): 394-398.
- 30 Burdge DA, Libourel IGL. Open source software to control bioflo bioreactors. *PLoS ONE*. 2014;9(3): e92108.
- 31 Schroeder M, Niebruegge S, Werner A, Willbold E, Burg M, Ruediger M. Differentiation and lineage selection of mouse embryonic stem cells in a stirred bench scale bioreactor with automated process control. *Biotechnol Bioeng*. 2005;92(7): 920-33.
- 32 Teo A, Mantalaris A, Mayasari Lim M. Hydrodynamics and bioprocess considerations in designing bioreactors for cardiac tissue engineering. *J of Reg Med and Tissue Eng*. 2012;1: 4.
- 33 Wu J, Rostami MR, Cadavid Olaya DP, Tzanakakis ES. Oxygen transport and stem cell aggregation in stirred-suspension bioreactor cultures. *PLoS ONE*. 2014;9(7): e102486.
- 34 Kaul H, Cui Z, Ventikos Y. A multi-paradigm modeling framework to simulate dynamic reciprocity in a bioreactor. *PLoS ONE*. 2013;8(3): e59671.
- 35 Orr DE, Burg KJ. Design of a modular bioreactor to incorporate both perfusion flow and hydrostatic compression for tissue engineering applications. *Annals of Biomed Eng*. 2008;36(7): 1228-41.
- 36 Consolo F, Fiore GB, Truscillo S, Caronna M, Morbiducci U, Montevecchi FM, Redaelli A. A computational model for the optimization of transport phenomena in a rotating hollow-fiber bioreactor for artificial liver. *Tissue Eng Part C Methods*. 2009;15(1): 41-55.

- 37 Eckmann L, Freshney M, Wright EG, Sproul A, Wilkie N, Pragnell IB. A novel in vitro assay for murine haematopoietic stem cells. *Br J Cancer Suppl.* 1988;9: 36-40.
- 38 Coanda H. inventor, Procédé de propulsion dans un fluide. Brevet Invention République Française, Gr. Cl. 2, No. 762688, 1932.
- 39 Ismadi M-Z, Gupta P, Fouras A, Verma P, Jadhav S, Bellare J, et al. Flow characterization of a spinner flask for induced pluripotent stem cell culture application. *PLoS ONE.* 2014;9(10): e106493.
- 40 Shen Y, Hou Y, Yao S, Huang P, Yobas L. In vitro epithelial organoid generation induced by substrate nanotopography. *Sci Rep.* 2015;19,5: 9293.
- 41 Gidaspow D, Bezburuah R and Ding J. Hydrodynamics of circulating fluidized beds, kinetic theory approach. In *Fluidization VII, Proceedings of the 7th Engineering Foundation Conference on Fluidization.* 1992;75-82.

Chapter 4

Application with human induced Pluripotent Stem Cells: Preliminary Study

4.1 Introduction

Human induced pluripotent stem cells (hiPSCs) have the potential to revolutionize biomedical sciences. The development of the induced pluripotent stem cell (hiPSC) technology by somatic cell reprogramming [1] can facilitate the development of personalized regenerative therapies [2,3], and personalized disease modelling [4], constituting as well a superior renewable cell source for basic stem cell research [5]. Indeed, the use of hiPSCs overcomes the obstacles related to ethical or moral concerns about the use of human embryonic stem cells (hESCs) and, being the basis of autologous and syngeneic cell therapies, might solve the problem of immunological rejection after transplantation [6].

Although many problems still remain before iPSC medical and pharmaceutical applications can be fully realized [7], their possible widespread usability for clinical and industrial applications is one of the most trending topics in

stem cell research [4]. In this scenario, the high number of required cells demands the development of hiPSC (and their progenies) mass production by means of Good Laboratory/Manufactory Practices (GLP/GMP). Moreover, each technical solution for mass production must be integrated within a robust, cell-specific, safe and cost-effective cell culture process, which will accelerate the translation from laboratory to industrial/clinical scale [8].

As an example, to replace the loss of contractile cells in diseased post-infarction hearts, ~1-10 billions of hiPSC-derived cardiomyocytes per patient are estimated to be necessary. The same estimation, based on clinical data, have been calculated for the treatment of diabetes mellitus with hiPSC-derived β -like cells [8,9]. The routine production of such cell numbers by conventional two-dimensional (2D) hiPSC culture is extremely space- and labour-intensive, and the lack of culture monitoring technologies makes this approach not economically viable. Moreover, 2D hiPSC cultures do not allow either the scale-up or the scale out without the employment of complex automation systems [10].

Three-dimensional (3D) suspension cultures have been proposed to overcome the characteristic limitations of the 2D culture methods [11,12,13]. The most promising technique is the *matrix-free* expansion, exploited starting from hiPSC single-cell suspensions to the generation of *cell-only-aggregates*. This method do not make use of feeder cells and microcarriers (or other matrices) which might lead to regulatory problems in the scope of clinical applications [14], but requires the generation of suspension cultures, avoiding sedimentation. Taking inspiration from the biopharmaceutical industry processes, dynamic suspension cultures for pluripotent stem cells has been realized proposing the use of stirred tank bioreactors [12,15,16,17,18]. Dynamic

suspension allows to promote *i)* homogenous distribution of culture components, *ii)* mass transfer of gases and nutrients into cell aggregates, *iii)* cell aggregation, and *iv)* easier monitoring and control of process parameters. As a matter of fact, this devices are more compatible with the final process up-scale.

However, conventional stirred tank bioreactors suffer from some limitations. In particular, the interaction between cells/aggregates with the moving impeller and the onset of turbulent flow regions can induce detrimental stress on cells, reduce cell viability and interfere with cell pluripotency state with possible undesired differentiation and consequent culture inhomogeneity [2,15,19,20,21].

Given the limitations related to the moving impeller inside the stirred tank bioreactors, the bioreactor platform presented in this thesis was tested for hiPSC culture in order to investigate, in a feasibility study framework, the effects of impeller-free dynamic suspension culture on hiPSCs. In detail, this preliminary test phase investigated the effects of the characteristic low shear stress fluid dynamic structures developing inside the bioreactor culture chamber (described in Chapter 2) on hiPSC suspended aggregates, by evaluating the preservation of the morphological features of hiPSC aggregates (e.g. maintenance of spheroid shape avoiding spheroid fusion). Consecutively, the capability of cell aggregation of the bioreactor platform was preliminary tested inoculating hiPSCs as single-cell suspension to have a measure of impeller-free suspension on cell aggregation.

The obtained results indicated that the bioreactor platform produces a favourable environment to hiPSC cultures, giving good bases for the possible

further optimization of the bioreactor platform, with the aim to provide a device, based on the same impeller-free suspension functioning, specifically-improved to this type of cultures.

4.1. Materials and Methods

4.1.1. Bioreactor Platform

For this study the bioreactor platform presented in Chapter 2 was employed. The platform was equipped with a pH and a dissolved oxygen (DO) sensor which were positioned immediately downstream the bioreactor culture chamber with the aim to have a readout of oxygen consumption inside the bioreactor culture chamber. The tubing length for the oxygenator module was adjusted according to the tubing sizing method and computation presented in Chapter 2 - Appendix I, and resulted in a minimum total culture medium volume of approximately 250 mL. The bioreactor platform configuration used in this application is shown in Figure 4.1.

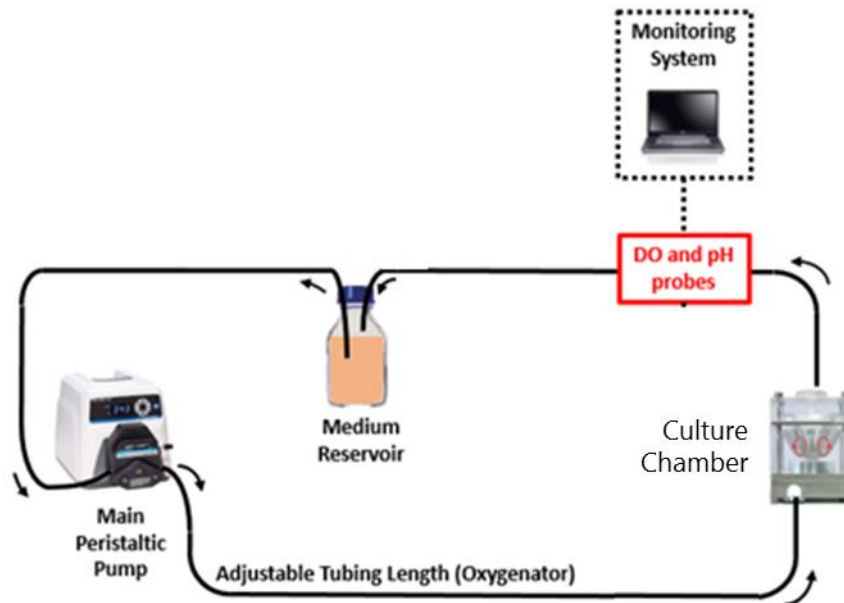


Figure 4.1: Schematics of the bioreactor platform configuration used for the preliminary tests with hiPSCs.

4.1.2. Qualitative Suspension Analysis

Preliminary performance tests were conducted to investigate the suitability and performance of the bioreactor platform. Cytodex 1 microcarriers with an average particle size of 190 μm and a density equal to 1030 kg/m^3 (GE-Healthcare) were prepared and stained with Coomassie blue (in order to be more visible). These microcarriers were chosen to simulate the suspension of hiPSC spheroid aggregates, which typically have similar values of density and diameter. Approximately 1:100 dilution of stained microspheres were inoculated into the bioreactor culture chamber to verify the symmetry and the homogeneity of the applied suspension. To allow the visualization of the inlet symmetry, the bioreactor culture chamber was kept open without lid, imposing an inlet flow rate from 20 to 50 mL/min .

4.1.3. Monolayer Culture Passaging of hiPSCs

Experiments were performed using hiPSCs generated from hematopoietic stem cells, in particular the hHSC1285iPS2 cell line. This cell line was maintained at standard conditions on mouse embryonic fibroblast (MEF) feeder-culture and then pre-cultured in monolayer for a maximum of 11-12 split passages with Essential (E8) culture medium, before being used for suspension culture. The E8 medium is a fully-defined albumin-free culture medium which was firstly proposed by James Thomson and colleagues [22] in 2011. This medium was prepared starting from DMEM/F12 basal medium and supplementing 7 more essential medium components:

- **L-ascorbic acid** (Vitamin C) to promote cell proliferation;
- **Selenium** for sustained cell expansion;
- **FGF2** for maintaining pluripotency, cell survival and proliferation;
- **insulin** to maintain cell survival and proliferation;
- **Transferrin** to support high cloning efficiency;
- **TGF β** to increase pluripotency expression marker such as NANOG;
- **NaHCO₃** for pH adjustment at 7.4 (together with the further addition of 5 M NaOH) and improving buffering capability at 5% CO₂.

Monolayer culture was done seeding 4×10^4 cell/cm² in Geltrex-coated T25 or T75 flasks, culturing each passage for 3-4 days. Each passage was performed washing the flask with PBS without Ca²⁺/Mg²⁺, followed by accutase treatment (5 min at 37 °C) in order to obtain a single cell suspension, and

seeding the cells into new flasks. Thereby culture medium for seeding was supplemented with ROCK inhibitor Y27632 to permit cell survival after the dissociation into single cells [23]. At each passage, before the re-seeding, vital cell count was performed by trypan blue staining enabling seeding at defined cell densities (4×10^4 cell/cm² as outlined above).

4.1.4. Orbital-Shaker Spheroid Aggregate Formation of hiPSCs

Small-scale low-density suspension culture was performed using Cellstar 6-well suspension culture plates (Greiner bio-one), positioned on an *orbital shaker* moving at 70 rpm. To initialize suspension culture, hiPSC monolayer were enzymatically treated with accutase (PAA laboratories) for 5 mins at 37 °C, to obtain a single cell suspension. In each well, 3.4×10^5 cell/mL were inoculated into 3 mL of pre-warmed E8 medium with supplementation of 10 μM ROCK inhibitor Y27632 and maintained under constant shaking.

4.1.5. hiPSCs Dynamic Suspension Culture with the Bioreactor

Platform

The bioreactor platform components were sterilized and assembled under laminar flow hood. pH probe (EasyFerm, Hamilton) was calibrated with a three-point calibration procedure integrated inside the monitoring and control software described in Chapter 2 - Appendix II. Since the DO probe (OxyFerm, Hamilton) needs approximately 10 hrs of polarization time, the probe was inserted in the recirculation closed-loop bypassing the bioreactor culture chamber after sterilization. Consequently, the culture medium was aerated (21% O₂, 5% CO₂ at 37 °C), and finally calibrated with the in-house made software when stable values of DO were reached.

The first experimental phase consisted in the inoculation of 24 hrs-old spheroid aggregates, previously obtained by means of orbital shaker small-scale hiPSC suspension (see 4.2.4). One of the most important requisites for hiPSC cultures is the capability of the culture device to preserve the spherical dimension of the aggregates and to limit and modulate spheroid diameters, with the aim to maintain hiPSC pluripotency properties, as well as to improve nutrient transport inside the aggregate [13]. To investigate the capability of the herein proposed bioreactor in modulating aggregate dimensions, three different experiments were performed modifying flow rate, bioreactor platform functioning mode, and inoculated cell number (summarized in Table 4.1 and schematized in Figure 4.3). Consecutively, evaluating the platform's capability of preserving typical hiPSC aggregate spherical morphology, a single bioreactor run was performed inoculating a single cell suspension with a cell density of 6×10^5 cell/mL for 24 hrs imposing a continuous flow rate equal to 30 mL/min. In order to obtain preliminary indications on cell aggregation potential of the bioreactor platform starting from a free single-cell suspension (generated from monolayer culture), hiPSC aggregates generated by means of dynamic suspension culture within the bioreactor were compared with the aggregate generated with the same cell source by means of small-scale suspension culture on orbital shaker. Since hiPSCs have not high survival rates when suspended as single-cells, the capability of generating hiPSC aggregates is crucial to determine the suitability of the device to be employed for pluripotent stem cell culture applications, starting from single cell suspensions.

Table 4.1: Prospect of dynamic suspension culture of hiPSCs within the bioreactor platform inoculated as spheroid aggregates.

Experiment	Flow rate (mL/min)	Medium	Cell Density ($\times 10^6$ cell/mL)
1	50-70-100	E8+penicillin/streptomycin	2.6
2	100	E8+penicillin/streptomycin	2.6
3	100 (pulsed 15/45s - on/off)	E8+penicillin/streptomycin	0.8

4.1.6. Flow Cytometry

Single cell suspensions were prepared and aliquots were incubated for 15 mins at 4 °C within 96 v-bottom plates with primary antibodies and corresponding isotype controls against OCT4 and NANOG. In detail, primary antibody against OCT4 and its isotype (mIgG2b) were incubated at 1:40 and 1:20 dilution, respectively; while primary antibody against NANOG and its isotype (rIgG) were incubated at 1:100 and 1:10000 dilution, respectively. After washing, cells were incubated with the corresponding secondary antibodies: donkey Cy5 anti-mouse IgG (1:300) for OCT4 and its isotype, donkey Cy3 anti-rabbit IgG (1:300) for NANOG and its isotype, for 30 mins at 4 °C in the dark. The cells were analysed by using fluorescence-activated cell sorting (FACS). In detail, FACS is a specialized type of flow cytometry which provides a method to sort heterogeneous populations of cells. It permits to recognise different cell populations by fast recording fluorescent signals from individual cells, according to fluorescent markers attached to primary antibodies.

4.2. Results

4.2.1. Qualitative Suspension Analysis

The suitability of the device in generating buoyant vortices and the establishment of suspension condition was confirmed by the suspension analysis performed with Cytodex 1 microcarriers. As previously described as result of multiphysics simulations (Chapter 2 - 2.3.1 Multiphysics Modelling for Fluid Dynamics Characterization), Figure 4.2 illustrates the development of vortical fluid structures in the bottom of the culture chamber (top view of the culture chamber without lid). These structures generate a flow mixing in laminar flow regime which homogeneously transports suspended particles throughout the culture chamber (i.e. blue-stained Cytodex 1), counterbalancing their weight. Modulating the flow rate from 10 to 50 mL/min, it was possible to evaluate that for particles with properties similar to hiPSC aggregates (diameter equal to 190 μm , and density equal to 1030 kg/m^3), flow structure generated imposing flow rates lower than 50 mL/min did not have enough energy to produce good mixing and suspension. The distribution of Cytodex 1 microcarriers in Figure 4.2A shows highly packed particles on the bottom of the culture chamber indicating the absence of transport and mixing, with a very clear tendency towards sedimentation. Increasing the flow rate (Figure 4.2B-C), particles were homogeneously suspended within the culture chamber, reaching a good mixing with a flow rate equal to 50 mL/min (Figure 4.2C). According to these results, the flow rate of 50 mL/min was identified as the minimum flow rate required to produce hiPSC aggregate suspension within the bioreactor culture chamber. This value was used as initial flow rate value

to be imposed for the first hiPSC dynamic suspension culture experiment (first row in Table 4.1).

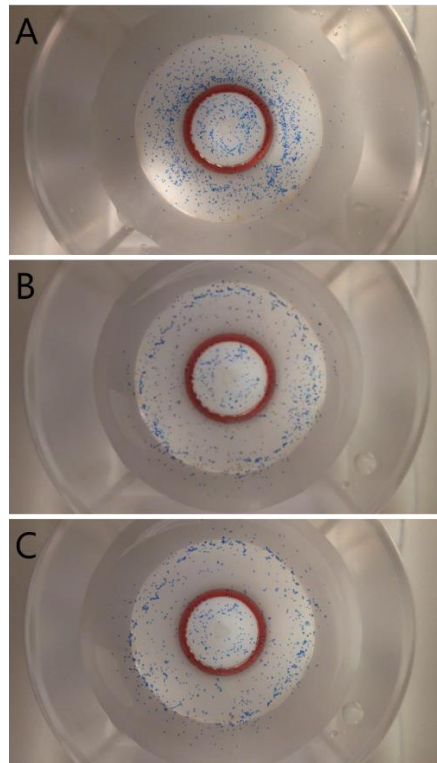


Figure 4.2: Representation of the Cytodex 1 microcarriers: low flow rate are not capable of generating particle suspension (A, 20 mL/min). With increasing the imposed flow rate particles are suspended and homogeneously distributed within the culture chamber (B, 30 mL/min; C, 50 mL/min).

4.2.2. hiPSCs Dynamic Suspension Culture within the Bioreactor Platform

Cells were cultured in monolayer before being inoculated into the 6-well plate small-scale low-density suspension culture on orbital shaker. The monolayer condition of the cultured cells is shown in Figure 4.3: after three culture days the flask reached confluency and cells were detached and cultured in small scale suspension culture forming spheroid hiPSC aggregates.

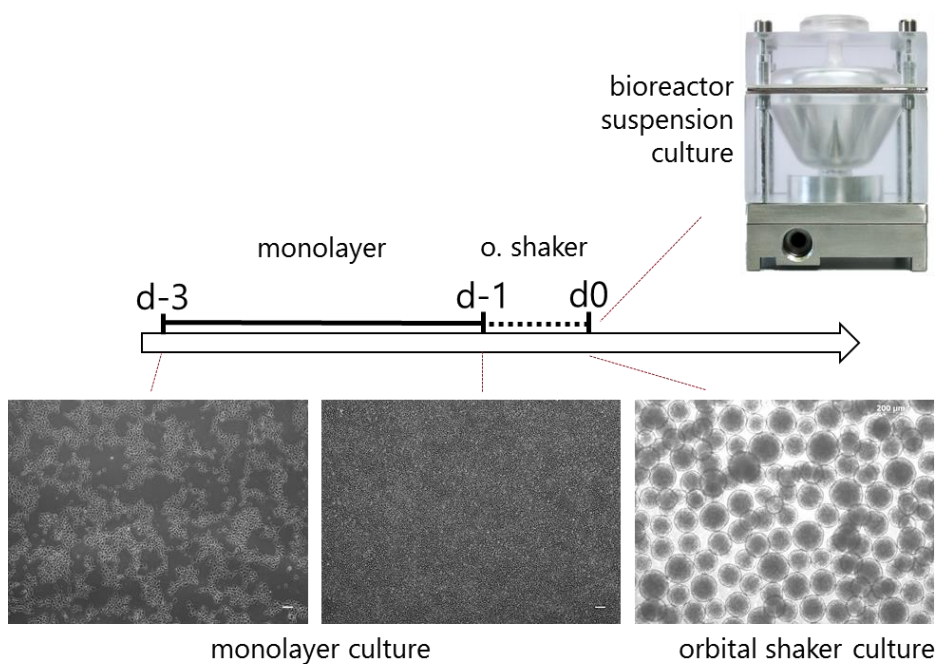


Figure 4.3: Schematics showing the experiment design: from monolayer pre-expansion to small-scale suspension culture in orbital shaker, prior the inoculation inside the bioreactor culture chamber.

The first experiment (Table 4.1, first row) was performed starting from imposing a flow rate equal to 50 mL/min (i.e. the flow rate which was detected as the minimum flow rate capable of producing the suspension of the Cytodex 1 microcarriers). After a few hours the cell aggregates started fusing and, becoming bigger (Figure 4.4), the flow rate was iteratively increased up to 100 mL/min.

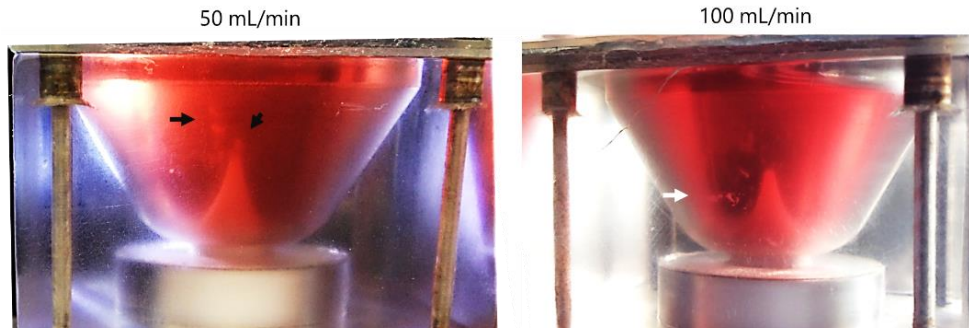


Figure 4.4: Observation of suspended hiPSC aggregates during the culture through the translucent polycarbonate wall of the bioreactor culture chamber. At 50 mL/min black arrows indicate the fusion of several aggregates with the formation of clumps. Increased the flow rate up to 100 mL/min, aggregate suspension was improved and the dimensions of clumps was reduced (white arrow).

After 24 hrs of dynamic suspension within the bioreactor, aggregates were harvested for qualitative evaluation of their morphology. The typical spherical shape of hiPSC aggregates was lost, and most of the aggregates tended to fuse to each other forming amorphous bodies, large in dimensions with shorter axis longer than 500 μm (Figure 4.5). Despite the large dimension of these bodies, the live/dead staining (ThermoFisher Scientific) microscopy visualization revealed a low rate of mortality (green-calcein for alive, red- ethidium homodimer for dead cells).

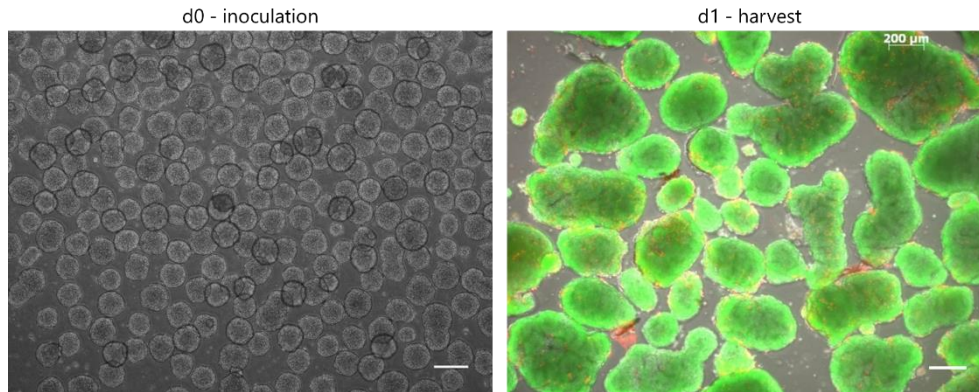


Figure 4.5: Experiment 1. Qualitative comparison between the hiPSC before inoculation and after 24 hrs dynamic suspension within the bioreactor (Experiment 1). The harvested aggregates were live/dead stained (green =live, red = dead). Scale bar 200 μm .

This result suggested that the dynamic suspension produced a favourable environment for massive undesired aggregation and fusion of the cultured hiPSC spheroids already in the first 24 hrs. Within this configuration aggregate dimension and shape was not preserved, probably due to the inappropriate imposed flow rate in the first hours of culture when the aggregates started clumping. As a result the second experiment (second row, Table 4.1, Figure 4.6) was performed culturing hiPSCs imposing a flow rate equal to 100 mL/min. After 24 hrs of dynamic suspension inside the bioreactor, aggregate tended to grow in dimension. The dynamic suspension promoted the enlargement of the hiPSC spheroids (mean diameter 140 μm , before inoculation in bioreactor, 196 μm after 24 hrs in dynamic suspension, respectively, around 90 measured diameters), but contemporarily increased the heterogeneity of the diameter values (standard deviation of 18 μm Vs. 68 μm , respectively). The wider estimated diameter distribution (i.e. estimated probability density function of diameter distribution) for the dynamic cultured cells in bioreactor is a result of the fusion of a great number of hiPSC spheroids,

which produces aggregates with diameter values larger than 200 μm . From the comparison of aggregate morphology before and after dynamic culture within the bioreactor, it is possible to note the smoother edges of the spheroid before being subjected to dynamic suspension. The 24 hrs of dynamic suspension inside the bioreactor produced rougher edges which are usually associated to not completely healthy hiPSC aggregates, and can increase the potential interaction and fusion of the spheroids to each other.

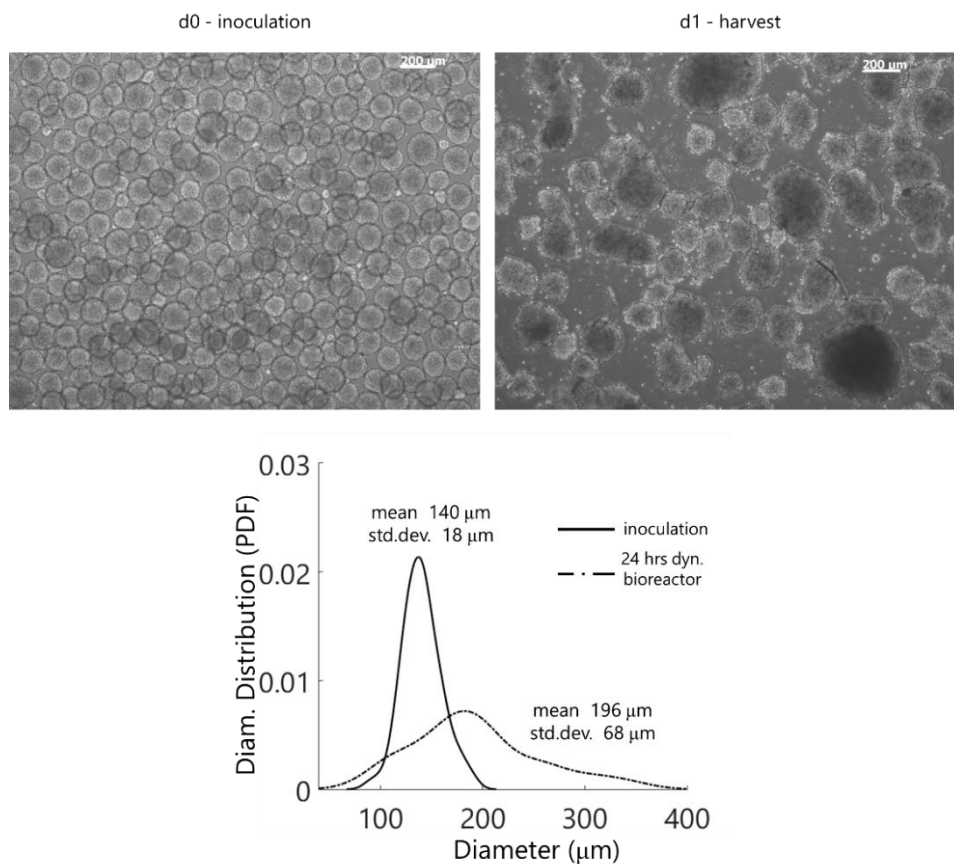


Figure 4.6: Experiment 2. Qualitative comparison between the hiPSC before inoculation and after 24 hrs dynamic suspension within the bioreactor (Experiment 2). The aggregates after 24 hrs within the bioreactor present rough edges, usually associated to not-completely healthy hiPSC aggregates. Scale bar 200 μm . Diameter distribution graph (bottom) for hiPSC aggregates before and after 24 hrs culture inside the bioreactor with mean and standard deviation values of each distribution.

Moreover, the visual inspection of the PDMS filter after the harvest highlighted that cells/aggregates reaching the filter can adhere on it, causing a moderate cell loss (cells adhering on the filter cannot be recovered, Figure 4.7), which may limit the efficiency of the culture procedure.

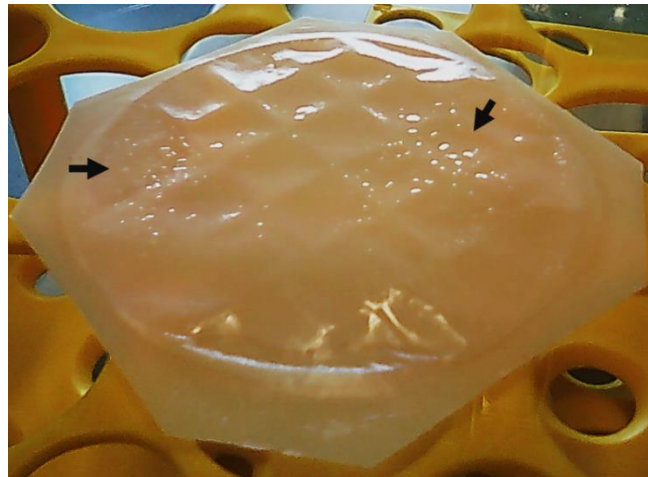


Figure 4.7: Experiment 2. Detail of the PDMS filter recovered after the cell harvest. Black arrows indicate aggregates and cells which adhered on the filter surface.

In order to reduce the heterogeneity of diameter distribution and to limit the number of cells adhering on the PDMS filter surface, the third experiment (third row, Table 4.1) was carried out taking advantage of the pulsed protocol developed by means of the multiphysics simulations and widely presented in Chapter 2. The rationale under this choice was to impose a cyclic moderate shear stress stimulation on hiPSC aggregates, in order to modulate the tendency of the aggregate to fuse, and contemporarily using the free-fall phase for a more efficient hiPSC spheroid suspension, thus reducing the number of cells and aggregate adhering on the PDMS filter surface. Starting from the indications obtained from the two previous experiments carried out with the continuous recirculation loop, the flow rate imposed by the pump was set to 100 mL/min (Figure 4.8). The operational graphs mentioned in Chapter 2

allowed to set the recirculation phase and the pump stop phase to 15 s and 45 s, respectively, obtaining a pulsation period of 1 min.

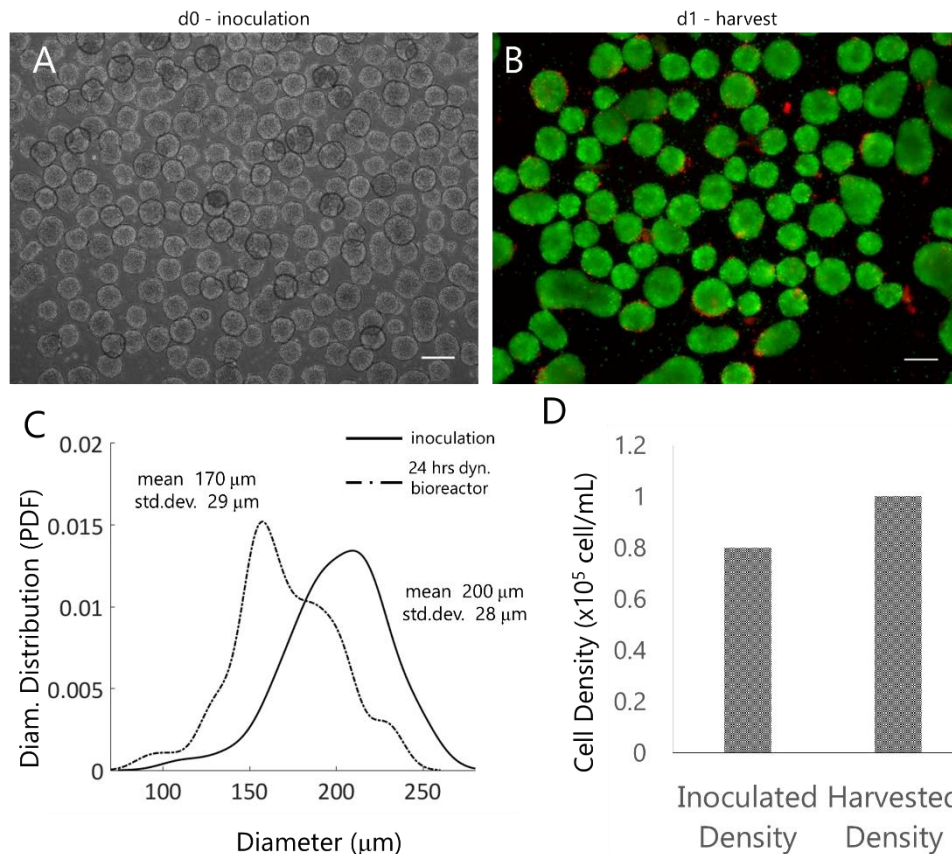


Figure 4.8: Experiment 3. Qualitative comparison between the hiPSC before inoculation (A) and after 24 hrs dynamic suspension within the bioreactor (B). Scale bar 200 μm . Diameter distribution graph (bottom) for hiPSC aggregates before and after 24 hrs culture inside the bioreactor with mean and standard deviation values of each distribution (C). Inoculated Vs. harvested cell density (D).

The pulsed functioning mode of the bioreactor platform allowed to improve the homogeneity of the hiPSC spheroid diameters. From the visual inspection of Figure 4.8, it is possible to evaluate the presence of some fused aggregate after 24 hrs of dynamic suspension inside the bioreactor. Nevertheless, the probability density function of diameter distribution depicts a reduction of the average aggregate dimension (mean value 170 μm for dynamic

suspension inside the bioreactor and 200 μm for inoculated aggregate, around 80 measured values), with comparable values of standard deviation before and after the bioreactor inoculation (29 μm Vs 28 μm , respectively). The cell density of cultured cells increased in 24 hrs from approximately 0.8×10^5 to 1×10^5 cell/mL.

As final experiment, the capability of the bioreactor of producing hiPSC spheroid aggregate was investigated. Monolayer culture of undifferentiated hiPSC were detached and inoculated as single cell suspension (6×10^5 cell/mL) within the bioreactor culture chamber imposing a suspension flow rate equal to 30 mL/min. The choice of the flow rate for the 24 hrs dynamic suspension culture took advantage of the preliminary multiphysics simulations used to characterize the flow structures inside the bioreactor culture chamber (presented in Chapter 2). In fact, according to the *in silico* results, it was selected as the minimum flow rate necessary to guarantee moderate shear stress levels with larger suspension vortices. Figure 4.9 presents a comparison between the result of 24 hrs dynamic suspension inside the bioreactor and, as a control, the result of 24 hrs of small-scale low density suspension culture on orbital shaker. The bioreactor was capable of producing small hiPSC aggregates among some bigger aggregates (with diameter up to 300 μm) and some clumps. In general very small spheroids were produced (mean diameter equal to 87 μm) compared to the spheroids produced by the small-scale suspension on orbital shaker (mean diameter equal to 157 μm). The standard deviation values reported in Figure 4.9 do not take into account the non-spherical aggregates formed during dynamic suspension within the bioreactor.

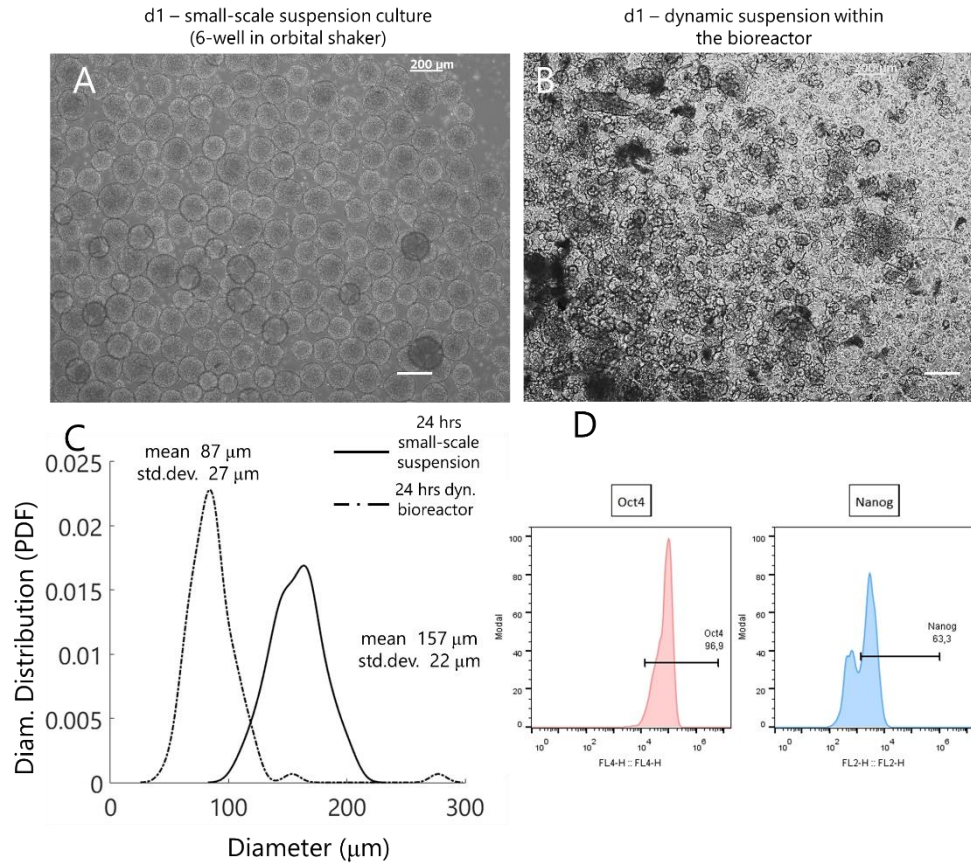


Figure 4.9: Experiment 4, single cell suspension. Qualitative comparison between the hiPSC aggregates after 24 hrs in small-scale suspension culture (A) and after 24 hrs in dynamic suspension within the bioreactor (B)(Experiment 4). Scale bar 200 μm . Diameter distribution graph (C) for hiPSC aggregates after 24 hrs of small-scale suspension culture and after 24 hrs suspension culture inside the bioreactor with mean and standard deviation values of each distribution. FACS analysis results on pluripotency marker expression (D).

The dynamic suspension within the bioreactor produced a heterogeneous hiPSC aggregate population compared to the homogeneity obtainable by means of the small-scale suspension, clearly observable in microscopy image in Figure 4.9A and 4.9B. Flow cytometry intracellular marker quantification confirmed that most of the cells maintained their state of pluripotency after 24 hrs of dynamic suspension within the bioreactor with 96% of OCT4 and 63% of NANOG expression (Figure 4.9D).

4.3. Discussion and Conclusion

In this chapter, a feasibility study on hiPSC culture performed using the dynamic suspension bioreactor platform proposed in this thesis work was presented and described. As presented in the previous chapters, the combination of peculiar geometric features of the bioreactor culture chamber with the closed-loop medium recirculation circuit enables the formation of laminar dynamic suspension culture in a tuneable range of shear stress values. This functioning principle avoids the use of impellers or rotational components for the generation of flow structures capable of suspending cells, aggregates, or microcarriers within the bioreactor chamber. According to this characteristics, this bioreactor platform was proposed for its possible usage in the field of hiPSC dynamic suspension cultures, as an alternative device to conventional stirred flask systems. In fact, it was established that within stirred bioreactors (e.g. stirred flask, stirred tanks) the interaction of cells with the moving blades of the impeller and the onset of non-homogeneous turbulent structures and high shear stresses could lead to cell damage limiting cell expansion efficiency and reproducibility [2,15,19,20,21]. As a matter of fact, the suspension bioreactor proposed in this thesis work (and widely described in Chapter 2 and Appendices) was employed for hiPSC dynamic suspension cell culture preliminary applications, in the scope of a feasibility study carried out in collaboration with Hannover Medical School (MHH). The effects of low shear stress impeller-free dynamic suspension on hiPSC spheroid aggregates was investigated inoculating aggregates previously generated by means of small-scale low-density suspension cultures (6-well plates on orbital shaker). As a requisite to maintain the pluripotency properties of hiPSC cell aggregates, the capability of the bioreactor chamber to preserve the spherical

shape of the suspended aggregates was studied carrying out three independent preliminary experiments imposing three different setups. The imposition of a continuous medium recirculation flow rate, after 24 hrs, enhanced the generation of massive agglomeration, which produced macroscopic and amorphous aggregates. This result suggests that the continuous low shear stress imposed by the peculiar fluid dynamics developing within the culture chamber are not able to counterbalance hiPSC agglomeration kinetics. A modulation effect on agglomeration kinetics was achieved by the combination of moderate intermittent shear stress and free-fall transport applied by the pulsed protocol. The cyclic succession of free-fall transport moments and moderate shear flow-driven transport increased the homogeneity of the suspended hiPSC aggregates (thinner diameter statistical distribution), interfering with aggregate fusion and keeping the original hiPSC morphology. The inoculation of single cell suspension allowed to elucidate that impeller-free flow dynamics established inside the bioreactor culture chamber is able, even weakly, to promote cell-cell interaction and consequently the formation of hiPSC aggregates. The harvest after 24 hrs of small spherical aggregates amongst bigger and amorphous aggregates indicated that the low shear stress environment stimulated cell aggregation.

Nevertheless, some limitations can weaken this feasibility study. In this bioreactor platform prototypal stage, the possibility to sample hiPSC aggregates directly during the culture was not feasible. For this reason, short 24 hrs bioreactor runs were performed with the aim to have an immediate idea of the impact of impeller-free fluid dynamics on hiPSCs. Longer culture periods may require the possibility to sample aggregates directly from the culture

chamber in order to monitor the aggregate evolution over time without stopping the suspension. Moreover, although the bioreactor culture chamber was conceived to be translucent, the visibility during the culture was not optimal and this limited the controllability of the process.

These outcomes, even though preliminary and not repeated, provide good indications for the possible usage of the presented bioreactor platform for hiPSC dynamic suspension culture. In detail, to perform more systematic and longer (more than 24 hrs long) statistically relevant studies, the bioreactor platform can be properly optimized for this specific biotechnological application on the basis of the results herein presented. In the future, the same functioning principle can be implemented in a different prototype design which may allow to parallelize the experiments accelerating the time necessary to obtain statistically significant results (more bioreactor culture chambers for more repetitions). The same culture chambers may be conceived to allow direct sampling and inoculation in order to prolong the culture periods while maintaining a full control of hiPSC aggregate evolution. All this optimization procedure will be carried out integrating computational multiphysics simulations in the design phase as presented in the previous chapters, shortening the pathway to the final device avoiding trial-and-error approaches.

Acknowledgements

Thanks to Dr. Robert Zweigerdt who gave me the opportunity to work with his research group for six months at Hannover Medical School. Thanks to all the Lab fellows: Christina, Emiliano, Diana RD, and all the others for the warm welcome: I felt at home.

References

- 1 Takahashi and Yamanaka. Induction of Pluripotent Stem Cells from Mouse Embryonic and Adult Fibroblast Cultures by Defined Factors. *Cell*, 126 (August 25, 2006), 663–676.
- 2 Teo, A., Mantalaris, A., and Mayasari, Lim M. Hydrodynamics and bioprocess considerations in designing bioreactors for cardiac tissue engineering. *Journal of regenerative medicine and Tissue Engineering*, 1, 4 (2012).
- 3 Robinton and Daley. The promise of induced pluripotent stem cells in research and therapy. *Nature*, 481 (May 13, 2012), 295-305.
- 4 Inoue and Yamanaka. The Use of Induced Pluripotent Stem Cells in Drug Development. *Clinical Pharmacology & Therapeutics*, 89, 5 (May 2011).
- 5 Murry and Keller. Differentiation of Embryonic Stem Cells to Clinically Relevant Populations: Lessons from Embryonic Development. *Cell*, 132 (February 22, 2008).
- 6 Guha, P., Morgan, J. W., Mostoslavsky, G., Rodrigues, N. P., and Boyds, A. S. Lack of immune response to differentiated cells derived from syngeneic induced pluripotent stem cells. *Cell Stem Cell*, 12, 4 (2013), 407-412.
- 7 Hong, So Gun, Dunbar, Cynthia E., and Winkler, Thomas. Assessing the risk of genotoxicity in therapeutic development of Induced Pluripotent Stem cells. *Molecular Therapy*, 21, 2 (2013), 272-281.
- 8 Zweigerdt, R. Chapter - Large Scale Production of Stem Cells and their Derivatives. In *Engineering of Stem Cells*. Springer, 2009.
- 9 Chong, J. J., Yang, X., Don, C. W., Minami, E., Liu, Y. W., Weyers, J. J., and et al. Human Embryonic-stem cell derived cardiomyocytes regenerate non-human primate hearts. *Nature*, 510, 7504 (2014), 273-277.
- 10 Terstegge, S., Laufenberg, I., Pochert, J., Schenk, S., Itskovitz-Eldor, J., Endl, E., and et al. Automated maintenance of embryonic stem cell cultures. *Biotechnology and Bioengineering*, 96, 1 (2007), 195-201.
- 11 Amit, M., Chebath, J., Laessky, I., Miropolsky, Y., Peri, M., Blais, I., and et al. Suspension culture of undifferentiated human embryonic and induced pluripotent stem cells. *Stem Cell Review*, 6, 2 (2010), 248-259.

- 12 Zweigerdt, Robert, Olmer, Ruth, Singh, H., Haverich, Axel, and Martin, Ulrich. Scalable expansion of human pluripotent stem cells in suspension culture. *Nature Protocols*, 6, 5 (2011), 689-700.
- 13 Olmer, Ruth, Lange, A., Selzer, S., Kasper, C., Haverich, Axel, Martin, Ulrich, and Zweigerdt, Robert. Suspension culture of human pluripotent stem cells in controlled, stirred bioreactors. *Tissue Engineering Part C Methods*, 18, 10 (2012), 772-784.
- 14 Wang, Y., Cheng, L., and Gerecht, S. Efficient and scalable expansion of human pluripotent stem cells under clinically compliant settings: a view in 2013. *Annuals of Biomedical Engineering*, 42, 7 (2014), 1357-1372.
- 15 Zweigerdt. Large Scale Production of Stem Cells and Their Derivatives. *Adv Biochem Engin/Biotechnol*, 114 (2009), 201-235.
- 16 Ismadi, M. Z., Gupta, P., Fouras, A., Verma, P., Jadhav, S., and Bellare, J. Characterization of a Spinner Flask for induced pluripotent stem cell culture application. *Plos One*, 9, 10 (2014), e106493.
- 17 Kemp, P. History of regenerative medicine: looking backwards to move forwards. *Regenerative Medicine*, 1, 5 (2006), 653-669.
- 18 Siti-Ismail, N., Samadikuchaksaraei, A., Bishop, A. E., Polak, J. M., and Mantalaris, A. Development of a novel three-dimensional, automatable and integrated bioprocess for the differentiation of embryonic stem cells into pulmonary alveolar cells in a rotating vessel bioreactor system. *Tissue Engineering Part C Methods*, 18, 4 (2012), 263-272.
- 19 Rodrigues, C. A., Fernandes, T. G., Diogo, M. M., da Silva, C. L., and Cabral, J. M. Stem cell cultivation in bioreactors. *Biotechnology Advances*, 29, 6 (2011), 815-829.
- 20 Cherry, R. S. Animal cells in turbulent fluids: details of the physical stimulus and the biological response. *Biotechnology*, 22, 2 (2004), 80-86.
- 21 King and Miller. Bioreactor development for stem cell expansion and controlled differentiation. *Current Opinion in Chemical Biology*, 11 (2007), 394-398.
- 22 Chen, Guokai, Gulbranson, Daniel R., Hou, Zonggang, Bolin, Jennifer M., Ruotti, Victor, and et al. Chemically defined conditions for human iPS cell derivation and culture. *Nature Methods*, 8, 5 (2011), 424-429.
- 23 Watanabe, K., Ueno, M., Nishiyama, A., Matsumura, M., Wataya, T., Takahashi, J. B., and et al. A ROCK inhibitor permits survival of

dissociated human embryonic stem cells. *Nature Biotechnology*, 25, 6 (2007), 681-686.

Chapter 5

Discussion and Conclusion

In this thesis, a versatile bioreactor platform for culturing cells in dynamic suspension was presented. Thanks to the peculiar shape of the culture chamber, combined with the recirculation circuit closed-loop, this bioreactor is able to produce a laminar dynamic suspension culture at tuneable low shear stress values. The presented device is proposed as an alternative to commercial dynamic suspension devices, in order to overcome some of the limitations of the most commonly-used suspension bioreactors for scalable production and differentiation of cells (stirred flask and rotating wall bioreactors). In particular, within stirred flask bioreactors, the interaction among cells and impeller blades can lead to detrimental stress on cells, reducing cell viability and interfering with cell pluripotency (in stem cell expansion applications) [1,2,3,4,5]. Rotating wall bioreactors can overcome this limitation but the complexity of technological solutions adopted for rotation makes these devices not easily scalable [3,6].

This thesis demonstrates that, starting from the current state-of-the-art knowledge in dynamic cell culture with commercial bioreactors, it is possible

to integrate a comprehensive modelling approach within the bioreactor mechanical design phase, in order to support the development of innovative and versatile devices to be used in the field of tissue engineering and regenerative medicine.

In this frameworks, the different aspects of the methods applied for the bioreactor platform optimization and development are discussed in the following.

Multiphysics Model

Computational fluid dynamics and multiphysics modelling are key tools (1) for the design and optimization of bioreactors, and (2) for the acquisition of a comprehensive description of their functioning [7,8]. For these reasons, multiphysics models have been made and adopted in the recent years to extract knowledge on biological processes inside the bioreactor culture chambers [9,10,11].

Here, the direct integration of in silico multiphysics modelling and experimental mechanical design was implemented to devise, produce, characterize, and use a dynamic suspension bioreactor platform. In fact, multiphysics simulations were useful to optimize the bioreactor platform design, obtaining a full characterization of the conditions developing inside the bioreactor culture chamber. This multiphysics model allowed to define two main flow conditions in culturing cells/constructs: (1) *ultralow* shear stress condition, obtained working with flow rates below 20 mL/min, and (2) *moderate* shear stress condition, established in flow rate range from 30 to 120 mL/min. The (tunable) shear stress values produced in this dynamic suspension bioreactor are:

(1) one order of magnitude lower than the shear stress values normally developing within a commercial spinner flask where, imposing agitation rates ranging from 15 to 50 rpm, mean shear stress values ranging from 20 to around 120 mPa are reached (with peak values reaching 200 mPa) [12]; (2) several orders of magnitude lower than the reference shear stress value considered critical (250 mPa) for sensitive cells like human embryonic stem cells or neonatal rat cardiomyocytes [1].

The same multiphysics modelling approach was adopted to identify, *in silico*, appropriate culture protocol. This allowed the identification of proper initial for experimental tests involving expensive small molecules, cells, and culture media. Accordingly, this *in silico* protocol determination strategy represents a useful tool to reduce the costs during the technical assessment of the device functioning.

In fact, the *in silico* strategy represents a valuable alternative to the traditional trial-and-error method within the range of approximations of the assumptions made at the basis of the modelling approach. Indeed, there are some assumption which can influence the outcome of the model, particularly referring to the use of the bioreactor platform for mammalian cell suspension culture. Firstly, this study considered spherical non-deformable suspended particles with constant diameter. In the real applications with mammalian cells or aggregates, suspended particles are characterized by variable diameters and different, sometimes irregular, shapes. Concerning the pulsatile-flow working condition, cells/aggregates are cyclically transported by flow-driven transport and by free-fall motion. The predicted cell/aggregate transport (with particular attention on free-fall cell/aggregate motion) does not account for the realistic geometric shape irregularities, which could in principle affect

the applicability of Stokes' law for the calculation of the particle terminal velocity. Contemporarily, the inhomogeneity of particle diameters, will determine different timing in the free-fall motion, thus provoking a more complex behaviour of the suspended particle cloud during the cycle evolution. Moreover, this model is useful to describe the early stage of the culture procedure, giving only indications on the initialization of the experimental process. In fact, the model does not take into account cell aggregation/disaggregation biomechanics, and cell proliferation, which may have an impact on the experimental outcome even if it has typical characteristic time of days (simulated time were in the order of magnitude of minutes).

Although these limitations could weaken the findings of this study, the validity of the proposed process optimization method could be the basis for more complex studies which, validated *in vitro*, can consistently help the biotechnological experimental work and confer an *in silico*-based *a priori* knowledge useful to limit the experimentation costs. The use of this computational method supports the design and optimization procedure, limiting the trial-and-error approach and costs related to the technical assessment of the device functioning. The information obtained by means of the computational setup demonstrates the potential offered by the multiphysics model when used as a tool for the design phase of a bioreactor platform, giving further insights on the fluid dynamics established inside the culture chamber and consequently allowing the formulation of a more reliable and systematic experimental procedure.

Bioreactor Platform

The bioreactor platform was optimized to allow the real-time monitoring and control of culture parameters, such as pH and DO partial pressure. A properly designed and realized control unit integrates the possibility to continuously acquire the signals from the sensors and interactively control the pump action. The possibility of real-time monitoring and control of the cell culture is a highly required feature for scalable and repeatable cell culture systems [2,13]. In fact, oxygen tension inside the culture environment is particularly important for stem cell culture, since DO partial pressure has been shown to have an impact on stem cell differentiation into specific lineages [2].

The online measurement of physicochemical parameters, implemented in the bioreactor platform and presented in this thesis, gives the possibility to integrate a secondary continuous feeding circuit to replenish the exhausted medium with fresh medium. This feature, usually implemented in commercial stirred flask bioreactors to overcome the limitations of batch culture [94], in the bioreactor platform herein proposed allows the automatization of the culture medium replenishment in response to pH and DO variations during the cell culture. As a matter of fact, the control software architecture is conceived for the future implementation of an automatic routine for the activation of the secondary continuous feeding pump in response to the acquired pH and DO signals.

The monitoring and control system, as well as the secondary continuous feeding circuit, were implemented in the bioreactor platform configuration, which is in its still prototypal stage.

The bioreactor platform was employed for two preliminary applications, with lung-tumour-derived epithelial cell line (Calu-3) and human induced pluripotent stem cell (hiPSC) culture under low shear stress conditions.

Calu-3 cell line was selected for the primary test under ultralow shear stress conditions because of their property to form multicellular spheroids, typically used for investigation of lung cancer biology and ontogeny of epithelial cells *in vivo* [15]. Calu-3 dynamic suspension culture by means of the bioreactor proposed in this thesis promoted the production of functional 3D cell aggregates with active intercellular connections. Compared to the static control, Calu-3 cells cultured in dynamics suspension condition showed an increase in cycling cell number, together with a reduction of double strand DNA damage. These data was not supported with quantitative measures of 3D cell aggregate diameter, which could have provided a quantitative difference between static and dynamic suspension culture.

As second validation biotechnological application of the herein proposed bioreactor platform, the effect of low shear stress impeller-free dynamic suspension culture on human induced pluripotent stem cells (hiPSCs) was investigated. Under continuous low shear stress conditions, pre-formed inoculated hiPSC aggregates tended to aggregate forming massive agglomerates, suggesting that low shear stress levels were not able to modulate hiPSC aggregation kinetics. The pulsed-flow rate recirculation loop devised by means of a multiphysics modelling approach (Chapter 2) allows the modulation of 3D hiPSC aggregate growth in diameter. Starting from the ‘a priori’ knowledge gained by the development of the *in silico* pulsed protocol, the modulation effect on agglomeration kinetics was achieved by the combination of moderate intermittent shear stress and free-fall transport applied by the

pulsed protocol. The cyclic succession of free-fall transport moments and moderate shear flow-driven transport increased the homogeneity of the suspended hiPSC aggregates (thinner diameter statistical distribution), interfering with aggregate fusion and keeping the original hiPSC morphology. The inoculation of single-cell suspension allowed to elucidate that the impeller-free fluid dynamics establishing inside the bioreactor culture chamber is capable, even if weakly, to promote cell-cell interaction and consequently the formation of hiPSC aggregates.

Some limitations can waken this two preliminary experimental feasibility studies. In this bioreactor platform prototypal stage, the possibility to sample cell aggregates directly during the culture was not feasible. For this reason, short bioreactor runs were performed with the aim to have an immediate idea of the impact of impeller-free fluid dynamics on hiPSCs. Longer culture periods may require the possibility to sample aggregates directly from the culture chamber in order to follow the aggregate evolution over time without stopping the suspension. Moreover, although the bioreactor culture chamber was conceived to be translucent, the visibility during the culture was not optimal (high deformation of the visualized objects) and this limited the controllability of the process.

Nevertheless, these outcomes provide good indications for the possible usage of the presented bioreactor platform for human cell cultures. The combination of *in vitro* experiments and numerical simulations has demonstrated the potential of the device in culturing cells under low shear stress conditions. Importantly, the results herein presented as obtained by the use of the bioreactor platform in its prototypal stage suggest that the impeller-free func-

tioning principle, for producing dynamic suspension of human cells, is promising and it could be extended to dedicated cell culture applications in stem cell research and cancer biology.

In the future, this bioreactor platform will be considered as a starting point for the realization of dedicated impeller-free dynamic suspension bioreactors. In detail, the same impeller-free functioning principle currently implemented within the bioreactor culture chamber will be transferred to a modular platform in order to parallelize independent cultures. The bioreactor chambers will be modified to overcome the limitations arisen during the preliminary tests herein presented. The most important features to be guaranteed will be the direct sampling of culture specimens (cell/cell aggregates), an injection port, and direct pH and DO probing ports. This requirement will allow to speed up to the obtainment of a dynamic suspension impeller-free bioreactor for culturing stem and cancer cells under low shear stress conditions, which use would be adjusted starting from the multiphysics model results.

References

- 1 Teo, A., Mantalaris, A., and Mayasari, Lim M. Hydrodynamics and bioprocess considerations in designing bioreactors for cardiac tissue engineering. *Journal of regenerative medicine and Tissue Engineering*, 1, 4 (2012).
- 2 Zweigerdt. Large Scale Production of Stem Cells and Their Derivatives. *Adv Biochem Engin/Biotechnol*, 114 (2009), 201-235.
- 3 Rodrigues, C. A., Fernandes, T. G., Diogo, M. M., da Silva, C. L., and Cabral, J. M. Stem cell cultivation in bioreactors. *Biotechnologu Advances*, 29, 6 (2011), 815-829.

- 4 Cherry, R. S. Animal cells in turbulent fluids: details of the physical stimulus and the biological response. *Biotechnology*, 22, 2 (2004), 80-86.
- 5 King and Miller. Bioreactor development for stem cell expansion and controlled differentiation. *Current Opinion in Chemical Biology*, 11 (2007), 394-398.
- 6 Hammond, T. G. and Hammond, J. M. Optimized suspension culture: the rotating-wall vessel. *American Journal of Physiology. Renal Physiology*, 281, 1 (2001), F12-25.
- 7 Truscello, S., Schrooten, J., and van Oosterwyck, H. A computational tool for the upscaling of regular scaffolds during in vitro perfusion culture. *Tissue Engineering Part C Methods*, 17 (2011), 619-630.
- 8 Bannari, R., Bannari, A., Selma, B., and Proulx, P. Mass transfer and shear in an airlift bioreactor: using a mathematical model to improve reactor design performance. *Chemical Engineering*, 66 (2011), 2057-2067.
- 9 Karim, M. N., Hodge, D., and Simon, L. Data-based modelling and analysis of bioprocesses: some real experiences. *Biotechnology Progress*, 19, 5 (2003), 1591-1605.
- 10 Wu, J., Rostami, M. R., Cadavid Olaya, D. P., and Tzanakakis, E. S. Oxygen transport and stem cell aggregation in stirred-suspension bioreactor cultures. *PLoS ONE*, 9, 7 (2014), e102486.
- 11 Raimondi, M. T., Causin, P., Lagana, M., Zunino, P., and Sacco, R. Multiphysics computational modelling in cartilage tissue engineering. In *Computational Modeling in Tissue Engineering*. Springer-Verlag, Berlin Heidelberg, 2012.
- 12 Ismadi, M. Z., Gupta, P., Fouras, A., Verma, P., Jadhav, S., and Bellare, J. Characterization of a Spinner Flask for induced pluripotent stem cell culture application. *Plos One*, 9, 10 (2014), e106493.
- 13 Zweigerdt, Robert, Olmer, Ruth, Singh, H., Haverich, Axel, and Martin, Ulrich. Scalable expansion of human pluripotent stem cells in suspension culture. *Nature Protocols*, 6, 5 (2011), 689-700.
- 14 Olmer, Kropp, and Zweigerdt. Impact of Feeding Strategies on Expansion of Human Pluripotent Stem Cells in Stirred Tank Bioreactors Using mTeSR™1 (2014).

15 Shen, Y., Yao, S., Huang, P., and Yobas, L. In vitro epithelial organoid generation induced by substrate nanotopography. *Scientific Reports*, 19, 5 (2015), 92-93.

Industrial Bioengineering Group Activity

In this section a contribution to Industrial Bioengineering Group activity carried out during the first year of PhD is reported. The work herein presented was published in *Journal of Vascular Interventional Radiology*. Timothy Clark, the first author, proposed the study and wrote most of the paper, while the study presented was entirely done at Politecnico di Torino.

Abstract: Comparison of Symmetrical Haemodialysis Catheters using Computational Fluid Dynamics

Purpose:

Symmetrical tip dialysis catheters have become alternatives to split tip and step tip designs owing to low access recirculation and ease of tip positioning. Flow characteristics of three symmetrical tip dialysis catheters using computational fluid dynamics (CFD) as they relate to catheter function were compared.

Methods:

Palindrome, GlidePath and VectorFlow catheters were compared. A CFD-based approach was used to assess a) regions of flow separation, which are prone to thrombus development), b) shear-induced platelet activation potency, c) recirculation, and d) venous outflow deflection. A steady-state, laminar flow CFD model was used to simulate catheters tip position within the superior vena cava (SVC). Catheters performance was investigated at high hemodialysis flow (400 mL/min). Blood was assumed as a Newtonian fluid.

Results:

Wide regions of flow separation downstream of the Palindrome side slot and close to the distal tip were observed both in forward and reversed line configurations. Geometric asymmetry of the distal guidewire aperture of the GlidePath produced highest observed levels of inverted velocity flow when run in reversed configuration. The lowest shear-induced platelet activation average values were exhibited by GlidePath and VectorFlow catheters, whereas the Palindrome exhibited 152% higher overall platelet activation potency. All catheters were associated with a recirculation close to zero; the helically contoured lumens of the VectorFlow produced the greatest amount of deflection of venous flow away from the arterial lumen.

Conclusion:

The VectorFlow catheter was associated with less shear-induced platelet activation than the Palindrome and less flow separation than the Palindrome and GlidePath catheters irrespective of line configuration. These findings have potential implications for differences in thrombogenic risk during clinical performance of these catheters.

Introduction

Over 400,000 Americans receive renal replacement therapy through hemodialysis. Despite native fistula placement is the preferred form of permanent access, catheters remain the initial access for the majority of patients and they serve as a bridge to new access creation in patients with failed arteriovenous access (1).

Catheter thrombosis and infection remain causes of vascular access-related morbidity (2). Catheter performance during dialysis is also a challenge, since catheters with higher recirculation and/or reduced clearance will result in inadequate dialysis sessions (3). Inadequate dialysis has been shown to be an independent predictor of increased hospitalizations, hospital days, and Medicare inpatient expenditures among hemodialysis patients (4).

Differences in catheter tip design can produce significant differences in flow characteristics during the high-flow conditions required during dialysis, and in turn can have important implications for catheter thrombogenicity, recirculation and other critical parameters of catheter performance (5). Symmetrical tip catheters have become alternatives to conventional step-tip and split-tip catheters, owing in part to the ability to reverse lines during dialysis without an increase in recirculation (6). These differences were assessed between three commercially available symmetrical tip catheters using computational fluid dynamics, widely applied to study the hemodynamic performance of catheters (8-9).

Materials and Methods

Computational Fluid Dynamics

CFD simulations were designed to investigate and compare local hemodynamics in three commercially available symmetrical tip dialysis catheters: Palindrome (Covidien, Dublin, Ireland), GlidePath (Bard Access Systems, Salt Lake City, UT) and VectorFlow (Teleflex, Wayne, PA). High resolution CAD models of each catheter (**Figure 1**) were created as follows: the Palindrome catheter was measured with a touch probe coordinate machine and the resultant measurements were used to generate a high resolution 3D model in SolidWorks (Dassault Systems Inc., France). For the GlidePath, catheter internal and external surfaces were scanned within a high-resolution industrial computed tomography system (GKS Services Corp., USA) and the resultant 3D dataset was then rendered into SolidWorks. Both techniques ensured high accuracy in the reconstruction of every geometrical characteristic of the catheter models. The VectorFlow catheter was rendered using design control SolidWorks files. The 3D models were coaxially placed inside a cylindrical conduit (see details in the forthcoming) ideally resembling the SVC and processed to build discrete grids (where the governing equations of fluid motion have to be numerically solved) using the general purpose solid modeler ICEM (ANSYS Inc., USA). The computational grid consisted of over 8 million discrete tetrahedral/hexahedral cells (0.2 mm average edge size).

Model Assumptions

A previously validated CFD model (9) was used to simulate catheter tip position within the SVC, since it is currently not feasible to simulate hemodialysis catheters within a robust right atrial model, owing to complexity of assumptions regarding atrial anatomy, proportion of flow from the IVC, and

tricuspid valvular function. The SVC flow conditions were realistically assumed to be of 3 L/min within an 18 mm diameter, 480 mm long conduit with standard assumptions of adult human blood (incompressible Newtonian fluid model (10) with viscosity $\mu = 3.5$ mPa s and density $\rho = 1060$ kg/m³). Catheters performance was evaluated at 400 mL/min flow rate, in accordance with optimal clinical practice, with the catheters run in forward and reversed line configurations.

A detailed description of the methodology applied to prescribe the conditions at boundaries is available in the Appendix.

CFD Simulations and Post Processing

For all models, flow fields were computed by solving the 3D, steady-state (assumption based on the low pulsatility characterizing venous flow) governing equations of fluid motion in discrete form using a finite volume-based commercial code (Fluent, ANSYS Inc, USA). Each catheter was initially studied using classical fluid-dynamic theoretical analysis which verified the soundness of the assumption of flow laminarity. Sensitivity analysis was carried out to assure grid independence of the solution. Each catheter was run in forward and reversed directions to simulate clinical practice. A detailed description of the computational settings is provided in the Appendix.

Analysis of Thrombogenic Flow Patterns inside Catheters

The thrombogenic potency of the geometric features of the catheters was evaluated in terms of position and dimension of the flow separation regions (i.e., the boundary layers of flow that separate from the wall of the catheter to form a recirculation vortex behind the separation point, where shear stress vanish to become zero) generated within the lumens of the catheters as a

result of shape, size, number and position of both distal tip and sideholes. From a hemodynamics standpoint, flow separation occurs in regions of disturbed flow, where it can promote thrombus formation and development. Flow separation regions of each catheter were visually rendered by color-encoding the three-dimensional isosurfaces of blood velocity components with flow in the direction opposite to the main direction of the flow.

To further characterize the thrombogenic potency of flow patterns, the percentage volume of blood within each catheter model experiencing flow inversion (flow in the opposite direction to the main direction of flow) was also calculated. To do this, the arterial blood lumen inside a catheter segment of length extending from the tip to a 5.0 cm distance from the more distal side hole was considered.

Analysis of Shear-Induced Platelet Activation

As in previous studies on blood recirculating devices (11), to gain better understanding of the mechanisms that lead to flow-induced thrombogenic complications, the relationship between catheter-induced hemodynamics and platelet activation was quantified. A previously validated Lagrangian-based mathematical model was used (12), accounting for cumulative dynamic shear conditions experienced by platelets and is expressed as the Platelet Activation State (PAS) (13). PAS quantifies the more global thrombogenic aspect of platelet prothrombinase activity, i.e., its contribution to thrombin generation; PAS values are expressed as a fraction maximal prothrombinase activity. Further details about this methodology are provided in the Appendix. For the computational protocol of tracking the platelet-like particles, a cluster of approximately 1600 identical platelet-like particles were seeded, uniformly spaced, at cross sections of both venous and arterial lumens at the same distance from the tip of each modeled catheter. Each individual particle was

then tracked both backwards and forward in its motion within the fluid domain, thus recomposing the backward and forward segments in one trajectory. As a result, shear-induced activation state is captured for all platelets entering or moving out from the distal tip and side holes. The evolution of the system was followed for a simulated time sufficient for all platelet-like particles to leave the fluid domain.

Analysis of Recirculation

Recirculation of dialyzed blood was evaluated by computationally labeling blood in the venous lumen of each catheter and solving a convection-diffusion equation to quantify the percentage of labeled blood recirculating inside the arterial lumen. This allows to consider the transport of a well-defined concentration of dialyzed blood as a problem of transport of a scalar; recirculation of dialyzed blood was then evaluated in terms of the quantity of scalar movement from the venous lumen of the catheter to the arterial lumen.

Deflection of Dialyzed Blood away from the Venous Lumen

The average deflection angle for fluid pathlines exiting from the venous tip of each catheter was also calculated. This angle is defined as the angle that the local tangent at each pathline forms with respect to the long axis of the SVC model.

Results

Impact of Tip Design on Overall Catheter Hemodynamics

Table 1 summarizes the local Reynolds numbers (Re) and proportions of flow within the distal lumens and side holes of all the catheter models. At

distal catheter tips local Re ranged from 104 - 515 in the arterial lumen and 17 - 909 in the venous lumen; within side holes, the highest Re (515) was seen in the Palindrome catheter in the arterial configuration. Results summarized in Table 1 demonstrate that the flow inside the catheter models at locations where intricate hemodynamics occur is laminar and that the assumption of laminar flow for the present study is valid. Considering flow repartition among distal lumens and side holes, it can be observed in Table 1 that both the number and size of side holes play a major role in the withdraw phase, with the VectorFlow characterized by the lowest percentage of flow rate through side holes (44%), and the highest percentages for GlidePath (76%) and Palindrome (86%). As expected, blood moves out of the catheters predominately from the distal lumen (84% for VectorFlow, 78% for GlidePath and 74% for Palindrome).

Analysis of Thrombogenic Flow Patterns

A comprehensive visualization of the flow features characterizing the streaming of blood inside the catheters is presented in the supplementary material (please refer to animation movies available in the additional material describing fluid streamlines inside the arterial and venous lumen of Palindrome, GlidePath and VectorFlow catheters). Small reattachment/separation regions were observed downstream of the side holes. These regions were common to all catheters and were characterized by three-dimensional fluid structures differing in terms of extension and location, as determined by the different geometric characteristics.

Flow separation regions were observed within the arterial lumen of all three catheter models, owing to the perturbation of flow from the distal tip and side holes. **Figure 2** depicts the extent of flow separation regions along the arterial lumen catheter tip of Palindrome, GlidePath and VectorFlow, by

color-encoding the isosurfaces of blood velocity components with flow in the direction opposite to the main direction of the flow. Wide regions of flow separation downstream of the Palindrome side slot and close to the distal tip were observed both in forward and reversed line configurations. The GlidePath was characterized by small flow separation regions located downstream of the side holes and the distal tip in forward direction of flow, but when run in the reversed configuration a wide flow separation region was seen at the distal tip due to the geometric asymmetry from its distal guidewire aperture. The VectorFlow showed small regions of flow separation similar to the GlidePath when the catheter was run in the forward configuration; line reversal of the VectorFlow did not produce a discernable increase in flow separation (Figure 2).

The GlidePath showed the highest percentage of inverted velocity within the arterial lumen (6.7% of blood volume in forward direction, 6.8% of blood volume in reversed direction) followed by Palindrome (5.6% forward, 5.6% reversed) and VectorFlow (3.3% forward, 3.7% reversed). Blood pathline analysis showed that the inverted velocity blood flow in the GlidePath derives also from geometric asymmetry of the distal guidewire aperture producing flow perturbation when run in reversed configuration.

Analysis of Shear-Induced Platelet Activation

To compare the shear-induced platelet activation potential of the catheters, the final PAS was calculated as the mean value of all the activation levels sustained by all platelet-like trajectories moving within the catheter lumens. Figure 3 shows mean PAS values in the arterial and venous lumen for each catheter model. Platelets leaving the venous lumen experienced higher levels of activation than the arterial lumen. This feature is common to all the catheter models and it can be ascribed mainly to the high velocity

jet-like structures characterizing the outflow of the catheter ports. Marked differences in the mean PAS of the venous lumens were observed, with the Palindrome exhibiting venous lumen mean PAS levels (1.23×10^{-5}) that were 345% and 255% higher than the VectorFlow catheter (2.77×10^{-6}) and the GlidePath (3.46×10^{-6}) catheter, respectively.

Within the arterial lumen, smaller differences between Palindrome, GlidePath and VectorFlow were observed (i.e., 1.32×10^{-6} for Palindrome, 1.69×10^{-6} for GlidePath and 2.49×10^{-6} for VectorFlow). The highest difference was observed between mean arterial lumen PAS values of the Palindrome and VectorFlow (47%). Arterial and venous PAS values were averaged in order to assess the overall platelet activation potency of each catheter (dashed lines in **Figure 3**). As a result, the lowest overall PAS values were exhibited by GlidePath (2.63×10^{-6}) and VectorFlow catheters (2.63×10^{-6}) whereas the Palindrome exhibited an overall platelet activation potency (6.81×10^{-6}), 159% higher compared to the other catheter models.

Analysis of Recirculation

A negligible (less than 0.5%) level of recirculation was found to affect all the catheter models, independent of their design features. Relative to the other catheter designs, the VectorFlow recirculation potential was found to be the highest, even if well below the clinically relevant values. Similar values of recirculation were found in all three catheter models when run in reversed configuration (**Figure 4**).

To further characterize the phenomenon of recirculation of dialyzed blood related to the design features of the devices, the mean deflection angle of pathlines moving out from the venous lumen was calculated at a distance from 1 to 5 SVC diameters from the catheter tip. The results are depicted in

Figure 5. By comparing deflection angles of pathlines in the different models, it is seen that the Palindrome model produces an approximately straight jet-like structure moving out of the venous lumen (negative mean angle deflection between -0.2 and -0.94 degrees), while GlidePath design features deflect the streaming blood with larger angles (up to -9 degrees). The blood streaming out of the VectorFlow is characterized by the presence of a markedly helical flow structure (Figure 5) with a maximal deflection angle of -14 degrees. This feature of the flow field is also confirmed by the switch from negative to positive deflection angles when venous outflow reaches two diameters of distance from the catheter tip.

From these findings, the low recirculation in the VectorFlow catheter can be attributed to a balancing effect of flow deflection from the design of its distal tip and the increased recirculation generated as a consequence of size, position and dimension of VectorFlow side holes.

Discussion

Chronic dialysis catheters remain widely utilized as a bridge for patients awaiting permanent access placement or maturation, and when remaining options for permanent access have been depleted. In 2011 over 27% of prevalent dialysis patients in the United States had catheters, and approximately 80% of patients initiating hemodialysis in the U.S. did so through a catheter (1). Despite widespread utilization, catheters are the least desirable form of access owing to higher rates of infection and dysfunction compared to grafts and fistulae (2).

Until viable alternatives to catheters can be found, catheter performance needs to improve and catheter-related morbidity decrease. Various strategies

have been used including antithrombotic (14) and/or antimicrobial (15) surface coatings, antimicrobial lock solutions (16) and catheter tip modifications intended to improve flow characteristics and decrease recirculation (17).

Early hemodialysis catheter tip designs from the 1980s were step-tip configurations, as typified by the Quinton-Mahurkar catheter. These catheters functioned well in the short term but required precise tip positioning to enable adequate flow (18). Reversing line configurations in step-tip catheter designs produced recirculation levels exceeding 25%, attributed to the close proximity of the arterial and venous lumens, and vein wall apposition to the arterial lumen (19). A strategy of spatially separating venous and arterial lumens was employed by the Tesio catheter introduced in 1994, whereby the arterial and venous lumens were free-floating and completely independent of each other. In 1996, the Ash split catheter was developed, whereby the arterial and venous lumens remained separate for a substantial portion of their tips but within a single device. The Tesio and Ash designs were less susceptible to positioning problems, and recirculation was reduced given the physical separation between the arterial and venous lumens (5,20,21). In 2005, the Palindrome symmetrical tip catheter was introduced, which enabled aspiration and return of dialyzed blood through lumens that terminated at the same position within the device. By offsetting the lumens 180 degrees and separating them through a septum with angled cross-cuts, the Palindrome catheter produced minimal admixture of arterial and venous blood, with low recirculation even when arterial and venous lines were reversed (22). A recent randomized trial comparing the Palindrome catheter to a step-tip design found a significantly higher dysfunction-free catheter patency at 60 days favoring the Palindrome (78.9% vs. 54.4%) (23).

Two additional symmetrical tip catheters have recently been introduced in the United States – the GlidePath in 2013 and the VectorFlow in 2014. The GlidePath has curved distal apertures on opposing sides of the catheter which are angled to minimize admixture of blood. The VectorFlow has helically contoured arterial and venous apertures to produce a spiral, three-dimensional transition of blood entering and leaving the catheter; these vectors are opposed to minimize admixture of dialyzed and nondialyzed blood.

No clinical trials have yet been performed to compare the performance of these three symmetrical tip catheters, therefore a comparison of these devices using computational fluid dynamics was sought to evaluate whether differences exist which could have clinical implications for the performance of these devices. Computational modeling is increasingly utilized in the development and assessment of medical devices, being able to simulate many complex physiologic conditions to generate data of medical device performance which would otherwise take months or years using bench and pre-clinical *in vivo* models.

Flow within the shaft of a dual-lumen dialysis catheter is laminar, notwithstanding complex flow structures may occur near the distal tip or side-holes of a catheter. An important phenomenon in these devices is that of flow separation, whereby coherent patterns of laminar flow become disrupted by blood flowing in a direction opposite to the main direction of flow, forming a low velocity recirculation eddy. The resultant slowing and stagnation of the blood stream can promote thrombus formation and development (24). The Palindrome catheter was found to have the largest regions of flow separation with these regions most prominent around the distal tip and the side-slots of the catheter. The GlidePath and VectorFlow catheters had areas of flow separation which were similar to each other, although greater in number for

the GlidePath owing to its two additional sideholes (which are flow separation generators). As seen in Figure 2, flow stagnation regions were found most prominently around catheter sideholes and terminal apertures where laminar flow entering from the catheter tip becomes interrupted by sidehole inflow with resultant areas of flow reversal (competitive flows). The hole at the venous lumen tip of the GlidePath (used for guidewire insertion of the device) was also a prominent source of flow separation, in that line reversal of this device produced a marked increase in flow separation when this lumen was reversed in the arterial direction.

The tendency of each device to cause shear-induced platelet activation and aggregation during typical flow conditions of dialysis was also compared, using a previously validated computational model (8,9). Historically, the development of blood recirculating devices has focused on hemolysis as an indicator of flow-induced blood trauma (25). More recent work has shown that device thrombogenicity is largely driven by platelet activation (26). Red blood cells are relatively resistant to mechanical effects of shear forces compared to platelets; platelets are more rigid and experience shear-induced activation at an order of magnitude less than what is required for hemolysis of red blood cells (26). We observed the highest potential for shear-induced platelet activation within the Palindrome catheter, with similarly lower levels within the GlidePath and VectorFlow catheters.

Catheter recirculation decreases the efficiency of solute clearance, and can result in the need for longer dialysis. Recirculation was very low with each studied catheter, with levels less than 1/20th of the K/DOQI threshold of 10% of clinically significant recirculation (27), and concordant with what has been reported with symmetrical tip catheters in animal and clinical studies (6, 23).

A previously studied design of the VectorFlow catheter without sideholes found the catheter had no detectable recirculation in CFD, bench and animal models of hemodialysis (9). The lack of recirculation was attributed to the flow deflection that occurs from the helical transition zone at the distal tip of the device, whereby dialyzed blood is deflected away from the catheter in a vector 180-degrees away from blood entering the catheter. However, that design of the VectorFlow did not include side holes.

In the current study, the flow deflection properties of each catheter were compared. VectorFlow catheter (with sideholes) continues to produce a deflection of blood away from the catheter. This phenomenon is not seen with the Palindrome catheter, as it does not have a flow-deflecting interface at the tip of the catheter to alter the vector of dialyzed blood leaving the catheter. The GlidePath catheter did produce a component of flow deflection at its tip, owing to the curvature of the distal lumens which change the direction of blood exiting the distal tip of the catheter (**Figure 5**).

Our study has several limitations. Catheters were compared at a single flow rate value (400 mL/minute) and may have observed differing performance at varying flow rates. Current clinical practice is to place the tip of chronic dialysis catheters within the right atrium, whereas an SVC model was used to provide uniform conditions for catheter assessment and performance comparison. There is as yet no robust CFD model of the right atrium owing to wide variation in patient anatomy, the effects of inflow from the inferior vena cava, and the variation in blood flow and direction from the tricuspid valve. Notwithstanding the robustness of CFD modeling, clinical performance of these vascular devices can only be definitively compared only through well-designed, randomized prospective trials. Other possible limitations could arise from assuming blood as a Newtonian fluid, while it is well

known that blood is a non-Newtonian fluid with a shear thinning behavior. However, previous findings (10) observed that shear rate values throughout the regions of interest inside hemodialysis catheters are high enough to neglect the non-Newtonian blood behavior (8). Moreover, the Newtonian fluid hypothesis does not compromise the generality of the conclusions.

In conclusion, substantial differences catheters performance were observed using CFD. The Palindrome catheter exhibited larger areas of flow stagnation owing to flow separation/reattachment from the combined effects of its distal tip and larger side-slots. It also showed the highest mean level of shear-induced platelet activation potency. Both attributes are considered risk factors for catheter thrombosis in clinical utilization. All three catheters exhibited minimal recirculation; low recirculation seen with Palindrome and GlidePath is mostly attributable to the presence of a wide septum dividing arterial and venous lumens. Conversely, low recirculation seen with the VectorFlow was attributable to flow deflection from the design of its distal tip (even in the presence of a smaller interposed septum between lumens): this feature partially cancels out the increased recirculation generated as a consequence of size, position and dimension of VectorFlow side holes). These findings suggest that catheter tip design remains an important functional attribute of symmetrical chronic dialysis catheters, and warrants further investigation in randomized clinical trials.

References

1. U.S. Renal Data System, *USRDS 2013 Annual Data Report: Atlas of Chronic Kidney Disease and End-Stage Renal Disease in the United States (Table D7)*, National Institutes of Health, National Institute of Diabetes and Digestive and Kidney Diseases, Bethesda, MD, 2014
2. Dhingra RK, Young EW, Hulbert-Shearon TE, Leavey SF, Friedrich KP. Type of vascular access and mortality in U.S. hemodialysis patients. *Kidney Int.* 2001; 60: 1443–1451.
3. Tan J, Mohan S, Herbert L, Anderson H, Cheng JT. Identifying hemodialysis catheter recirculation using effective ionic dialysance. *ASAIO Journal* 2012; 58: 522–525.
4. Sehgal AR, Dor A, Tsai AC. Morbidity and cost implications of inadequate hemodialysis. *Am J Kid Dis* 2001; 37: 1223-1231.
5. Trerotola SO, Kraus M, Shah H, Namyslowski J, Johnson MS, Stecker MS, Ahmad I, McLennan G, Patel NH, O'Brien E, Lane KA, Ambrosius WT. Randomized comparison of split tip versus step tip high-flow hemodialysis catheters. *Kidney Int.* 2002; 62:282-289.
6. Kakkos SK, Haddad GK, Haddad RK, Scully MM: Effectiveness of a new tunneled catheter in preventing catheter malfunction: a comparative study. *J Vasc Interv Radiol* 2008; 19:1018–1026.

7. Grigioni M, Daniele C, Morbiducci U, Di Benedetto G, D' Avenio G, Del Gaudio C, Barbaro V. Computational model of the fluid dynamics of a cannula inserted in a vessel: incidence of the presence of side holes in blood flow. *J Biomech* 2002; 35: 1599-1612.
8. Mareels G, De Wachter DS, Verdonck PR. Computational fluid dynamics analysis of the Niagara hemodialysis catheter in a right heart model. *Artif Organs* 2004; 28: 639–648.
9. Clark TWI, Van Canneyt K, Verdonck P. Computational flow dynamics and preclinical assessment of a novel hemodialysis catheter. *Semin Dial.* 2012; 25:574-578.
10. Mareels G, De Wachter DS, and Verdonck PR. Computational fluid dynamics-analysis of the Niagara hemodialysis catheter in a right heart model. *Artif Organs* 2004; 28(7):639–648.
11. Morbiducci U, Ponzini R, Nobili M, Massai D, Montevecchi FM, Bluestein D, Redaelli A Blood damage safety of prosthetic heart valves. Shear induced platelet activation and local flow dynamics: a fluid-structure interaction approach. *J Biomech* 2009; 42: 1952-1960.
12. Grigioni M, Morbiducci U, D' Avenio G, Di Benedetto G, Del Gaudio C. A novel formulation for blood trauma prediction by a modified power law mathematical model. *Biomech Mod Mechanobiol* 2005;4(4):249-260.
13. Nobili M, Sheriff JE, Morbiducci U, Redaelli A, Jesty J, Bluestein D. Platelet activation due to hemodynamic shear stresses: damage accumulation model and comparison to in vitro measurements. *ASAIO J* 2008;54:64-72.

14. Clark TWI, Jacobs D, Charles HW, Kovacs S, Aquino T, Erinjeri J, Benstein JA. Comparison of heparin coated and conventional split-tip hemodialysis catheters. *Cardiovasc Intervent Radiol* 2009; 32:703-706.
15. Trerotola SO, Johnson MS, Shah H, Namyslowski J, Johnson MS, Stecker MS, Ahmad I, McLennan G, Patel NH, O'Brien E, Lane KA, Ambrosius WT. Tunneled hemodialysis catheters: use of a silver-coated catheter for prevention of infection—a randomized study. *Radiology* 1998; 207:491–496.
16. Moore CL, Besarab A, Ajluni M, Soi V, Peterson EL, Johnson LE, Zervos MJ, Adams E, Yee J. Comparative effectiveness of two catheter locking solutions to reduce catheter-related bloodstream infection in hemodialysis patients. *Clin J Am Soc Nephrol* 2014; 9:1232-9.
17. Ash SH. Advances in tunneled central venous catheters for dialysis: design and performance. *Semin Dial.* 2008; 21: 504-515.
18. Schwab SJ, Buller GL, McCann RL, Bollinger RR, Stickel DL. Prospective evaluation of a Dacron cuffed hemodialysis catheter for prolonged use. *Am J Kidney Dis.* 1988; 11:166-169
19. Twardowski ZJ, Van Stone JC, Haynie JD. All currently used measurements of recirculation in blood access by chemical methods are flawed due to intradialytic disequilibrium or recirculation at low flow. *Am J Kidney Dis.* 1998; 32: 1046-58.
20. Perini S, LaBerge JM, Pearl JM, et al. Tesio catheter: radiographically guided placement, mechanical performance, and adequacy of delivered dialysis. *Radiology* 2000; 215:129–137.

21. Ash SR, Mankus RA, Sutton JM. Survival and hydraulic function of the Ash Split Cath hemodialysis catheter. *Nephrologie* 2001;22:403-405.
22. Tal MG. Comparison of recirculation percentage of the Palindrome catheter and standard hemodialysis catheters in a swine model. *J Vasc Interv Radiol* 2005;16: 1237–1240.
23. Hwang HS, Kang SH, Choi SR, Sun IO, Park HS, Kim Y. Comparison of the Palindrome vs. step-tip tunneled hemodialysis catheter: a prospective randomized trial. *Semin Dial* 2012; 25: 587-91.
24. Bluestein D, Chandran KB, Manning KB. Towards non-thrombogenic performance of blood recirculating devices. *Ann Biomed Eng.* 2010; 38(3): 1236–1256.
25. Paul R, Marseille O, Hintze E, Huber L, Schima H, Reul H, Rau G. In vitro thrombogenicity testing of artificial organs. *Int. J. Artif. Organs* 1998;21(9):548–552.
26. Klaus S, Korfer S, Mottaghy K, Reul H, Glasmacher B. In vitro blood damage by high shear flow: human versus porcine blood. *Int. J. Artif. Organs* 2002; 25:306–312.
27. National Kidney Foundation. Clinical practice guidelines for vascular access. *Am J Kidney Dis* 2006; 48 (Suppl 1):S176–273.

Figures

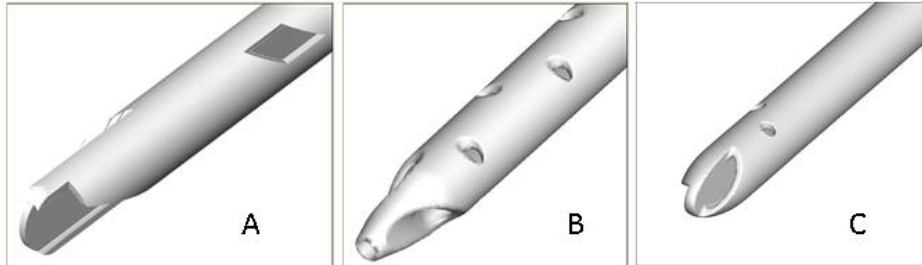


Figure 1

Three dimensional CAD models of the Palindrome, GlidePath and Vector-Flow catheters prior to tetrahedral/hexahedral meshing for analysis using computational fluid dynamics. The Palindrome catheter is completely symmetrical. The GlidePath catheter is not perfectly symmetrical due to a guide-wire aperture at the distal tip as part of the venous lumen, as well as offset sideholes. The VectorFlow catheter has complete symmetry of its distal tip but offsetting of its sideholes.

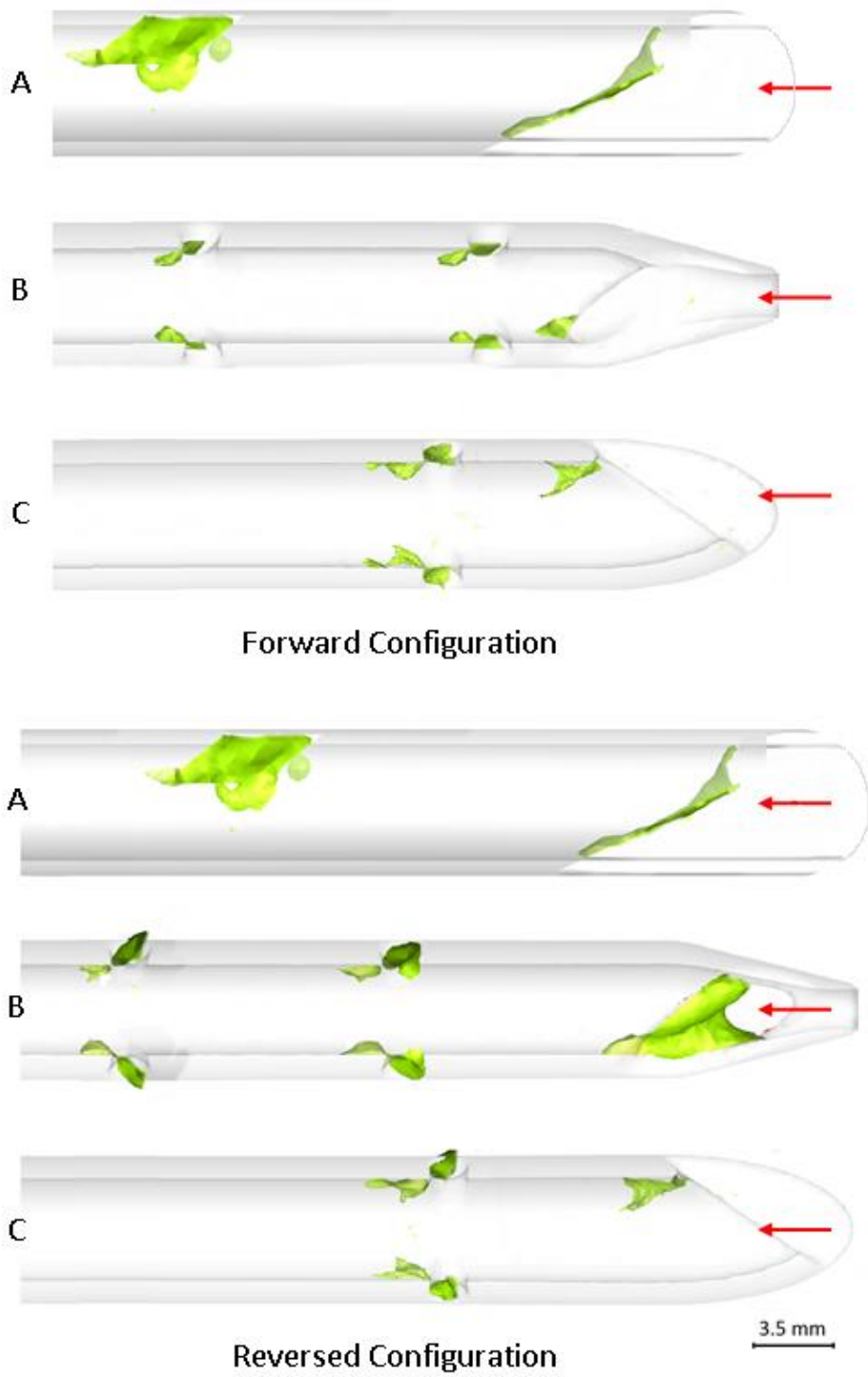


Figure 2

Flow separation regions for Palindrome (1), GlidePath (2) and Vector-Flow (3) in forward and reversed directions within the arterial lumen. The scale at the bottom of the image allows for quantitative analysis of the spatial extension of regions of disturbed flow inside the lumen; areas of flow separation appear in green. Red arrows indicate the main direction of flow.

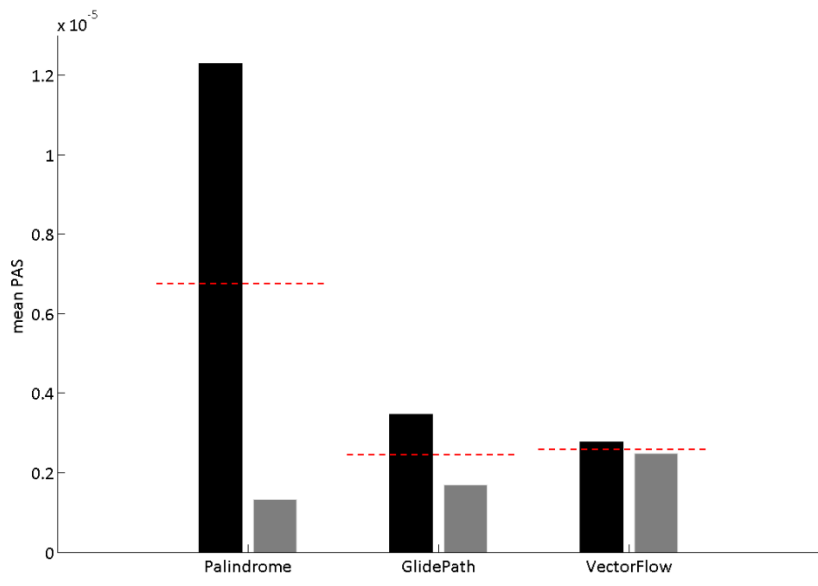


Figure 3

Mean Platelet Activation State (PAS) values for venous (black) and arterial (grey) lumens. Dashed line represents the average between arterial and venous PAS values.

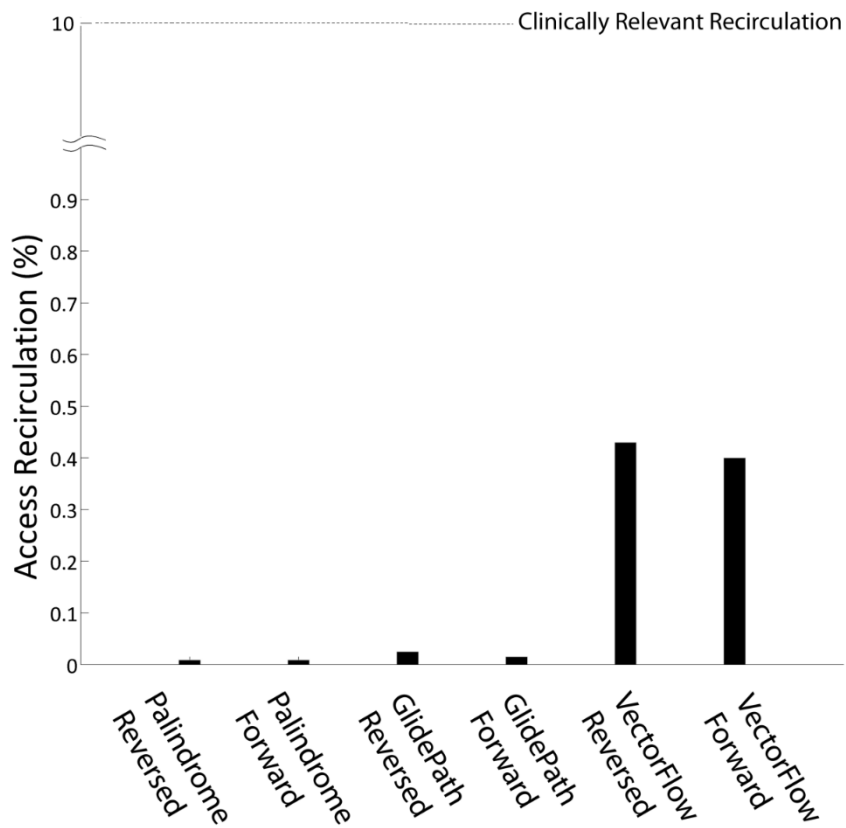


Figure 4 Recirculation of the Palindrome, GlidePath and VectorFlow catheters in reversed and forward direction, as a percentage of access recirculation. The dashed line denotes clinically significant recirculation as defined by K/DOQI (2).

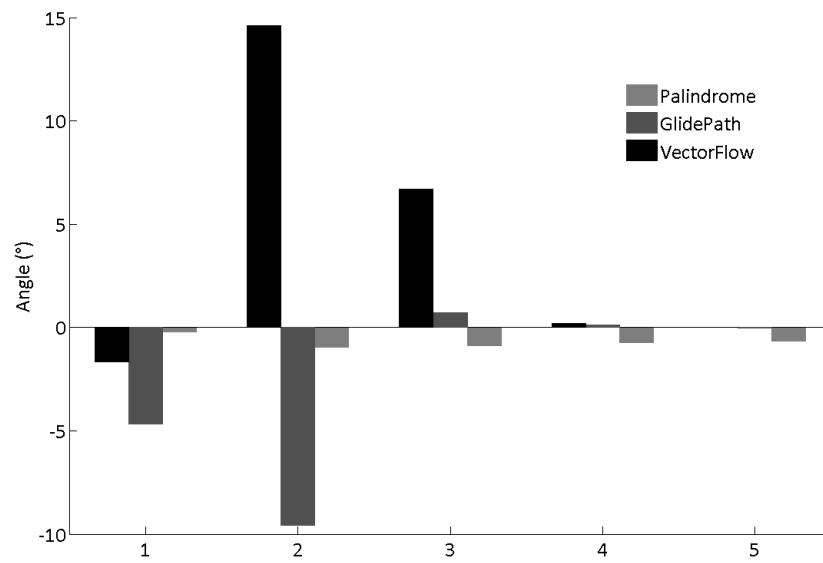


Figure 5: A. Mean angle deflection of flow pathlines at a distance (d) of 1 to 5 SVC diameters (D) downstream of the distal tip of the catheter in forward configuration.

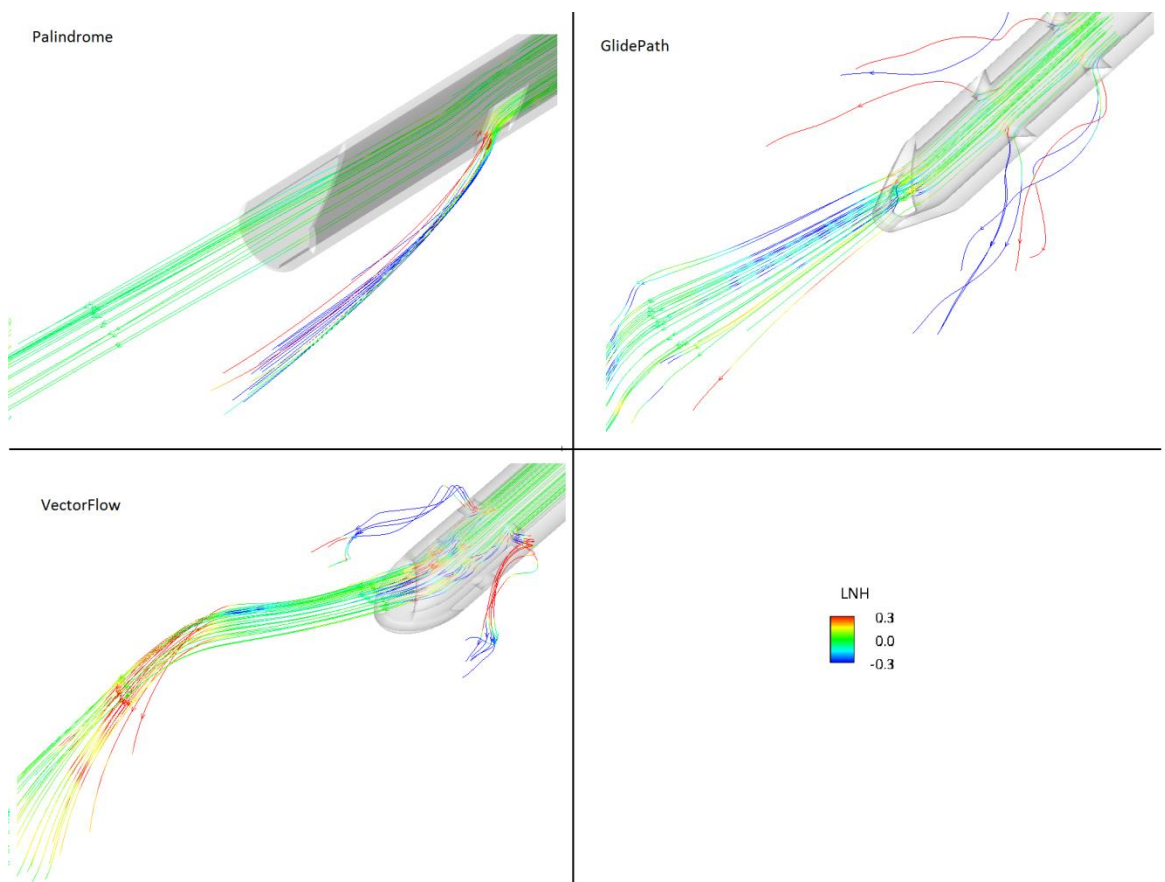


Figure 5:

B) Representation of blood streamlines exiting venous lumen in Palindrome (top left), GlidePath (top right) and VectorFlow (bottom) colored by velocity magnitude (in m/s).

Tables

Table 1: Flow split and Reynolds number through distal tip and side holes.

Arterial lumen		Reynolds Number	Split Ratio
VectorFlow	Distal Tip	496	53%
	Side Holes	412	47%
GlidePath	Distal Tip	224	24%
	Proximal Side Holes	214	26%
	Distal Side Holes	401	49%
Palindrome	Distal Tip	104	14%
	Side Holes	515	86%
Venous lumen		Reynolds Number	Split Ratio
VectorFlow	Distal Tip	909	84%
	Side Holes	35	16%
GlidePath	Distal Tip	720	78%
	Proximal Side Holes	17	2%
	Distal Side Holes	48	20%
Palindrome	Distal Tip	547	73%
	Side Holes	249	27%

Movies

Movie 1: Evolving streamlines in the Palindrome arterial lumen, color coded with respect to Velocity Magnitude (m/s).

Movie2: Evolving streamlines in the GlidePath arterial lumen color coded with respect to Velocity Magnitude (m/s).

Movie 3: Evolving streamlines in the VectorFlow arterial lumen color coded with respect to Velocity Magnitude (m/s).

Movie 4: Evolving streamlines in the Palindrome venous lumen, color coded with respect to Velocity Magnitude (m/s).

Movie 5: Evolving streamlines in the GlidePath venous lumen, color coded with respect to Velocity Magnitude (m/s).

Movie 6: Evolving streamlines in the VectorFlow venous lumen, color coded with respect to Velocity Magnitude (m/s).

Appendix

Computational settings applied for catheters flow dynamics simulations

The set of conditions applied at boundaries, taking device Palindrome as an example, is schematized in Fig. E1. Each catheter model was coaxially placed inside a cylindrical conduit (18 mm in diameter) which representing the superior vena cava. To ensure fully developed velocity profiles at the inlet and to minimize the influence of outlet BCs, straight flow extensions were added both to the inlet and outlet faces of the model. Technically, 200 mm long inlet and 100 mm long outlet flow extensions were added reaching a total axial extent of the computational domain of 480 mm. More in detail, steady-state flow simulations were carried out imposing the following boundary conditions: (1) a constant 3 L/min flow rate was prescribed at the SVC inlet section (T1, Fig. E1) in terms of flat velocity profile; (2) reference pressure was set at the outlet section of the SVC (T2); (3) a constant flow rate of 400 mL/min was prescribed at the venous inlet section of the catheter (V1) in terms of flat velocity profile; (4) a flow rate value equal to 400 mL/min was prescribed as outflow boundary condition at the arterial lumen of the catheter (A2) in terms of constant mass flow. All walls were assumed as rigid; the no-slip condition was applied.

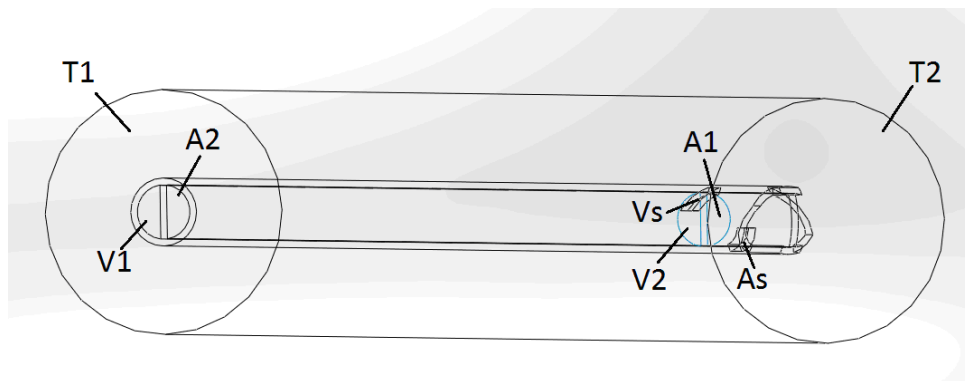


Figure E1: Conditions applied at the permeable boundaries. Schematics of the virtual bench test setup for Palindrome model (representation is not in scale). T1 and T2 are tube inlet and tube outlet, V1 and V2 are the venous inlet and outlet, A2 and A1 are arterial inlet and outlet, respectively. Vs and As represent the venous and arterial side holes.

For the finite volume method-based discrete solution of the governing equation of motion over the numerical grid, the segregated solver with SIMPLE scheme was used. Second Order accuracy was used for pressure and second order upwind for momentum. As for the quantification of access recirculation percentage, QUICK discretization scheme was applied for the convection-diffusion scalar transport equation solved for the dialyzed labeled blood, guaranteeing optimal accuracy to the numerical problem solution. Convergence was accepted when the residuals of continuity and velocity, fell below 10^{-6} . Simulations have been run in 8-CPU workstation parallel-architecture (Linux environment with a SUN cluster SunFire X4450).

Analysis of shear-induced platelet activation

We utilized a method which performs a comprehensive analysis of platelet-like trajectories and their shear histories during flow through dual lumen catheter models. The analysis uses information extracted from numerical simulations to resolve the flow field through the models of dual lumen catheters. The extent to which these devices to mechanically induce activation/damage of platelets was evaluated using the Lagrangian-based blood damage cumulative model proposed by Grigioni et al. (12). The Lagrangian-based mathe-

mathematical model is based on cellular damage theory, and accounts for the cumulative load history sustained by formed elements exposed to time-dependent stress levels. Originally developed for the evaluation of red blood cell mechanical damage (11) this model has since been adapted for the assessment of platelet activation state (PAS) under dynamic loading conditions (13). PAS quantifies the more global thrombogenic aspect of platelet prothrombinase activity, i.e., its contribution to thrombin generation. Developed within a hemodynamic shearing system to produce shear stress damage to human platelets, PAS values are expressed as a fraction maximal prothrombinase activity. A mathematical model has since been validated with the human platelet assay to calculate PAS values. Specifically, the activation state of the k -th platelet can be expressed as the integral sum of infinitesimal contributions:

$$\text{PAS}_k = \int_{t_0}^t Ca \left[\int_{t_0}^{\phi} \tau(\xi)^{b/a} d\xi + \frac{\text{PAS}_k(t_0)^{1/a}}{C} \right]^{a-1} \tau(\phi)^{b/a} d\phi \quad (1)$$

where $\text{PAS}_k(t_0)$ is the value of activation of the k -th platelet at the starting time of observation t_0 (i.e., senescence, or previous damage history during previous passages through a vascular access device), $\tau = \tau(t)$ is the shear stress and $a = 1.3198$, $b = 0.6256$, $C = 10^{-5}$ are the parameters of the model (14). Using this formulation the shear history experienced by blood cells is resolved: the effects of the shear stresses previously sustained on the subsequent activation/damage (senescence) is captured by Eq. (1), and the integral sum inside the square brackets represents the mechanical load sustained by the k -th platelet moving along a specific trajectory from the initial instance.

Over the whole dataset, we also calculated the mean PAS value for each time instant from the time of injection:

$$\text{PAS}_{\text{mean}}(t) = \frac{1}{N_p} \sum_{k=1}^{N_p} \text{PAS}_k(t) \quad (2)$$

where N_p is the number of platelets moving in the fluid domain.